Characterization of Fluid Flow & Heat Exchange Heterogeneity in Natural Rock Fractures

Noah Vriese, *University of Wisconsin-Madison*

Michael Cardiff, *University of Wisconsin-Madison*

Overview

I. Introduction

II. Methods

III. Flow Modeling

IV. Results & Discussion

V. Conclusions

Overview

I. Introduction
   I. Background
   II. Purpose & scope
   III. Review of fracture surface characterization, flow, & heat transport

II. Methods

III. Flow Modeling

IV. Results & Discussion

V. Conclusions

Overview

I. Introduction
   I. Background
   II. Purpose & scope
   III. Review of fracture surface characterization, flow, & heat transport

II. Methods

III. Flow Modeling

IV. Results & Discussion

V. Conclusions

I. Importance of Fractured Rock

- Fractured geologic formations are ubiquitous worldwide
- Fractures allow for the rapid transmission of subsurface fluid
- Important in variety of contexts:
  1. Reservoir exploration for water & hydrocarbons
  2. Geotechnical applications
  3. *Enhanced geothermal systems* (EGS)

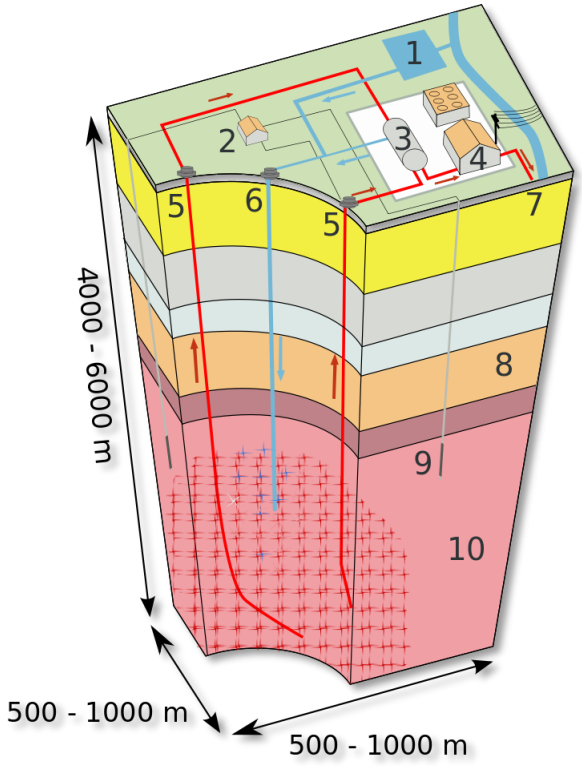

Figure. Enhanced Geothermal System

I. Fractures over Length Scales

- Typical fracture ***lengths*** range from *mm* (10^{-3} m) to *km* (10^{3} m)
- Typical fracture ***apertures*** range from *μm* (10^{-6} m) to *cm* (10^{-2} m)

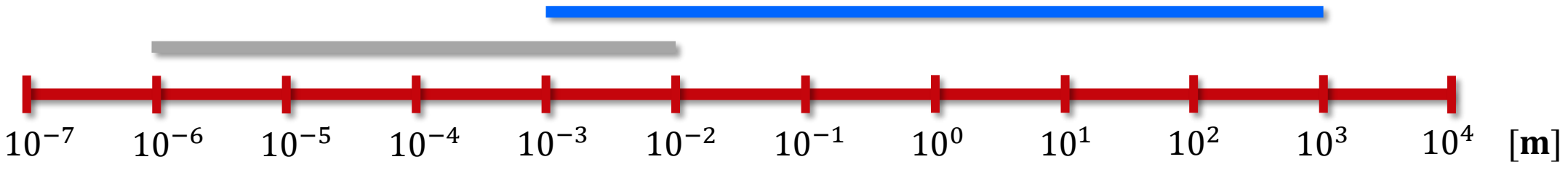

I. Fractures over Length Scales

- Typical fracture ***lengths*** range from *mm* (10^{-3} m) to *km* (10^{3} m)
- Typical fracture ***apertures*** range from *μm* (10^{-6} m) to *cm* (10^{-2} m)

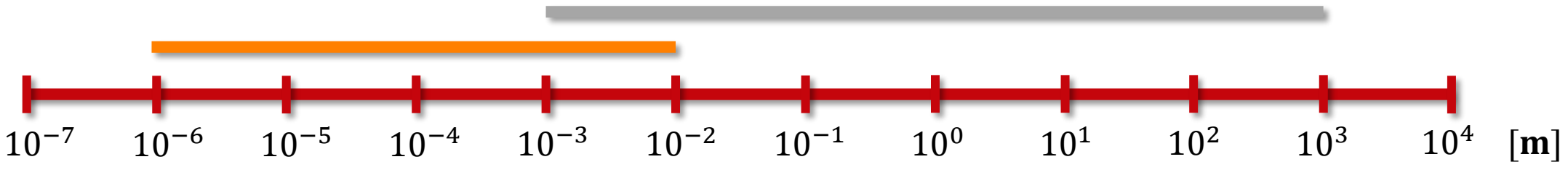

I. Fractures over Length Scales

- Typical fracture ***lengths*** range from *mm* (10^{-3} m) to *km* (10^{3} m)
- Typical fracture ***apertures*** range from *μm* (10^{-6} m) to *cm* (10^{-2} m)

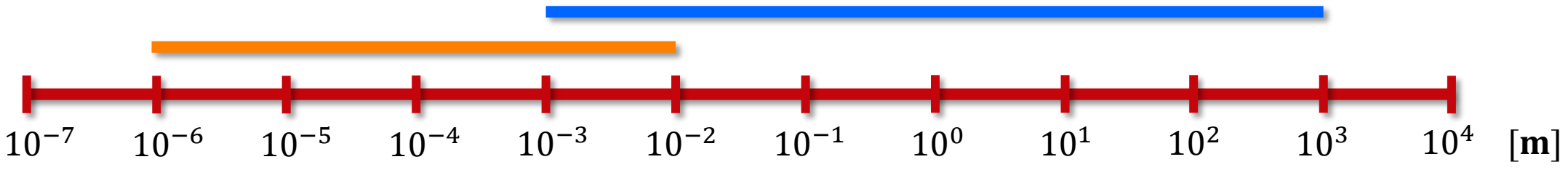

- Knowledge of flow within large scale *fracture systems* relies on a fundamental understanding of flow at the single *fracture* scale

I. Heterogeneity at all Scales

- Flow behaviors ***at all scales*** are complicated by ***heterogeneity***

- At the ***aquifer*** scale:
  - Fracture networks increase permeability anisotropy

- At the ***fracture*** scale:
  - Aperture variability increases tortuosity & flow dispersion

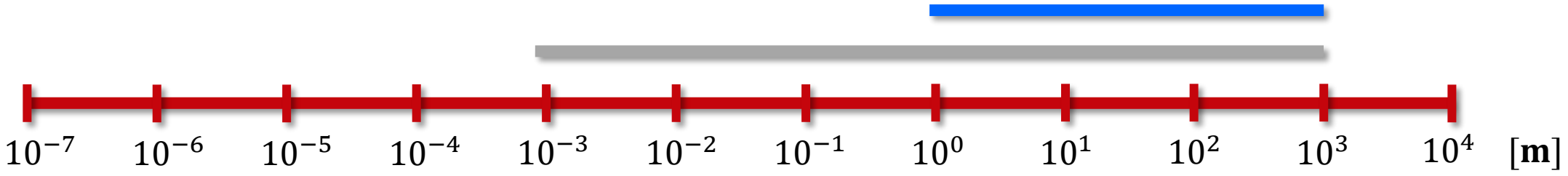

I. Heterogeneity at all Scales

- Flow behaviors ***at all scales*** are complicated by ***heterogeneity***

- At the ***aquifer*** scale:
  - Fracture networks increase permeability anisotropy

- At the ***fracture*** scale:
  - Aperture variability increases tortuosity & flow dispersion

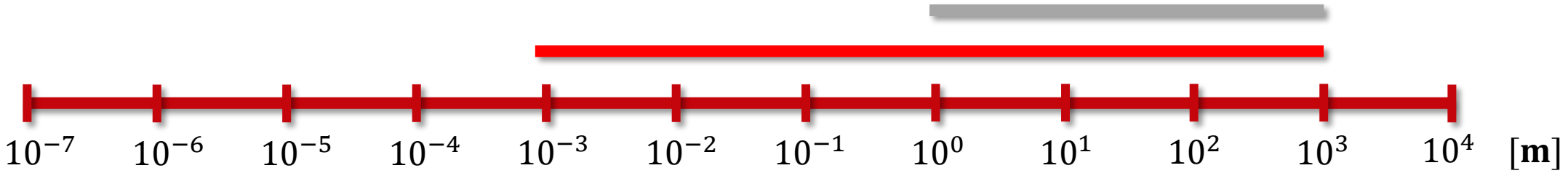

I. Fracture Aperture Heterogeneity

- The most common model of fracture-scale flow approximates a constant aperture

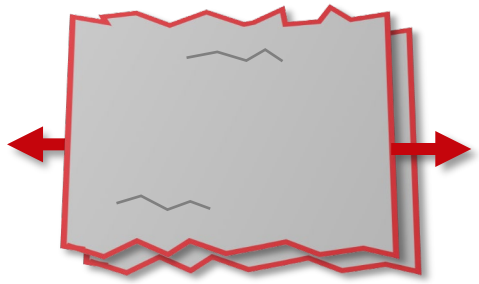

Fracture surfaces

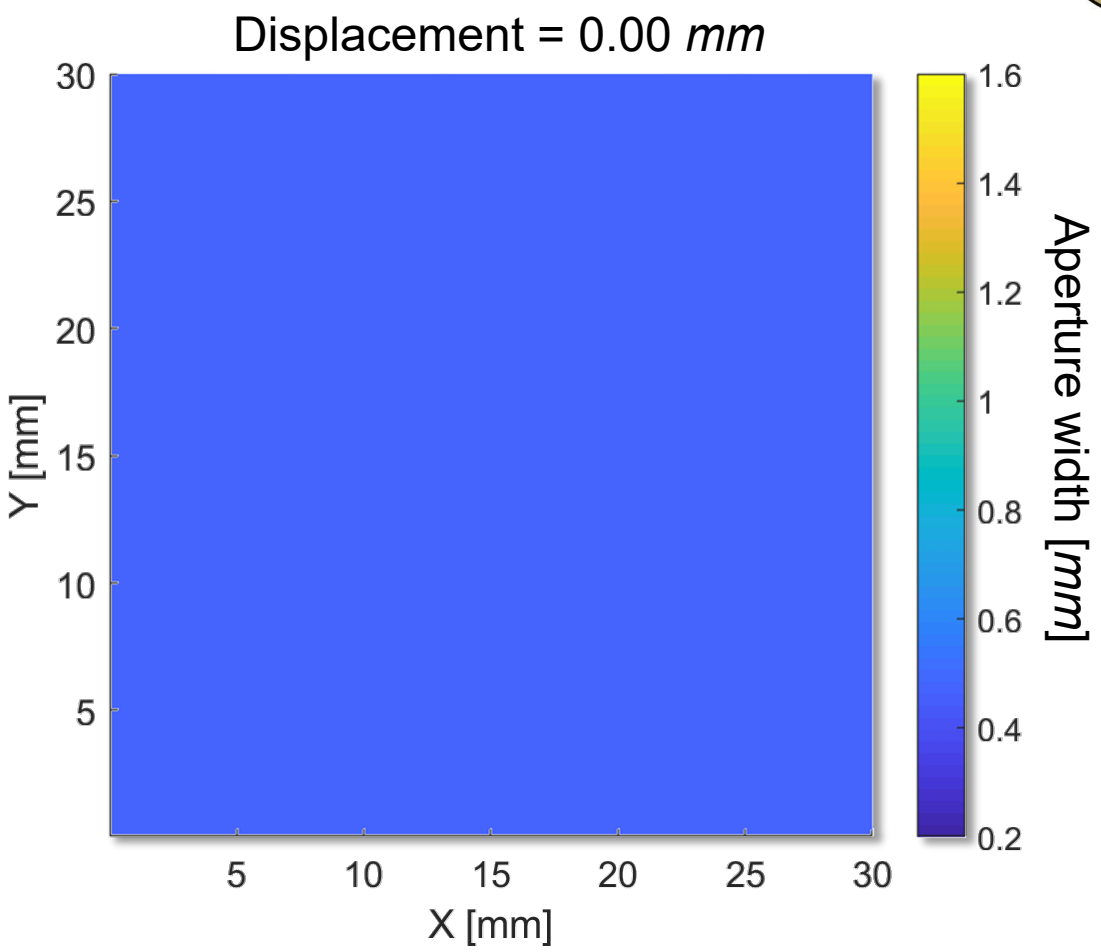

Figure. Aperture width as a function of shear slip.

I. Fracture Aperture Heterogeneity

- The most common model of fracture-scale flow approximates a constant aperture

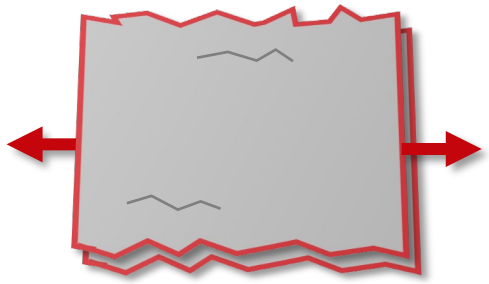

Fracture surfaces

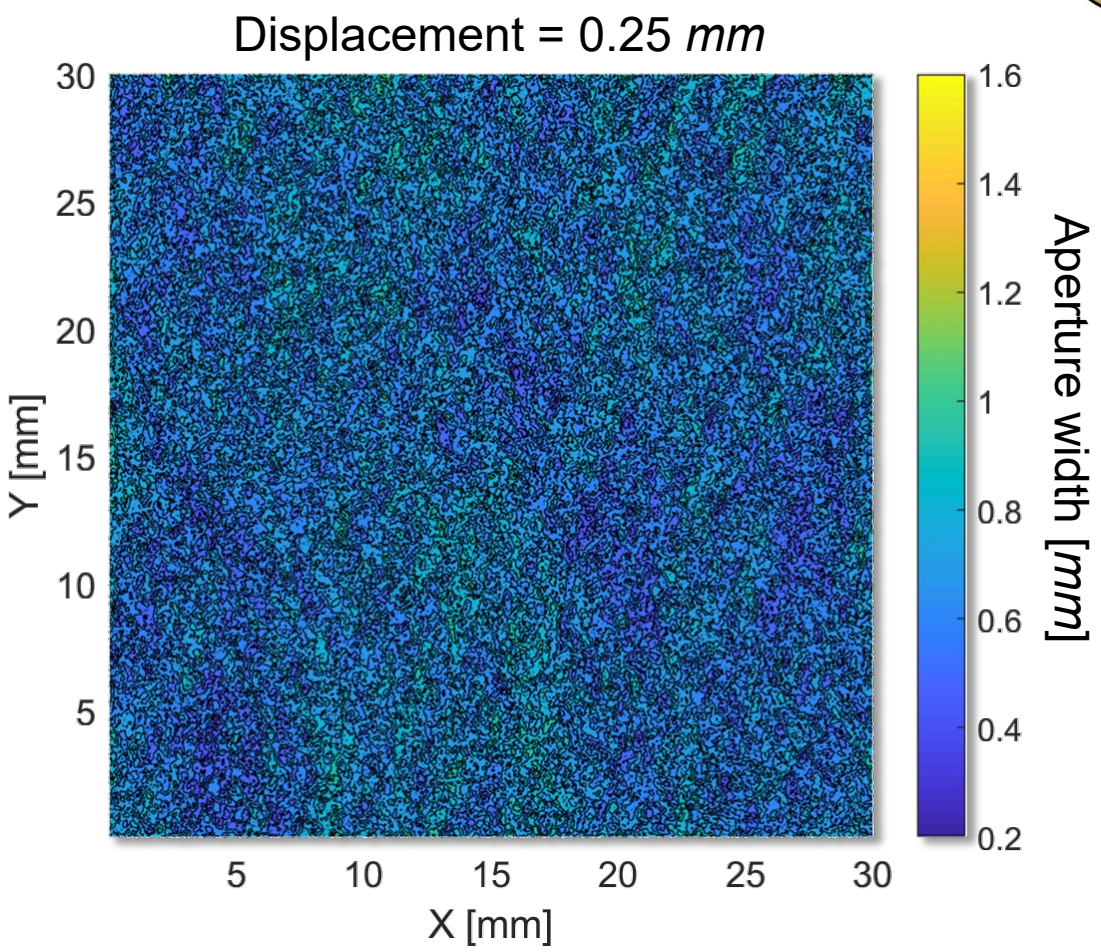

Figure. Aperture width as a function of shear slip.

I. Fracture Aperture Heterogeneity

- The most common model of fracture-scale flow approximates a constant aperture

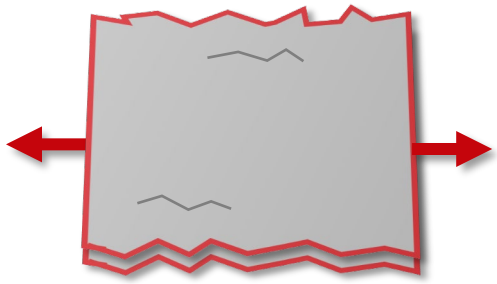

Fracture surfaces

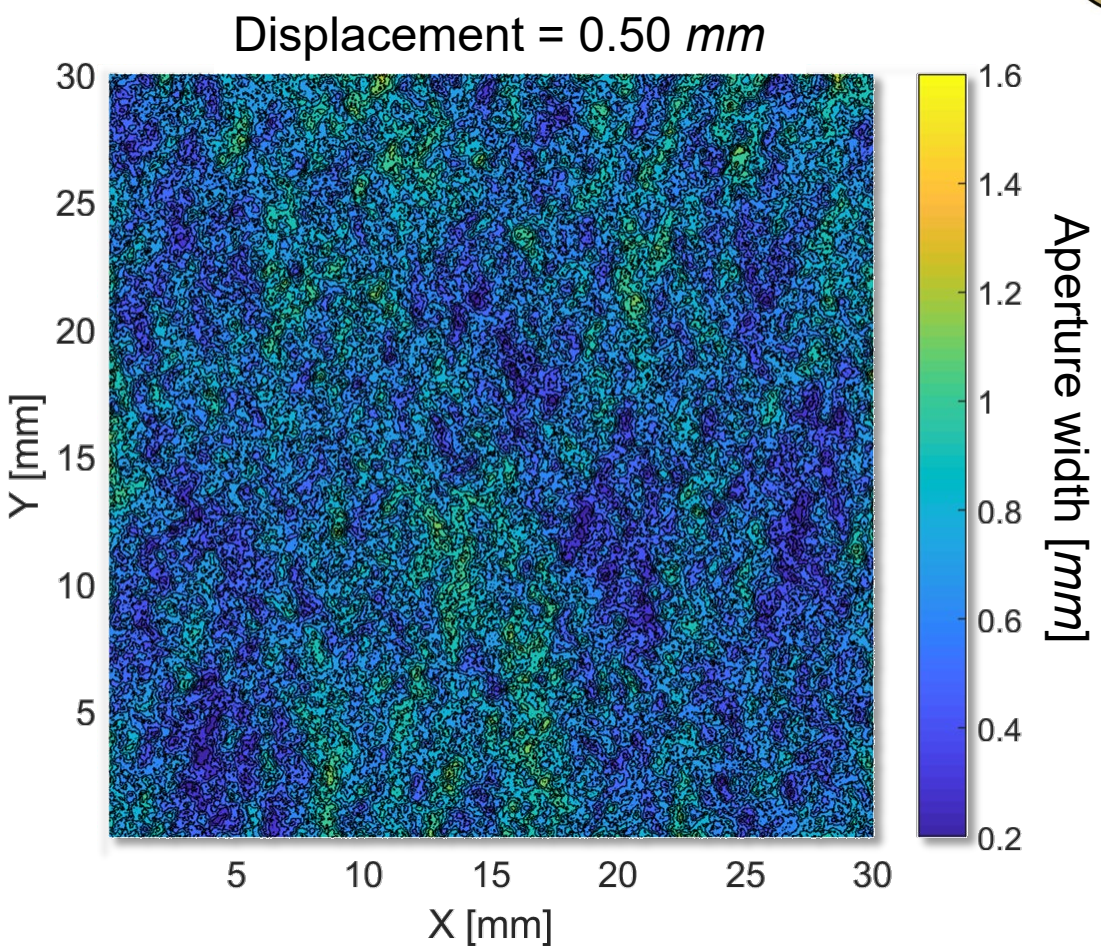

Figure. Aperture width as a function of shear slip.

I. Fracture Aperture Heterogeneity

- The most common model of fracture-scale flow approximates a constant aperture

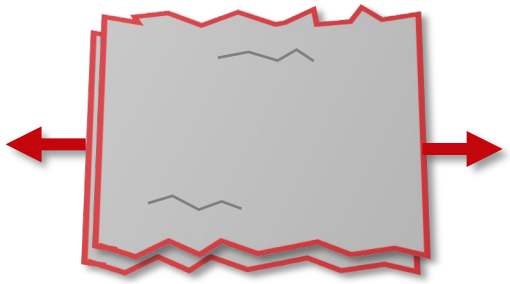

Fracture surfaces

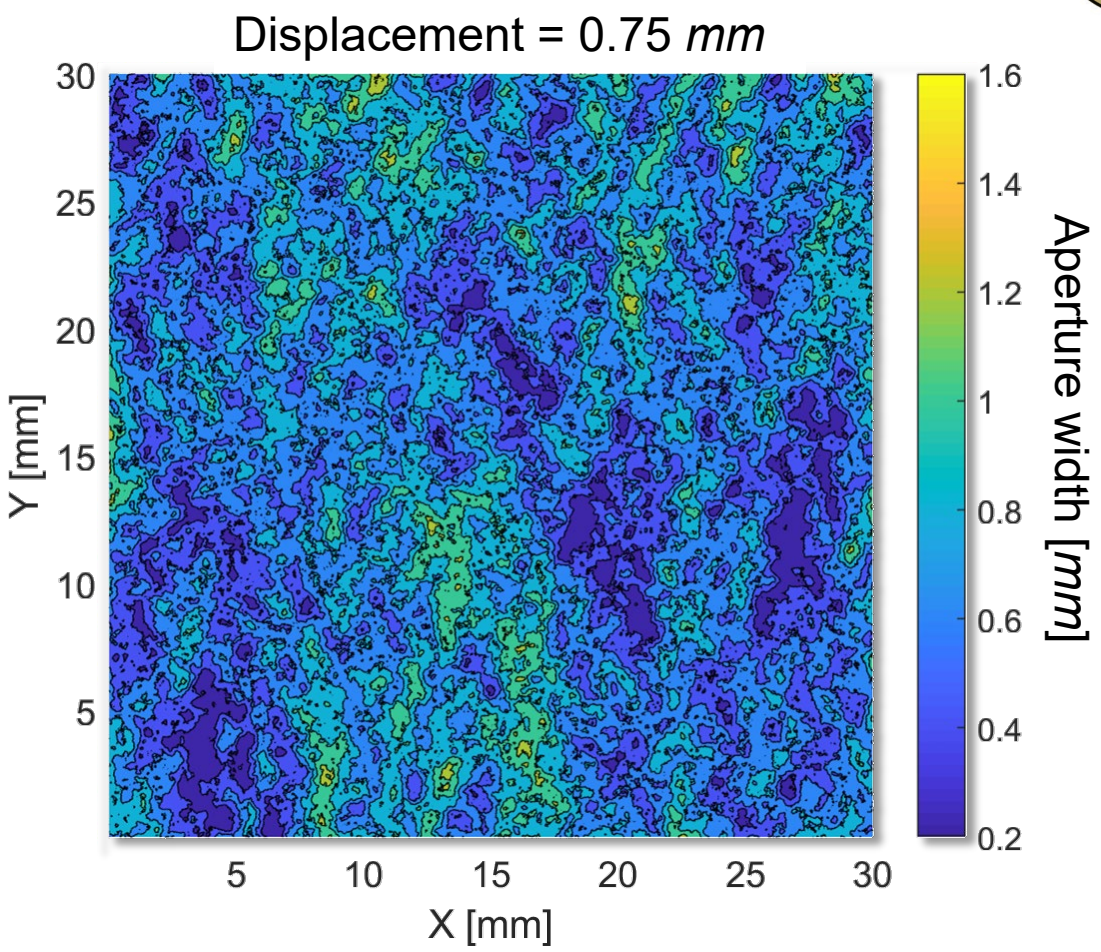

Figure. Aperture width as a function of shear slip.

I. Fracture Aperture Heterogeneity

- The most common model of fracture-scale flow approximates a constant aperture

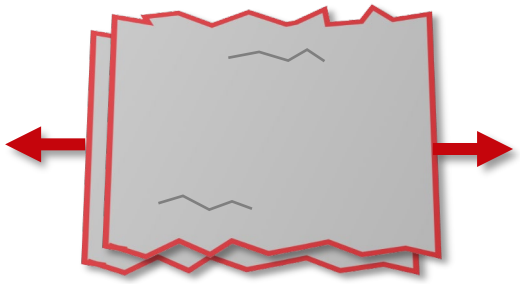

Fracture surfaces

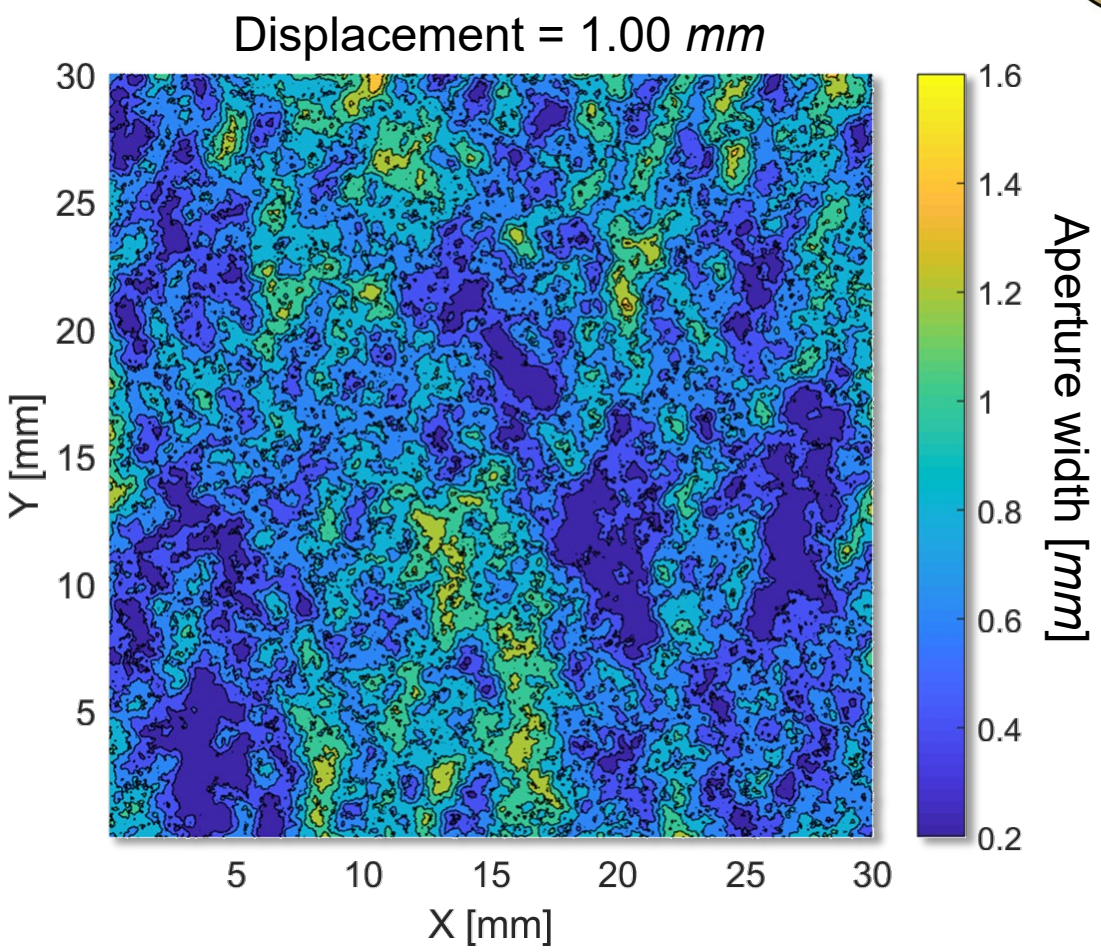

Figure. Aperture width as a function of shear slip.

I. Fracture Aperture Heterogeneity

- The most common model of fracture-scale flow approximates a constant aperture

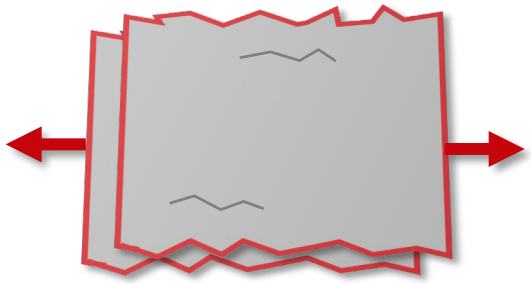

Fracture surfaces

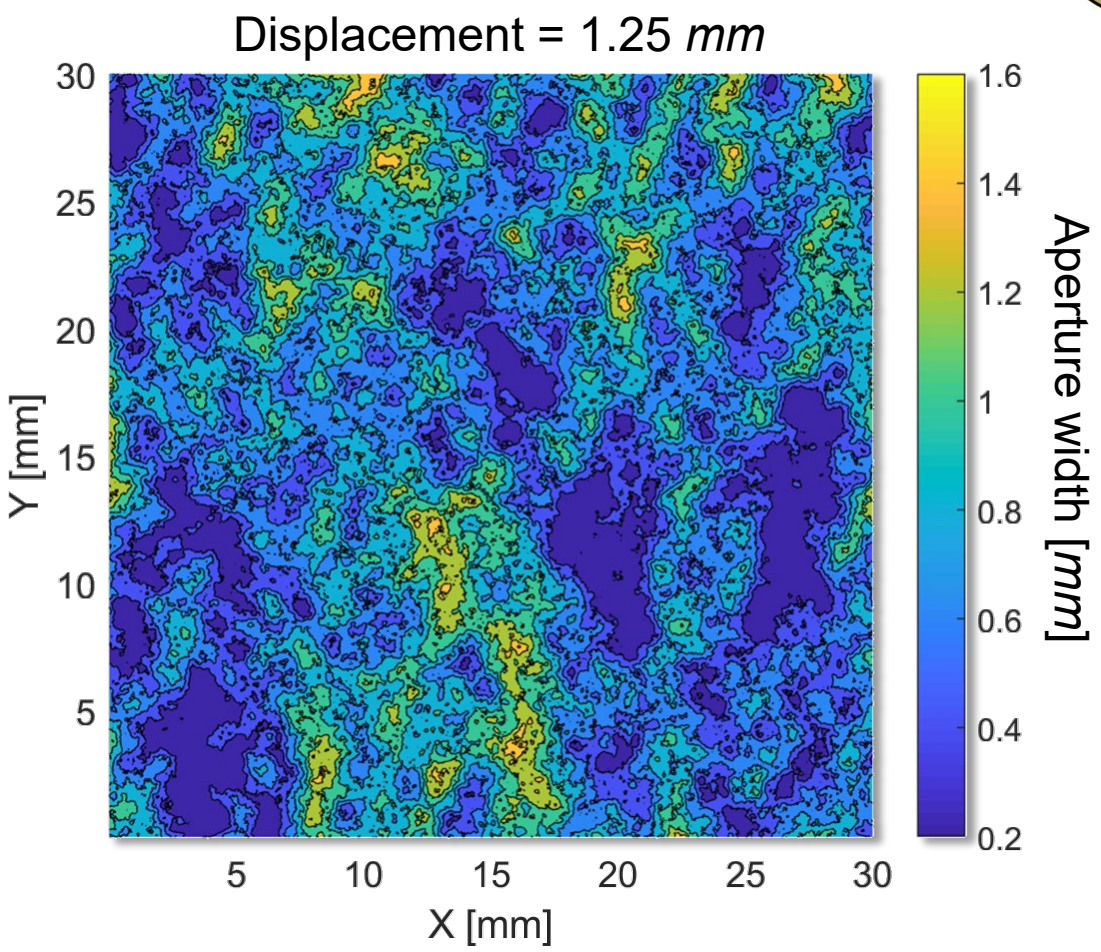

Figure. Aperture width as a function of shear slip.

I. Fracture Aperture Heterogeneity

- The most common model of fracture-scale flow approximates a constant aperture

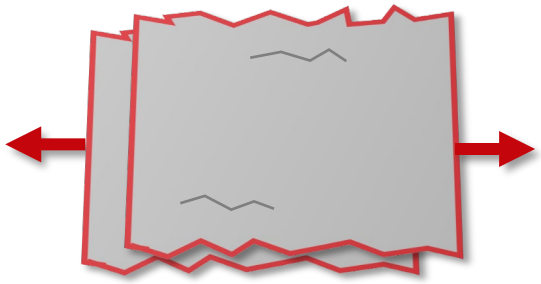

Fracture surfaces

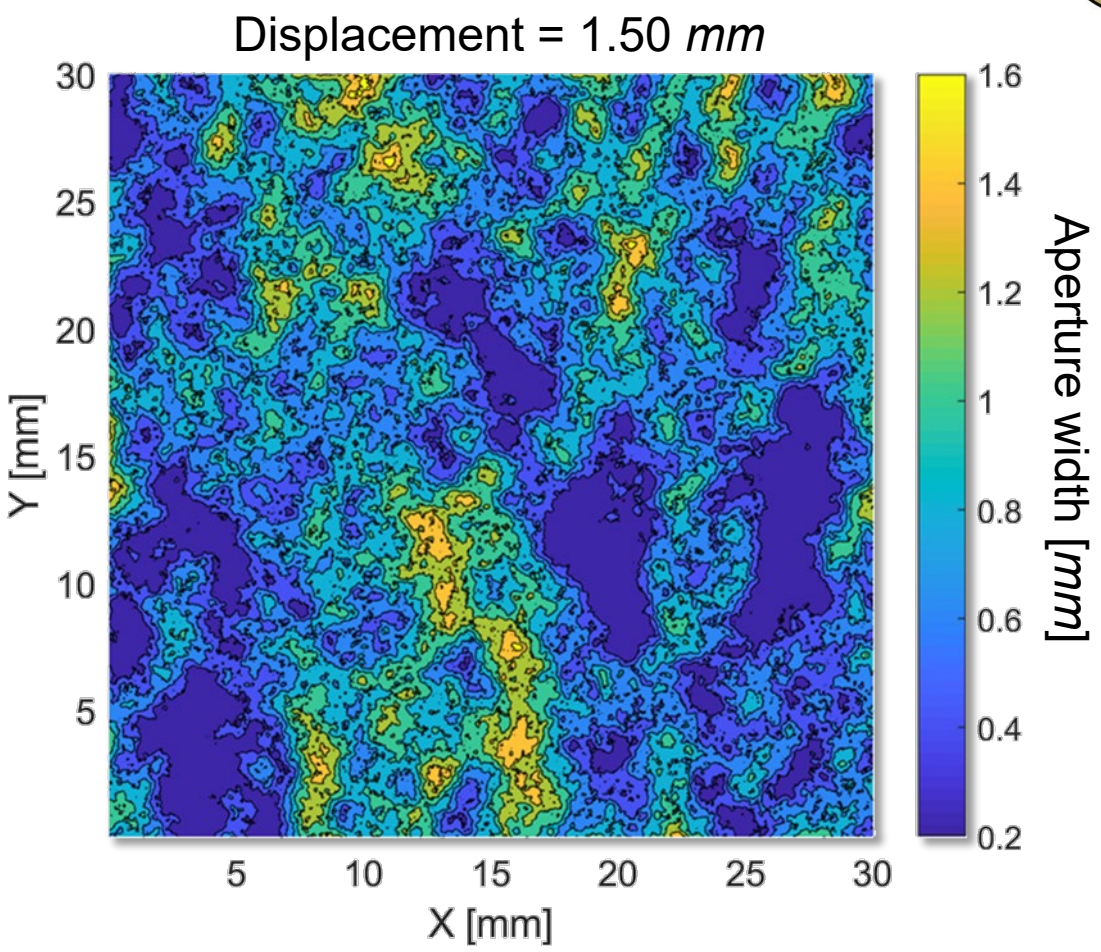

Figure. Aperture width as a function of shear slip.

I. Fracture Aperture Heterogeneity

- The most common model of fracture-scale flow approximates a constant aperture
- How might this aperture heterogeneity contribute to ***flow*** and ***heat transfer*** behaviors?

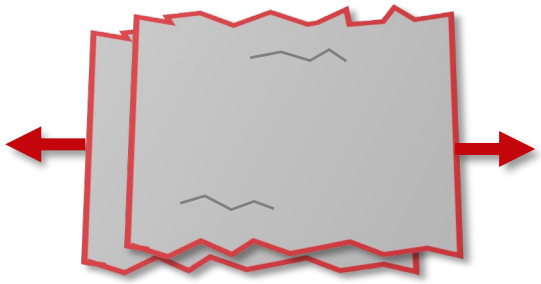

Fracture surfaces

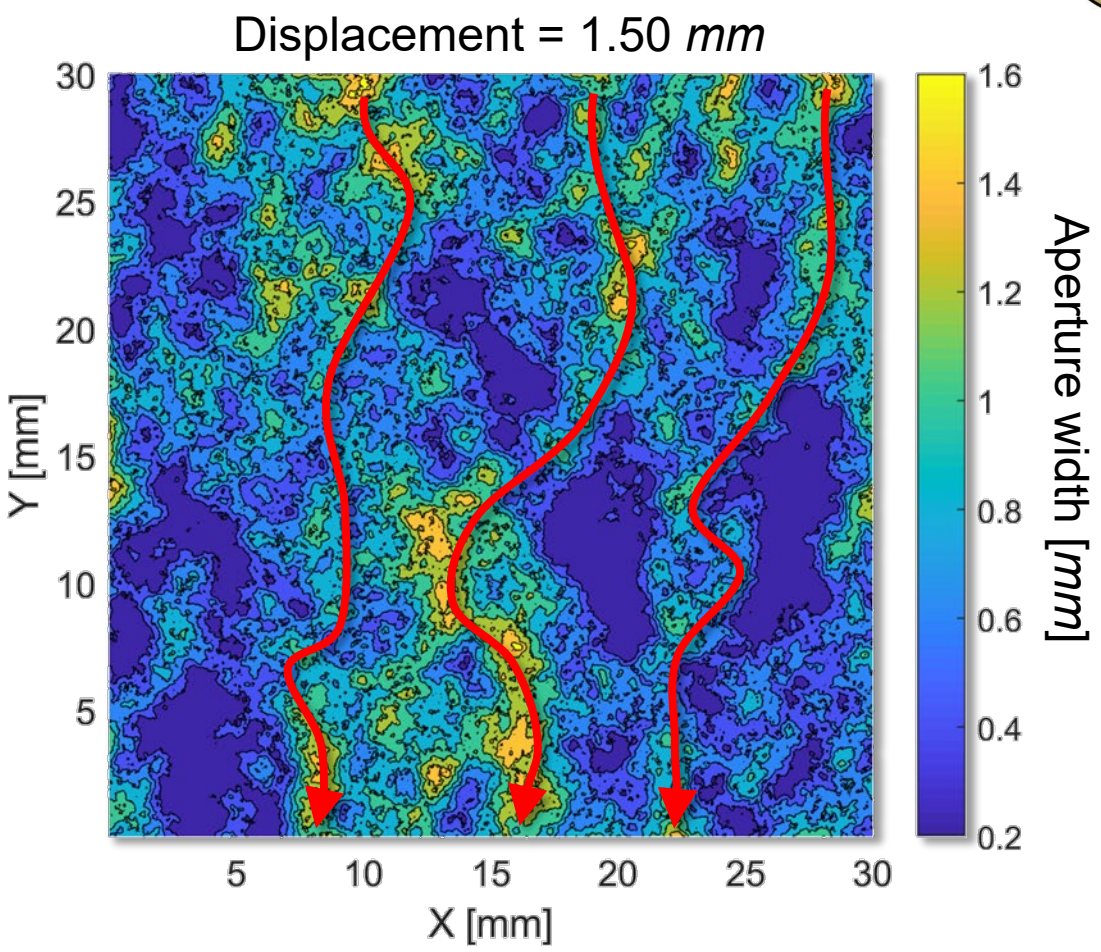

Figure. Aperture width as a function of shear slip.

I. Purpose & Scope

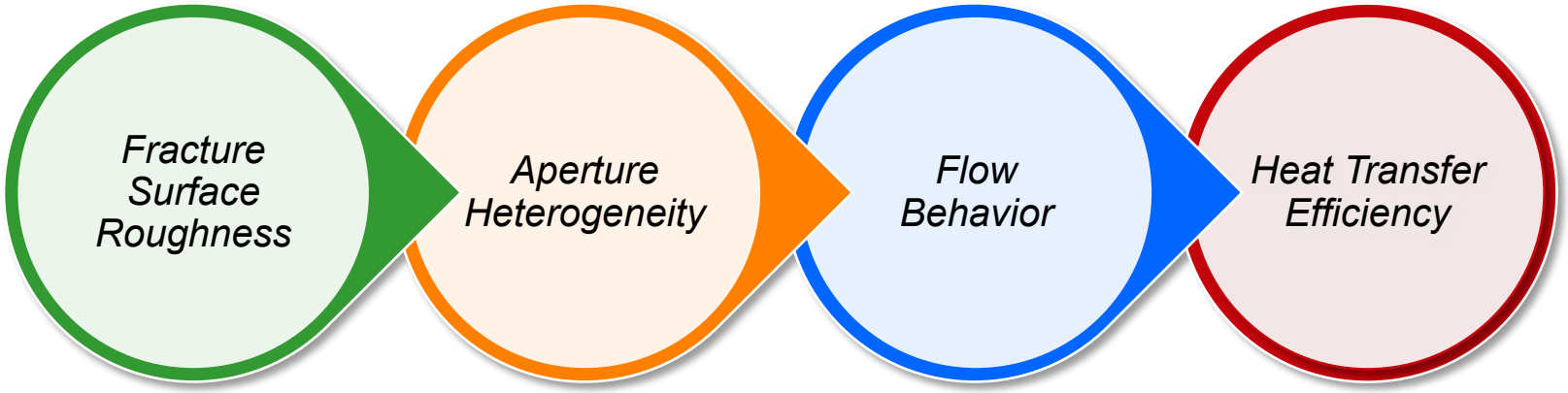

Purpose & Scope

Quantitatively assess the effect of [1]fracture surface roughness and [2]aperture heterogeneity, on [3]flow behaviors and [4]heat transfer efficiency within a single natural fracture geometry.

Overview

I. Introduction

   I. Background

   II. Purpose & scope

   III. Review of fracture surface characterization, flow, & heat transport

II. Methods

III. Flow Modeling

IV. Results & Discussion

V. Conclusions

I. Background: Fracture Roughness Measurement

How can fracture surface roughness be quantified?

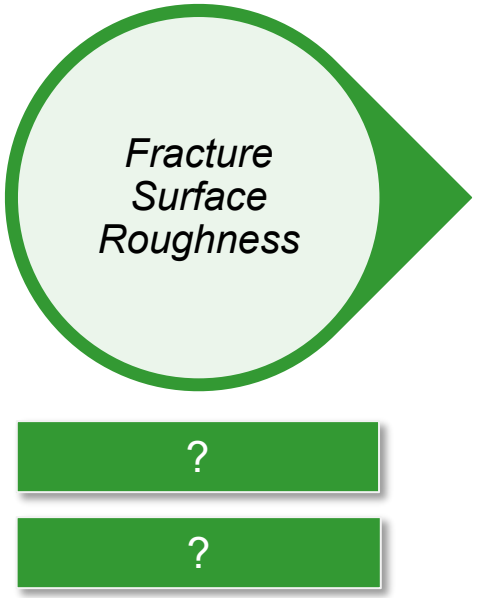

I. Fracture Surface Characterization

Components of fracture surface irregularity:

1. Waviness (long wavelength)

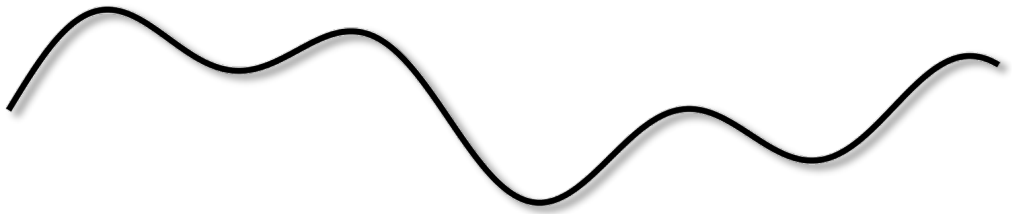

2. Roughness (short wavelength)

Surface (sum of components)

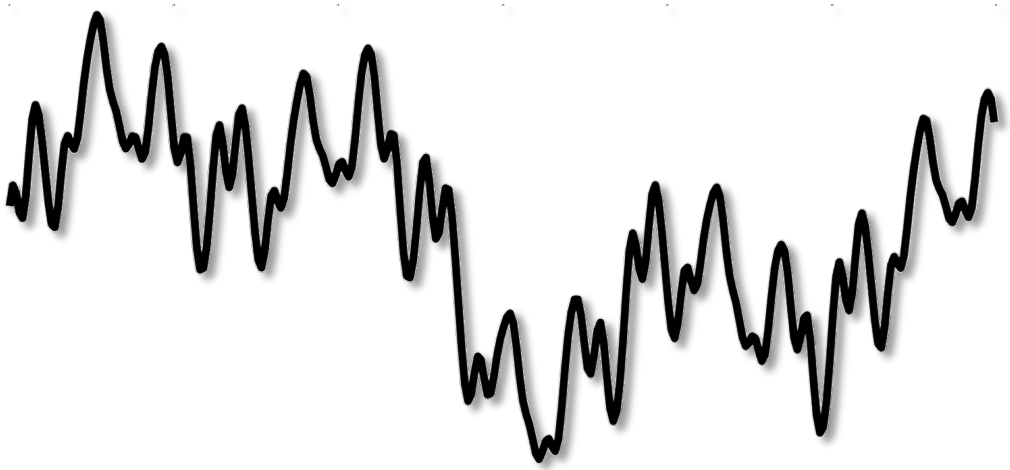

Figure. Conceptual fracture surface transect.

I. Surface Waviness Measurement via RMS Height

RMS height yields average waviness:

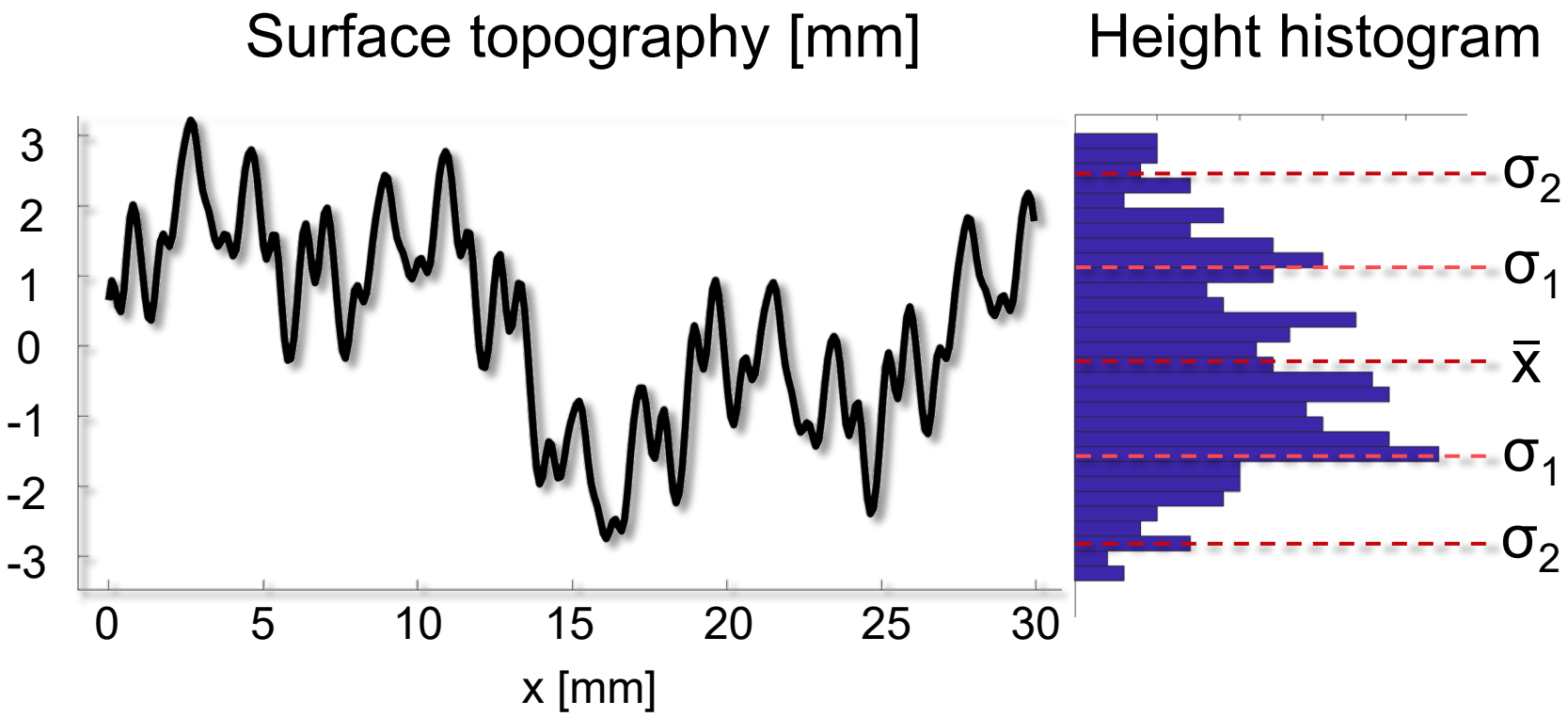

Figure. Conceptual fracture surface transect and height histogram.

σ = RMS height
= mean waviness
= 1.38 mm

I. Hurst Exponent (*H*) for Surface Roughness

Hurst exponent *H* used to quantify surface roughness

Values range from [0,1]:

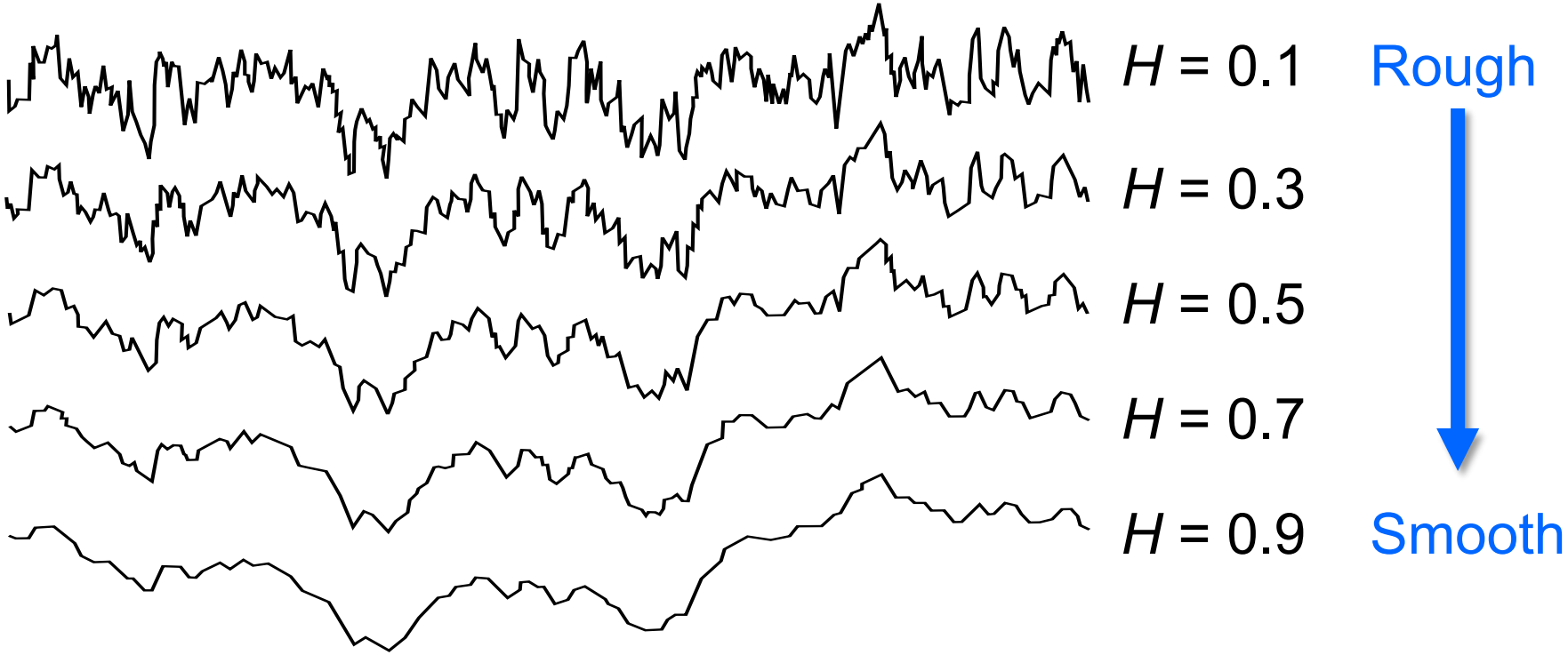

Figure. Surface profile with variable Hurst exponent (H).

I. Surface Roughness Estimation via Hurst Exponent

Hurst exponent is estimated via spectral methods:

Surface topography

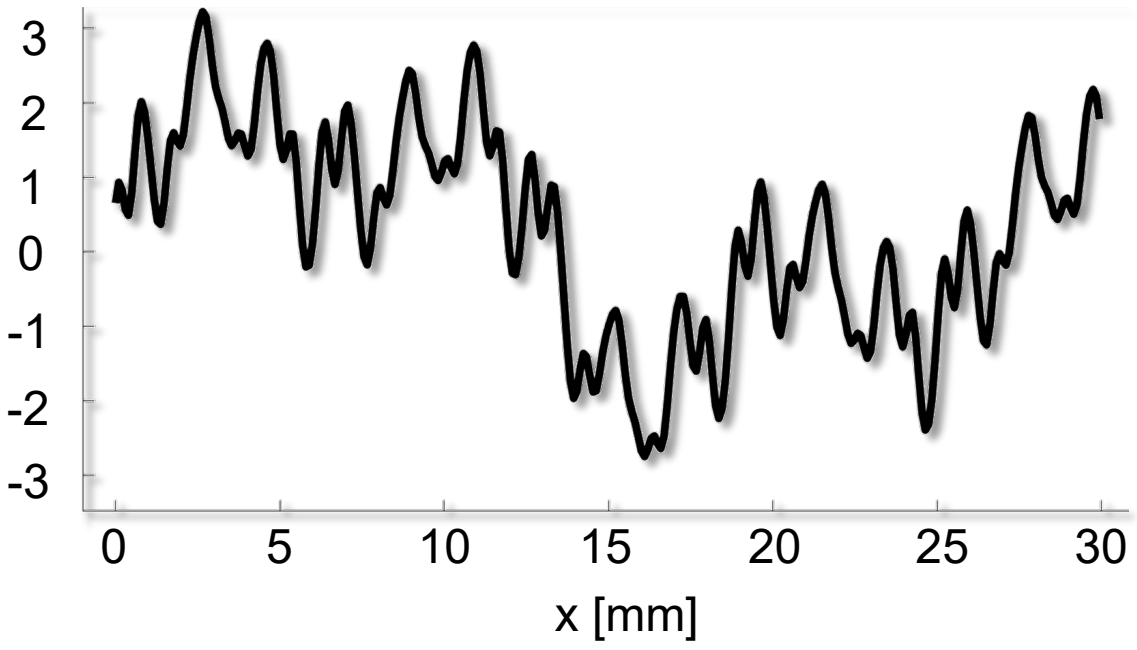

Fast Fourier Transform

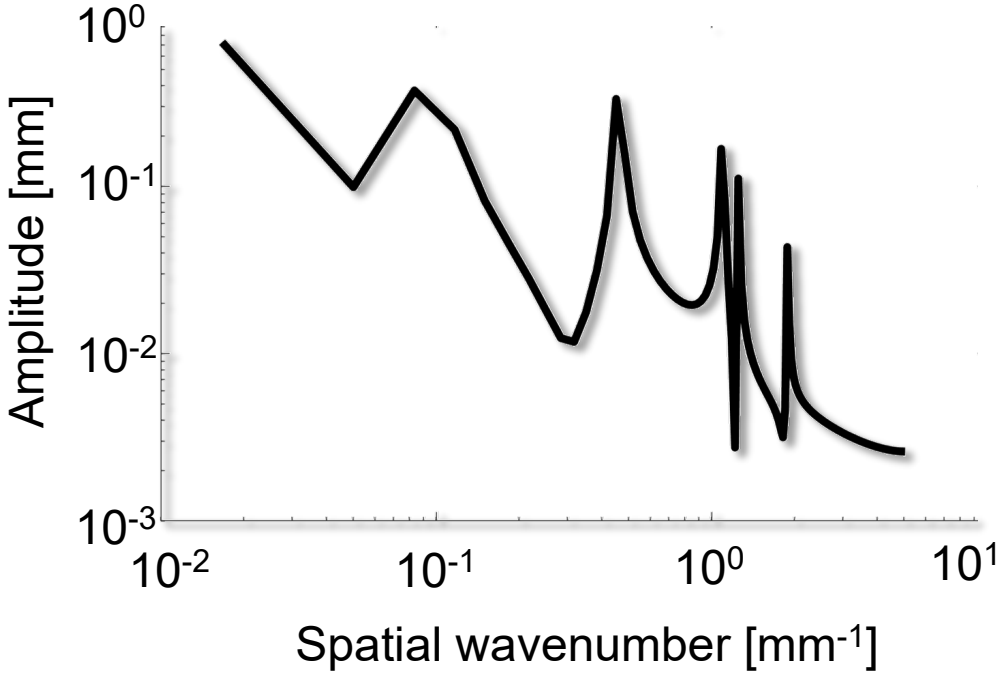

I. Surface Roughness Estimation via Hurst Exponent

Hurst exponent is estimated via spectral methods:

Surface topography

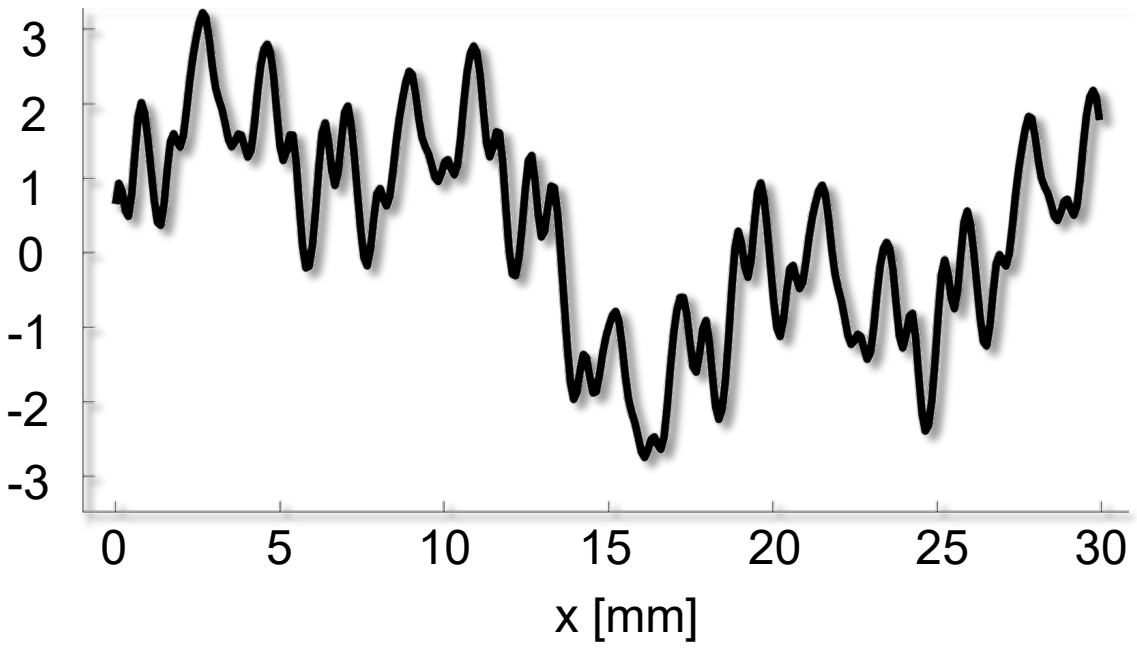

Power spectral density

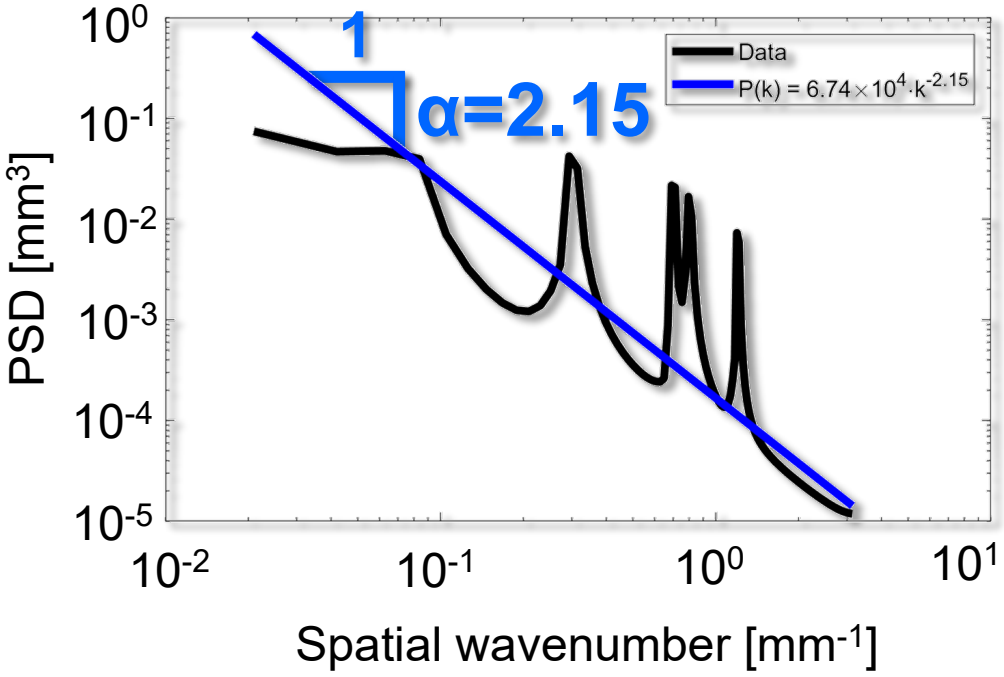

Hurst exponent = (α-1)/2 = 0.575

I. Background: Aperture Heterogeneity Characterization

How can we quantify aperture heterogeneity?

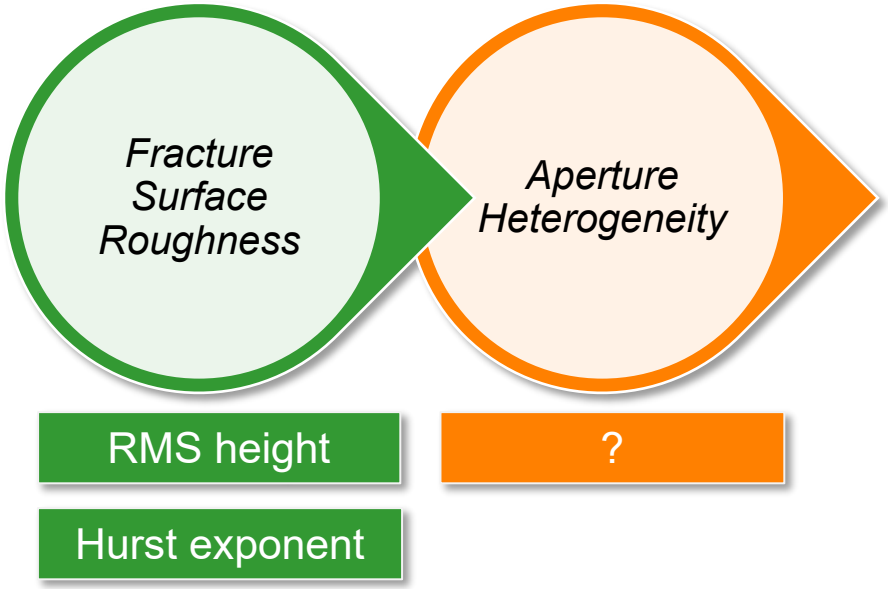

I. Aperture Heterogeneity Characterization

- Variogram function can be used to analyze trends in spatial variability of a dataset
- Correlation length: length of maximum spatial correlation

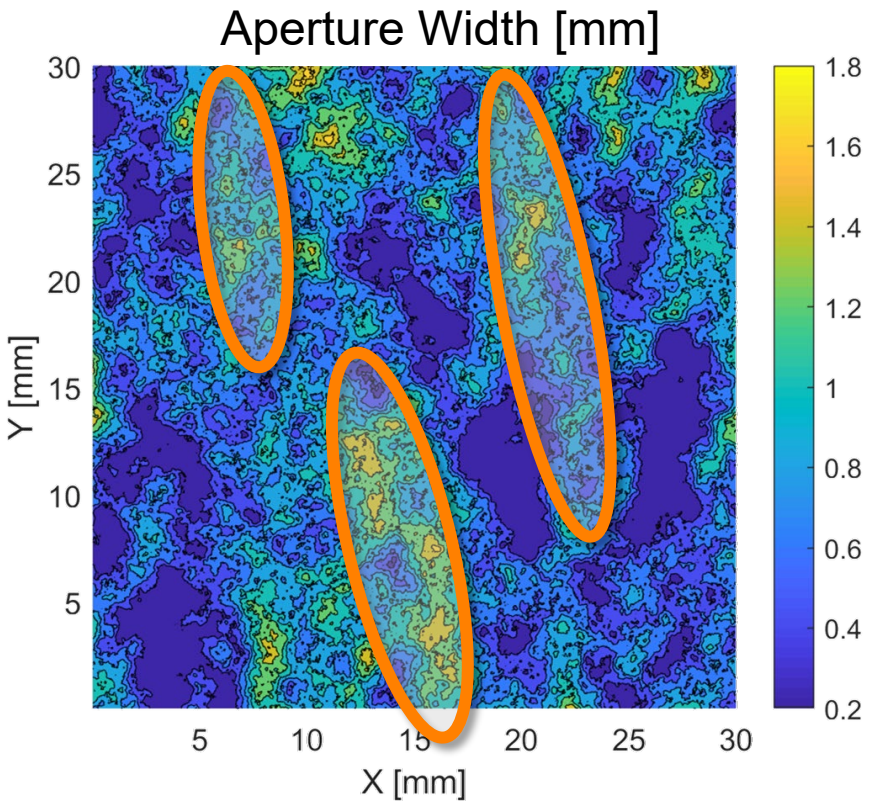

Figure. Aperture width distribution viewed perpendicular to the fracture plane.

I. Aperture Heterogeneity Characterization

- Variogram function can be used to analyze trends in spatial variability of a dataset
- Correlation length: length of maximum spatial correlation

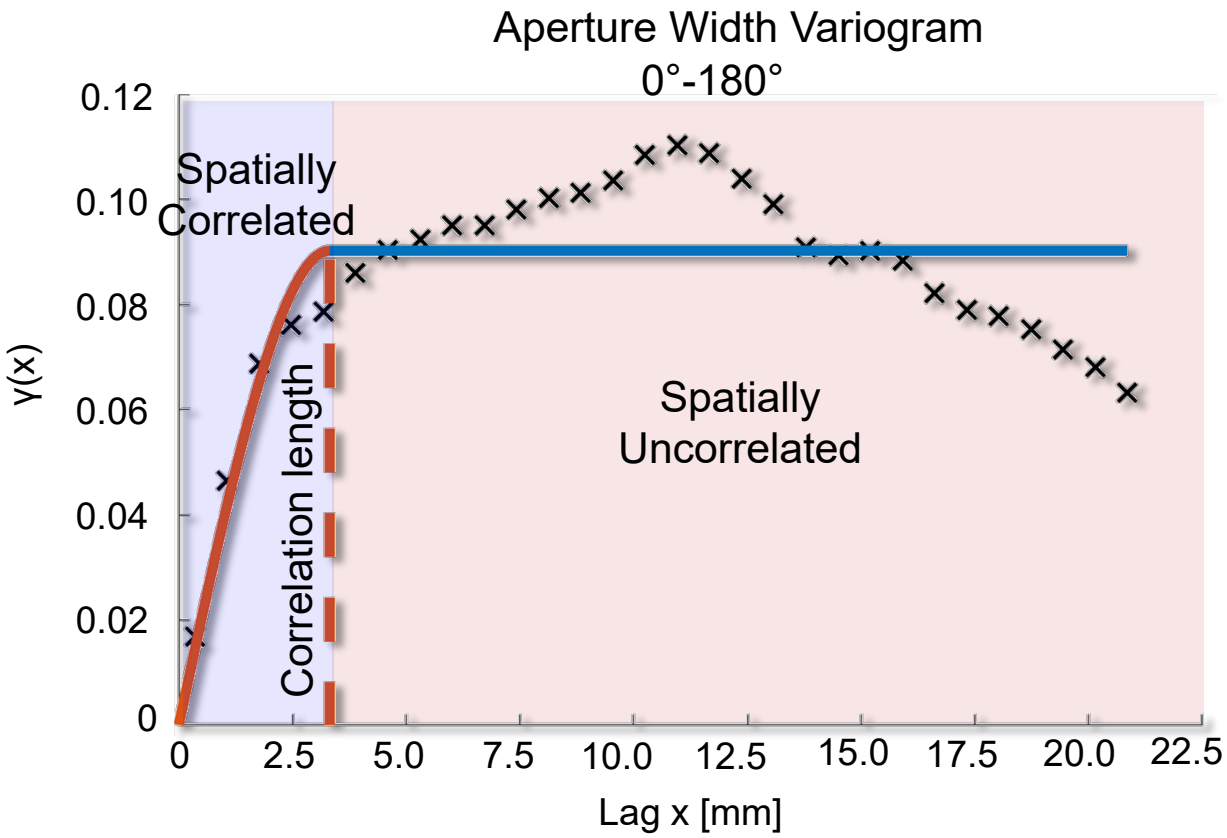

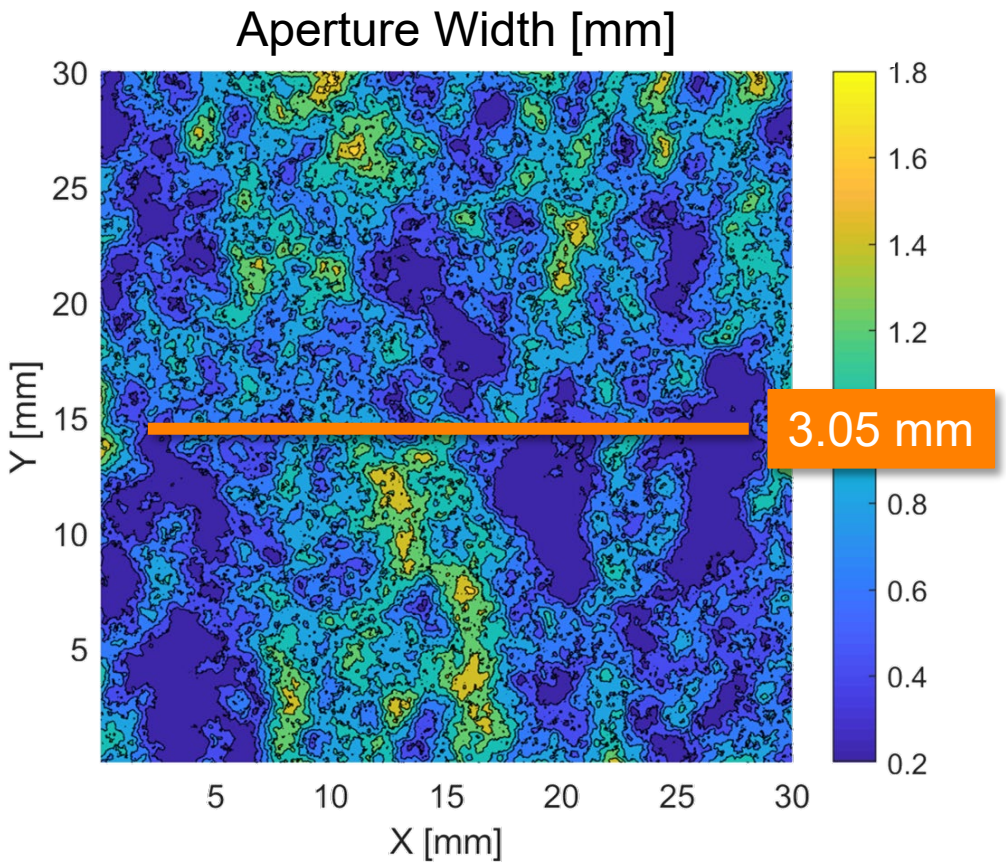

Figure. Aperture width distribution.

I. Aperture Heterogeneity Characterization

- Variogram function can be used to analyze trends in spatial variability of a dataset
- Correlation length: length of maximum spatial correlation

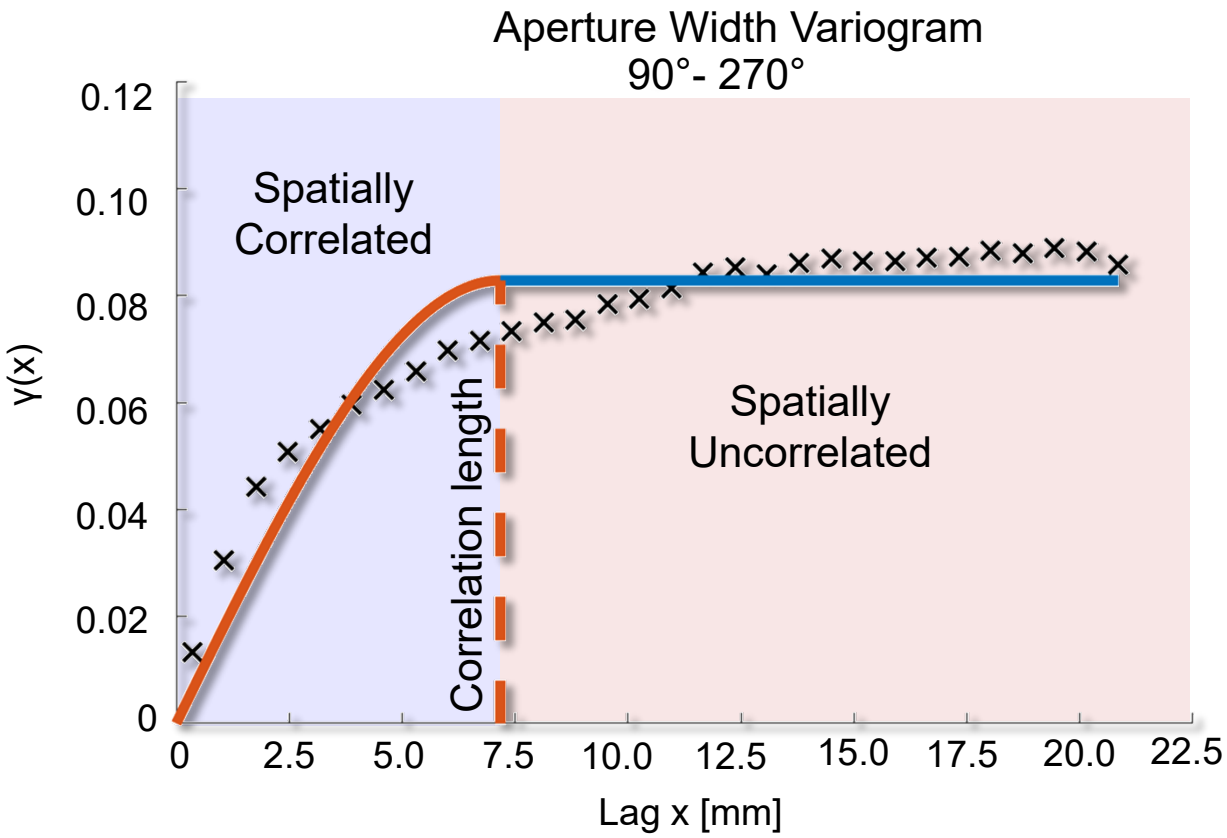

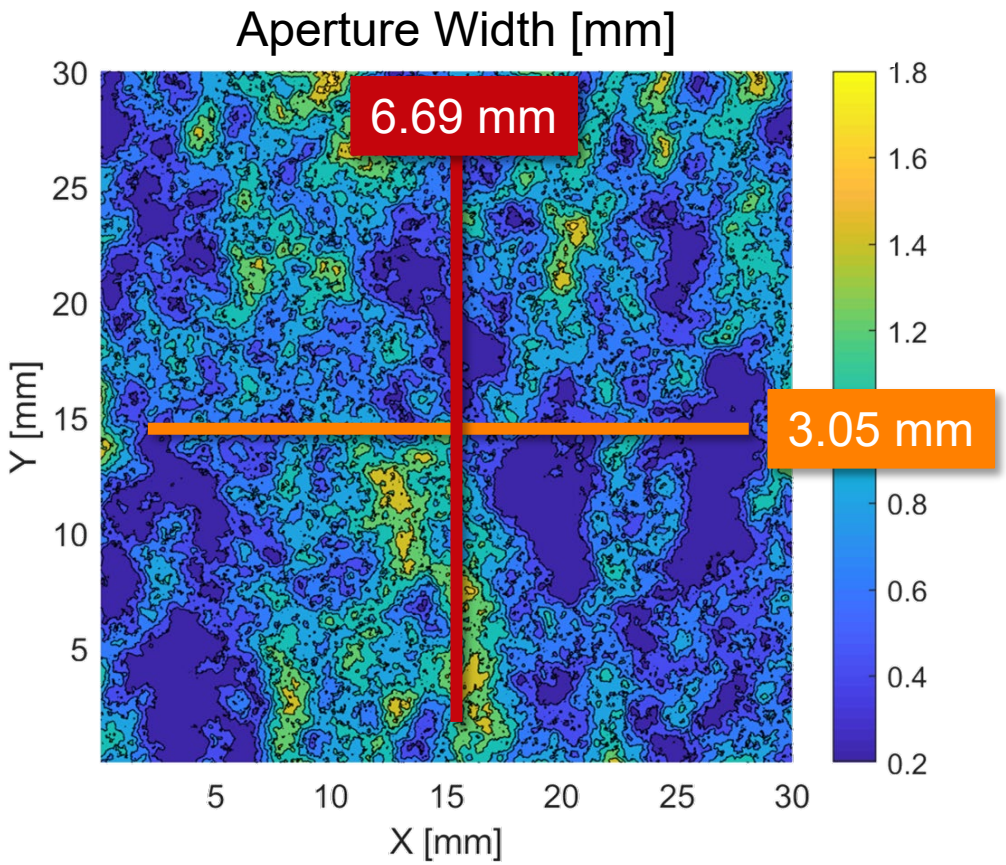

Figure. Aperture width distribution.

I. Background: Fracture Flow Processes

How does flow within fractures differ from parallel plate flow?

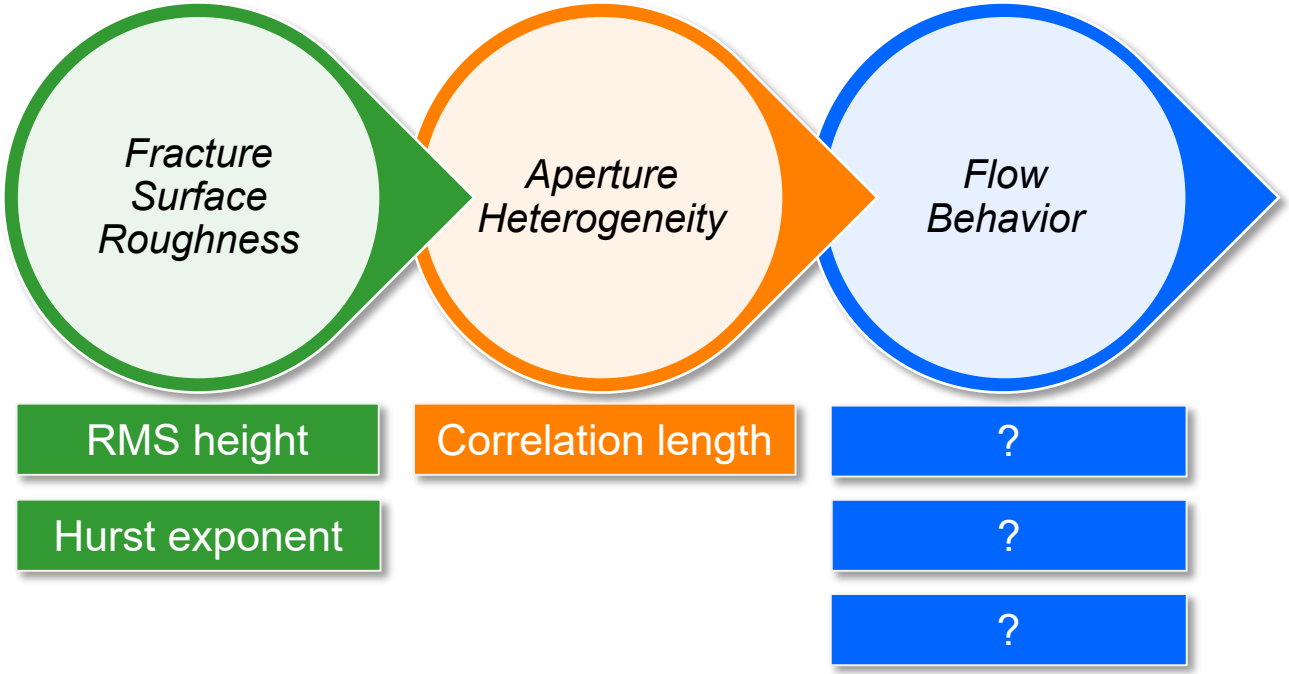

I. Deviations from Parallel Plate Flow in Natural Fractures

- Flow within natural fractures deviates from parallel plate flow in the following ways:

Channeling & Tortuosity | Directional dependence | Velocity ($\mathbf{u}$) variability

Parallel plate aperture

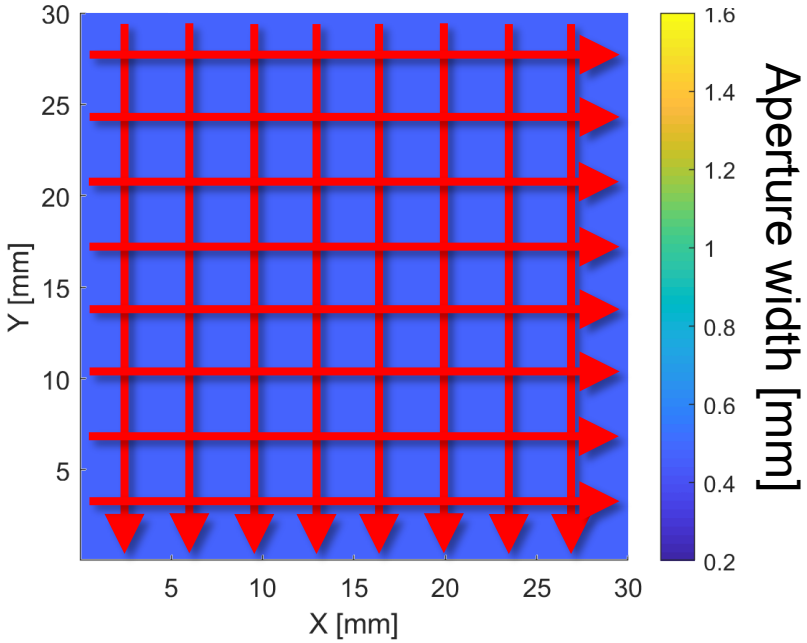

*Figure. Uniform flow behavior in a **parallel plate** aperture.*

Heterogeneous aperture

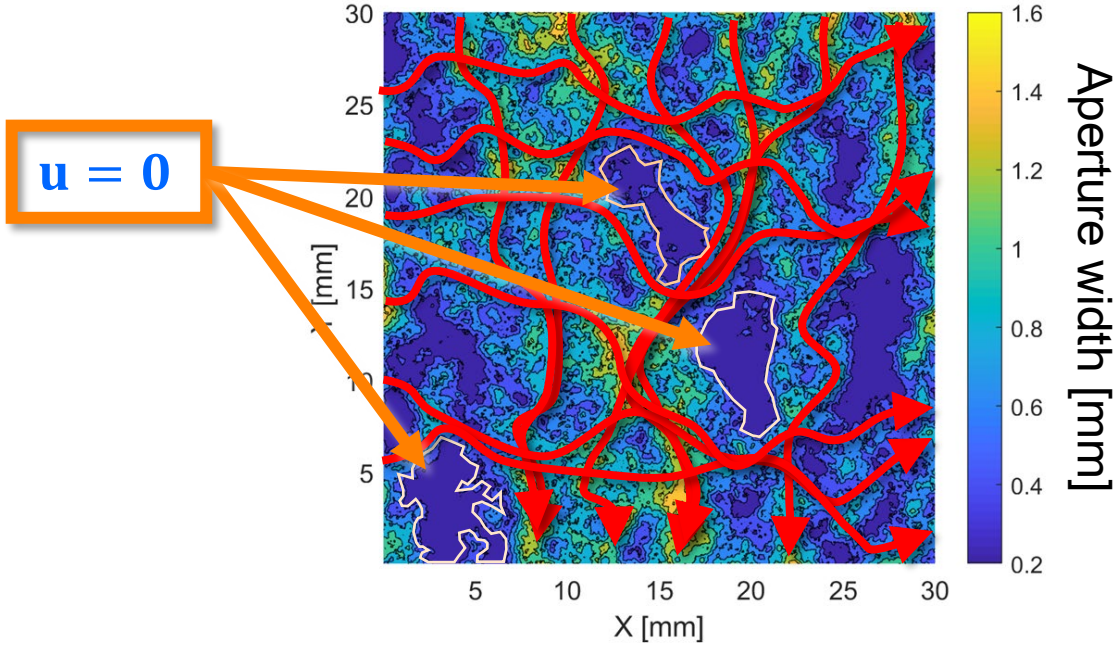

*Figure. Flow channeling behavior in a **heterogeneous** aperture.*

I. Background: Flow & Heat Exchange in Fractures

What are the relevant mechanisms for heat exchange in fractures?

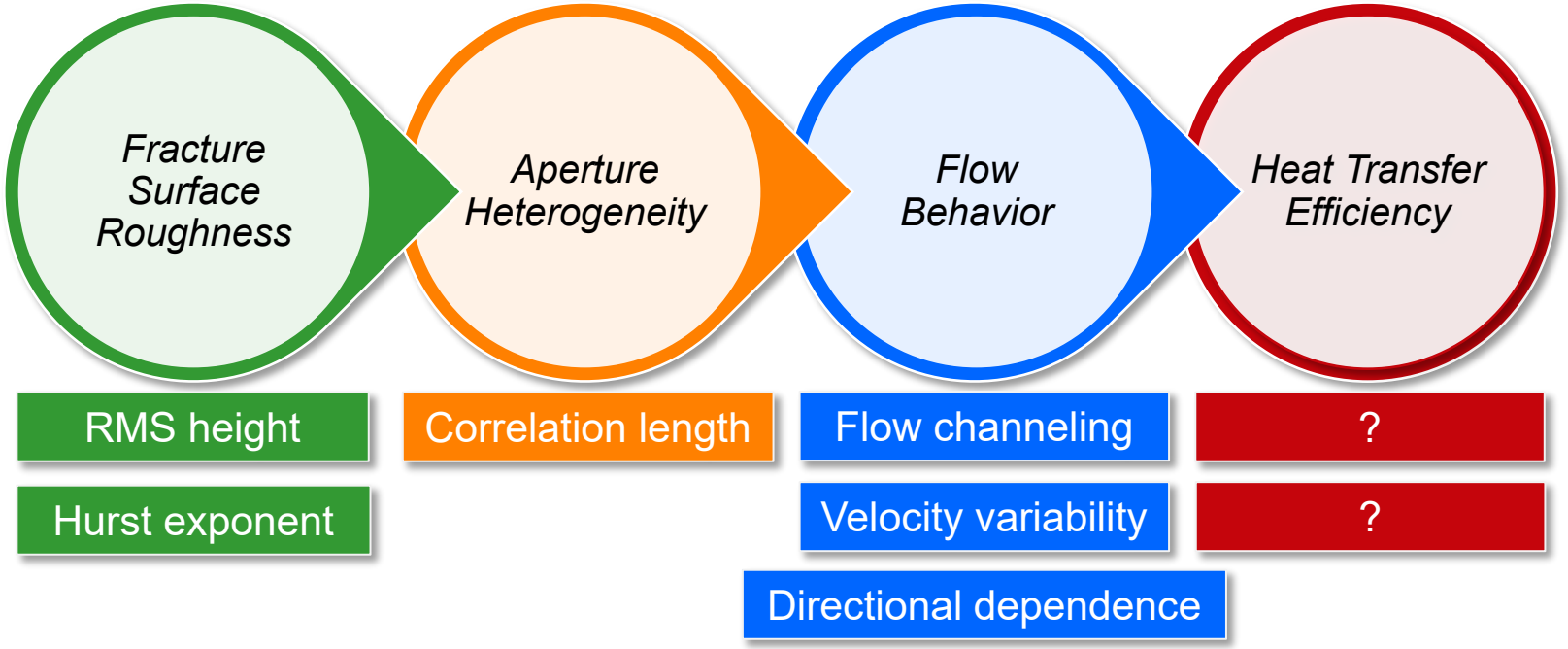

I. Background: Fracture Heat Exchange Mechanisms

- Mechanisms for heat transfer from fracture wall to outlet:

1. ***Diffusion***:

$$\mathbf{q} = -k\nabla T$$ (Fourier's law)

2. ***Advection***:

(**u**: fluid velocity)

$$\rho C_p \frac{\partial T}{\partial t} + \underbrace{\rho C_p \mathbf{u} \cdot \nabla T}_{\text{advection}} + \underbrace{\nabla \cdot \mathbf{q}}_{\text{diffusion}} = Q_{vd}$$

(heat advection-diffusion equation)

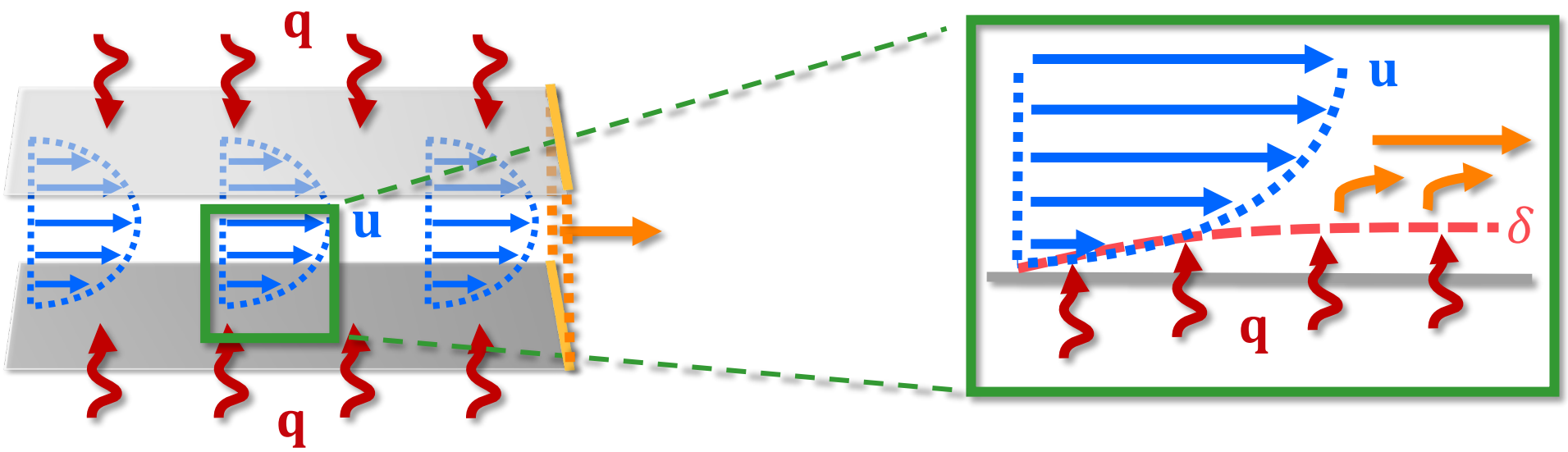

Figure. Parallel plate flow & heat exchange

Figure. Diffusive & advective heat flux

I. Background: Heat Exchange & Flow Channeling

- **Heat transfer q** to the fluid is **maximized** when the flow is **uniformly spread**.
- Aperture heterogeneity induces flow channeling **reducing heat transfer**.

Homogeneous aperture

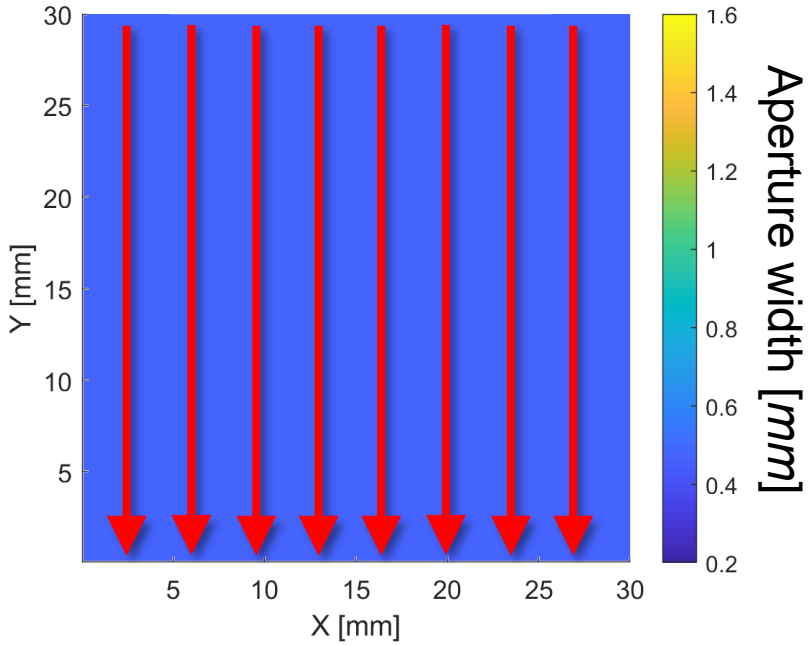

$q_{HOM} > q_{HET}$

Heterogeneous aperture

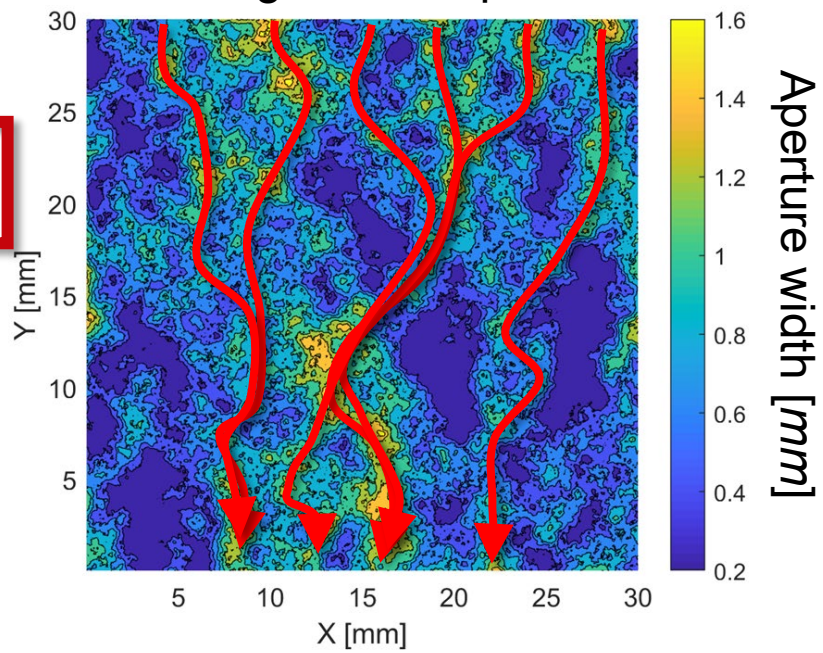

*Figure. Uniform flow behavior in a **homogeneous** aperture.*

*Figure. Flow channeling behavior in a **heterogeneous** aperture.*

I. Hypothesis: Linking the Hierarchy of Processes

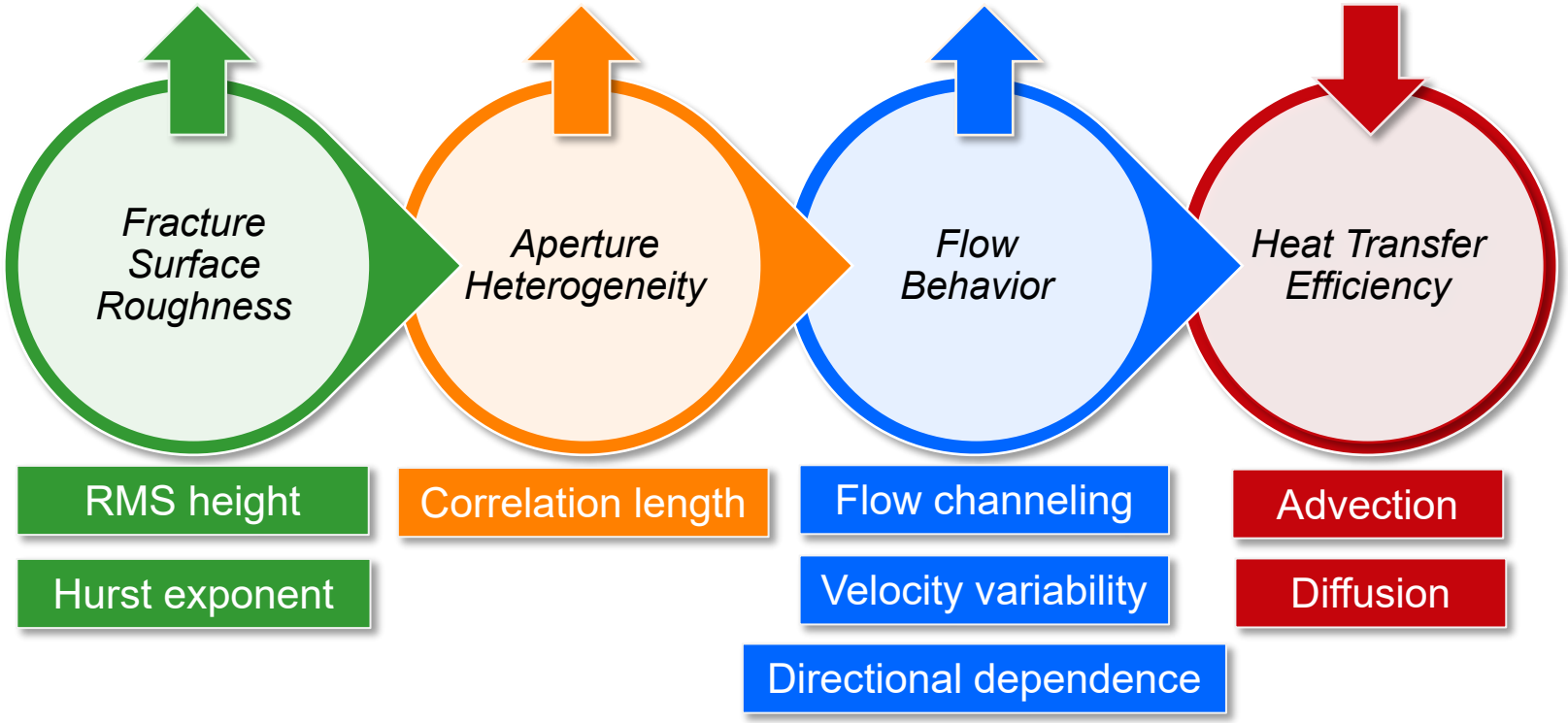

Hypothesis

Within a single fracture, increased fracture surface roughness increases aperture heterogeneity, thereby increasing flow channeling and velocity variability.

Overall heat transfer efficiency declines as a result.

Overview

I. Introduction

II. Methods

III. Flow Modeling

IV. Results & Discussion

V. Conclusions

Overview

I. Introduction

II. Methods

   I. Experimental design
   II. Fracture surface acquisition for model input
   III. Aperture composition & analysis

III. Flow Modeling

IV. Results & Discussion

V. Conclusions

II. Experimental Design: Fracture Roughness

Numerical flow modeling approach used to address hypothesis:

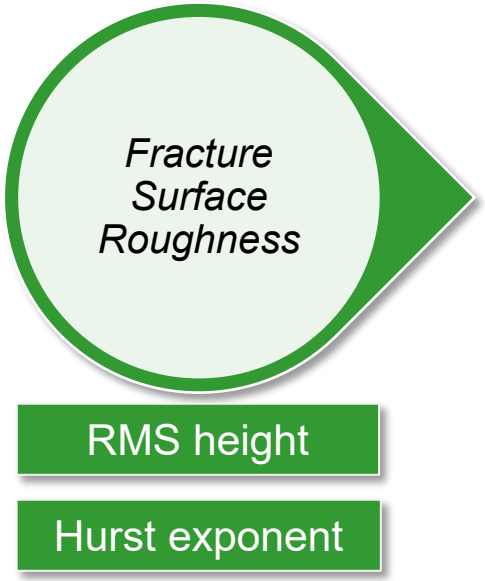

Variable fracture surface roughness' used to make apertures:

1. Natural granite surface

From natural granite measured **RMS height** & **Hurst exponent**:

2. Synthetic granite surface
3. Synthetic extra rough granite surface

II. Experimental Design: Aperture Heterogeneity

To capture the effects of aperture heterogeneity:

Aperture Heterogeneity

Correlation length

Half of model apertures made with surface shear-displacement.

Correlation length of aperture width measured in all directions.

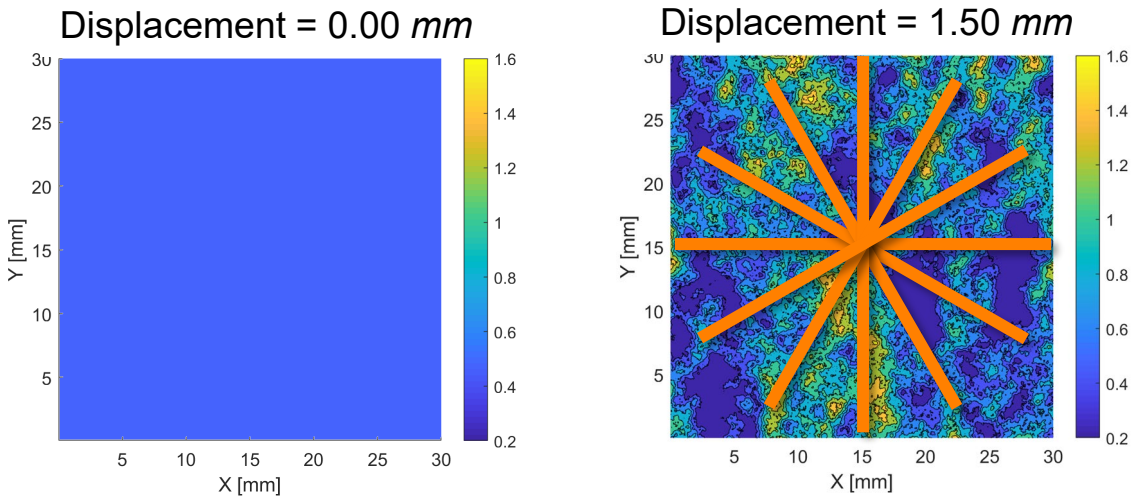

Figures. Homogeneous (left) and heterogeneous (right) aperture width distribution.

II. Experimental Design: Flow

To capture the variability of fracture flow behaviors:

Flow Behavior

- Flow channeling
- Velocity variability
- Directional dependence

Use of Stokes flow solution captures **flow channeling** & **velocity variance**

Directional dependence sampled via flow modeling in X & Y directions

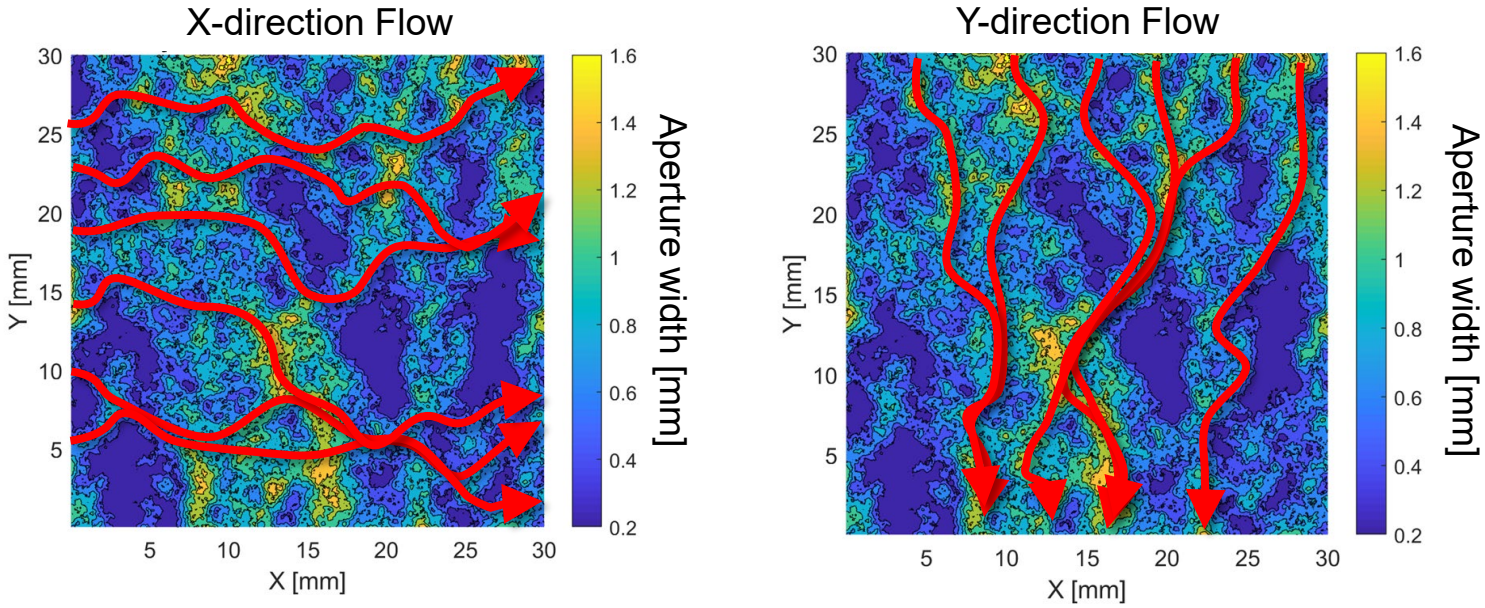

Figures. X-direction (left) and Y-direction (right) flow through a heterogeneous aperture.

II. Experimental Design: Heat Exchange

To quantify the resulting heat transfer efficiency:

Heat Transfer Efficiency

Advection

Diffusion

Advection calculated by coupling flow solution to heat transport equation.

Diffusive heat flow measured at fracture surface.

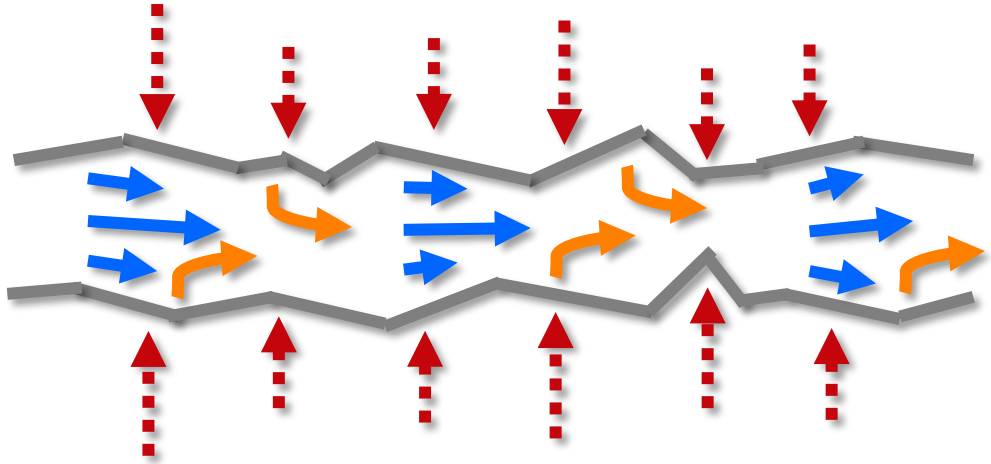

Figure. Conceptual fracture cross section illustrating diffusion and advection processes.

Overview

I. Introduction

II. Methods

   I. Experimental design

   II. Fracture surface acquisition for model input

   III. Aperture composition & analysis

III. Flow Modeling

IV. Results & Discussion

V. Conclusions

II. Natural Fracture Surface Acquisition

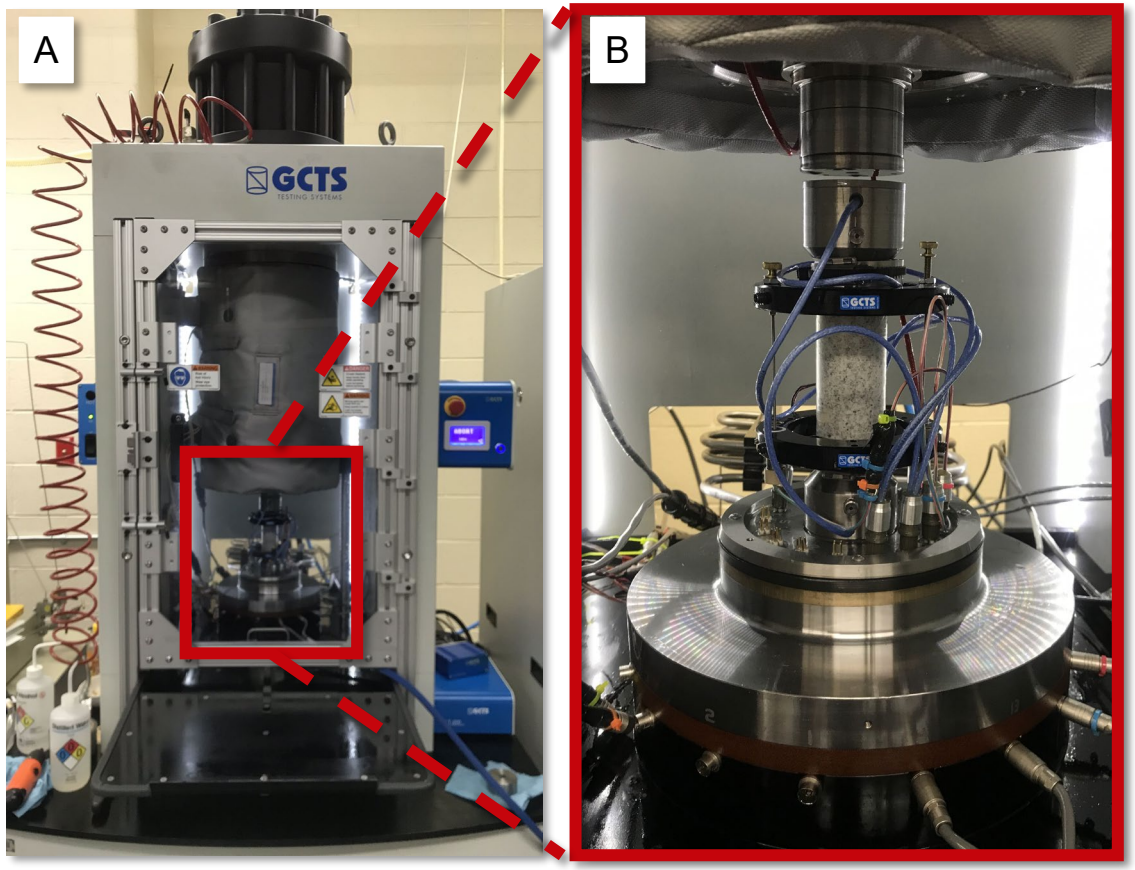

Figure. GCTS RTR-1000 Triaxial experimentation.

Figure. Fractured sample.

II. Natural Fracture Surface Acquisition

- Sample fracture surfaces scanned via white light interferometry (WLI)
- Surface denoised and outliers removed
- High resolution scan output: 10 µm X-Y spatial resolution

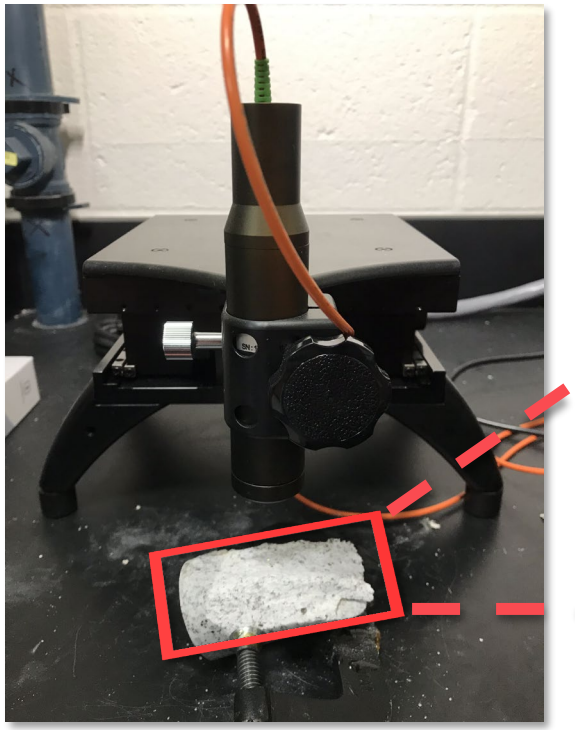

Figure. Fracture surface scan via Nanovea® JR-25 WLI.

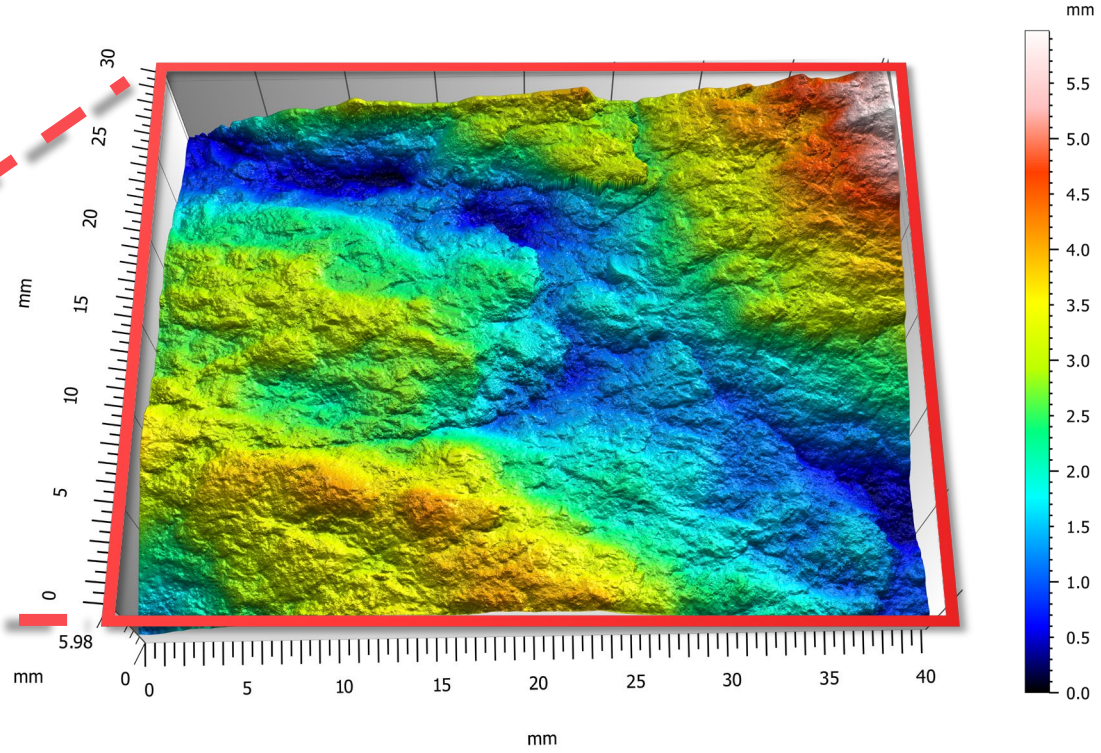

Figure. Fracture surface scan following denoising operations (MountainsMap® 7.4).

II. Natural Surface Roughness Measurement

RMS height (*Rq*) → waviness measurement

$$R_q = \sqrt{\frac{1}{n}\sum_{i=1}^{n} z(x_i)^2} \approx 1.1\ mm$$

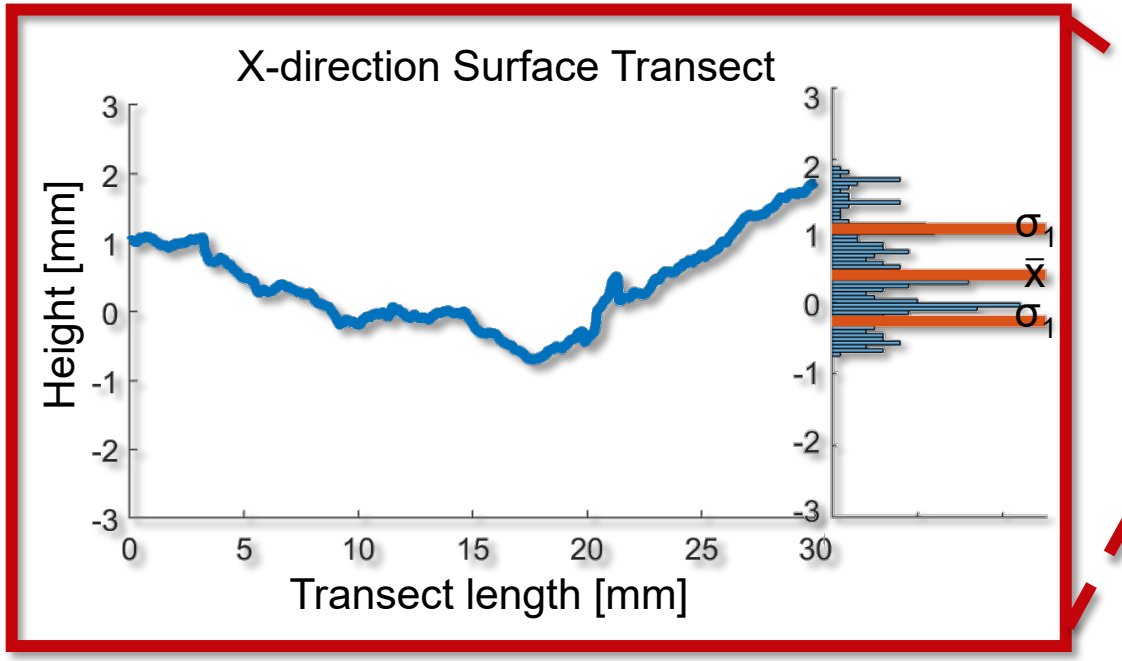

Figure. 1-D RMS roughness calculation.

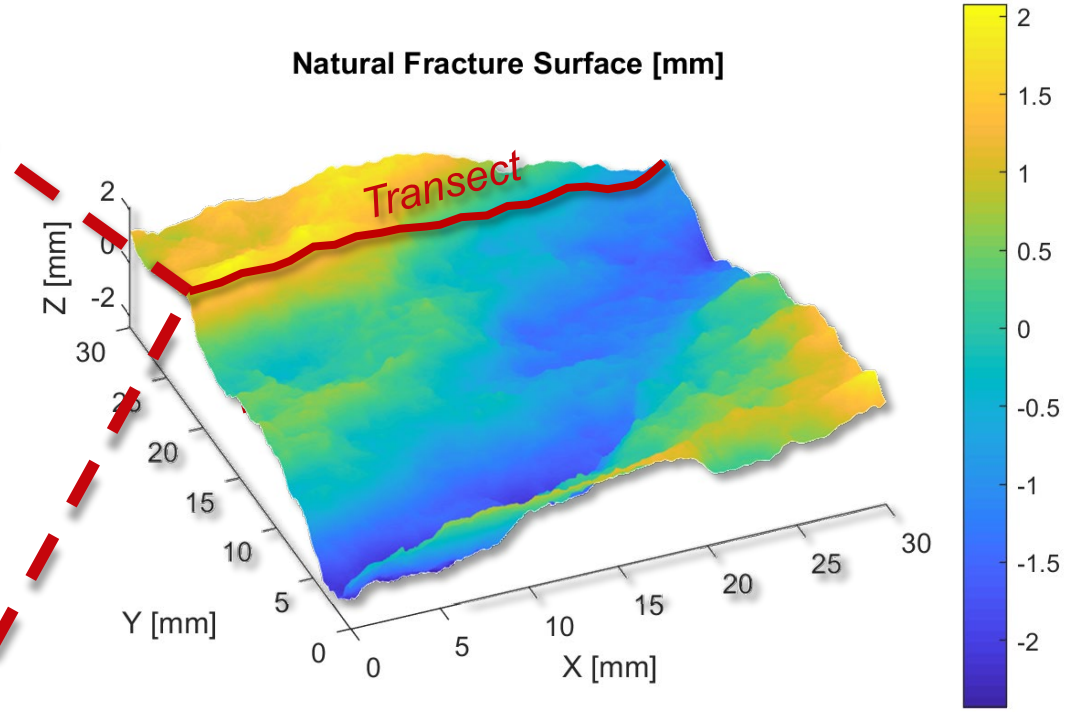

Figure. Fracture surface from WLI scan with selected transect.

II. Natural Surface Roughness Measurement

RMS height (*Rq*) → waviness measurement

$$R_q = \sqrt{\frac{1}{n}\sum_{i=1}^{n} z(x_i)^2} \approx 1.1\ mm$$

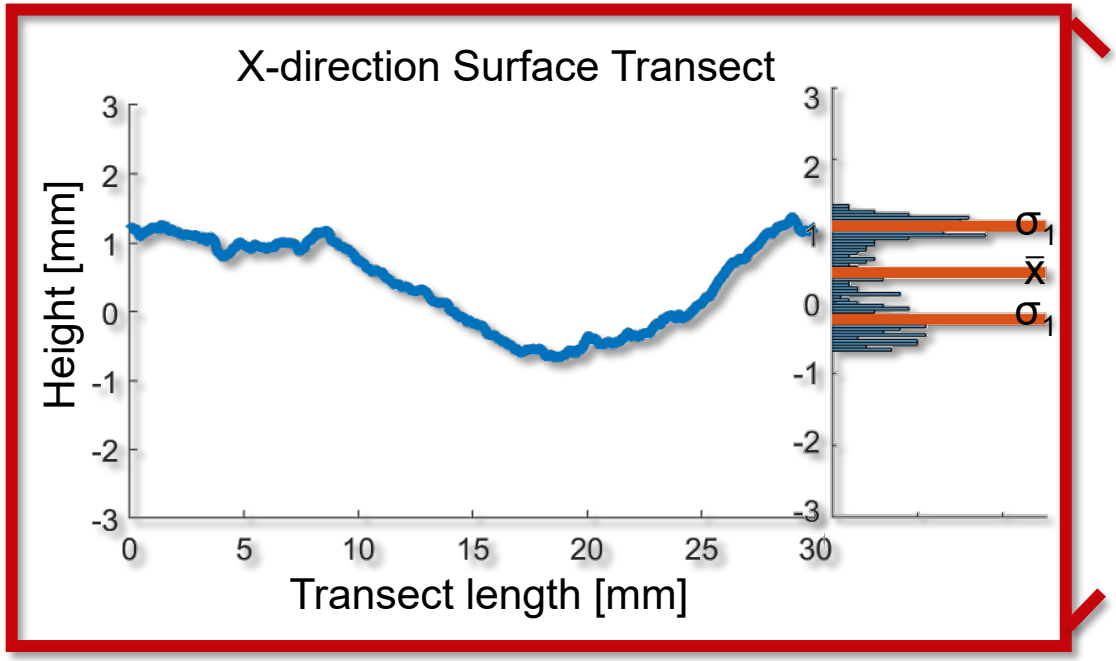

Figure. 1-D RMS roughness calculation.

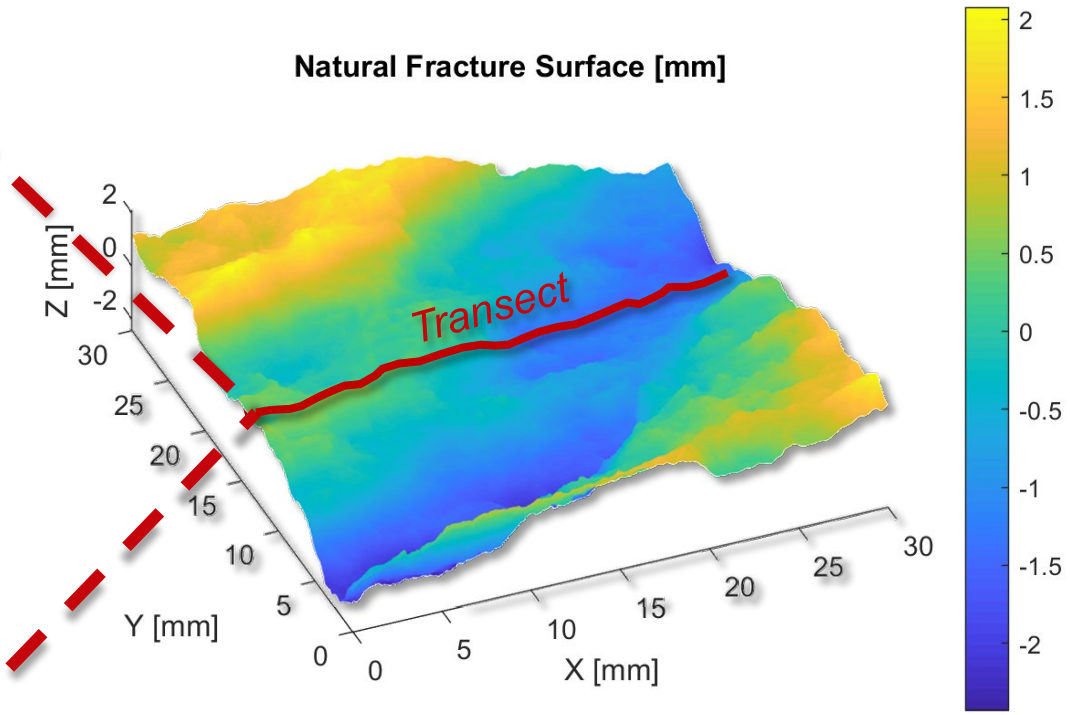

Figure. Fracture surface from WLI scan with selected transect.

II. Natural Surface Roughness Measurement

RMS height (*Rq*) → waviness measurement

$$R_q = \sqrt{\frac{1}{n}\sum_{i=1}^{n} z(x_i)^2} \approx 1.1\ mm$$

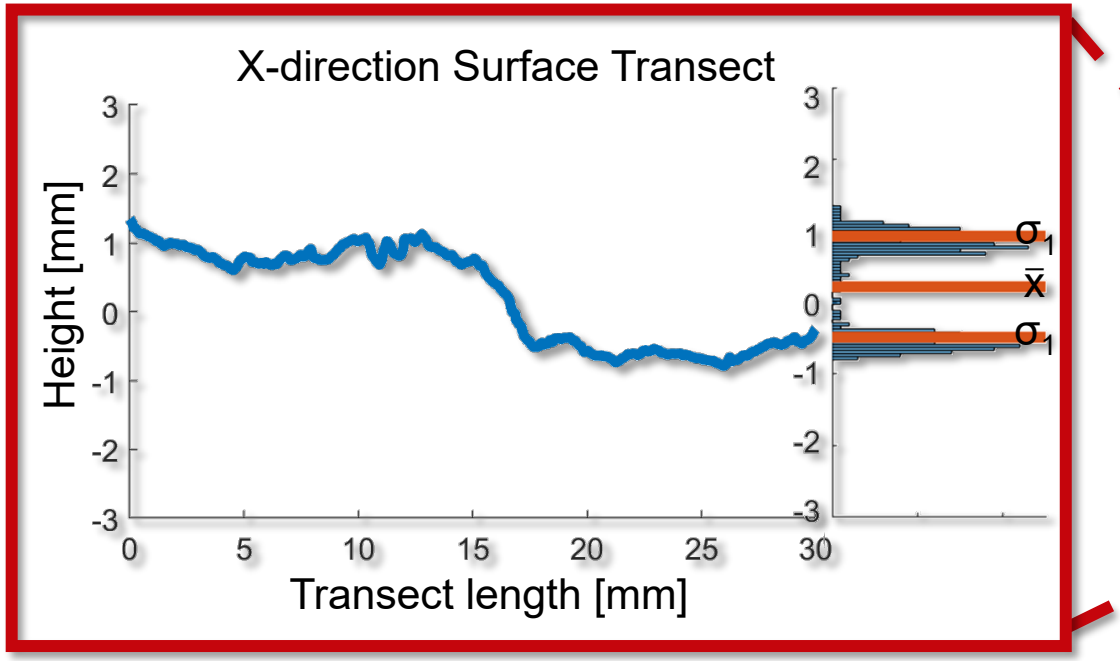

Figure. 1-D RMS roughness calculation.

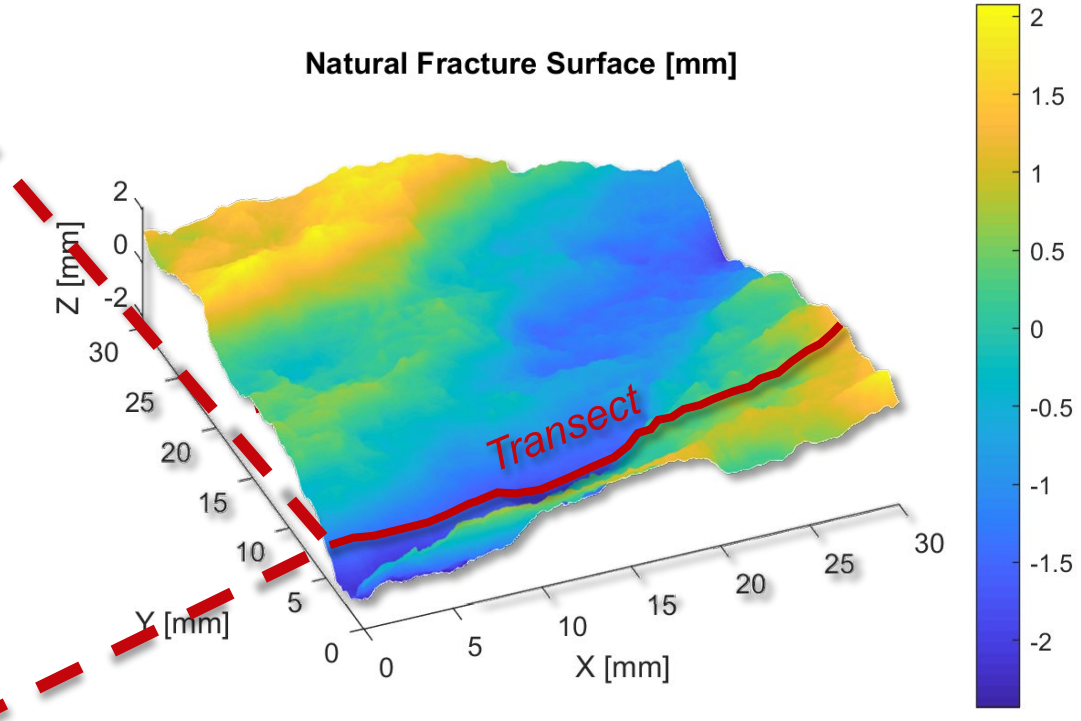

Figure. Fracture surface from WLI scan with selected transect.

II. Natural Surface Roughness Measurement

RMS height (*Rq*) → waviness measurement

$$R_q = \sqrt{\frac{1}{n}\sum_{i=1}^{n} z(x_i)^2} \approx 1.1\ mm$$

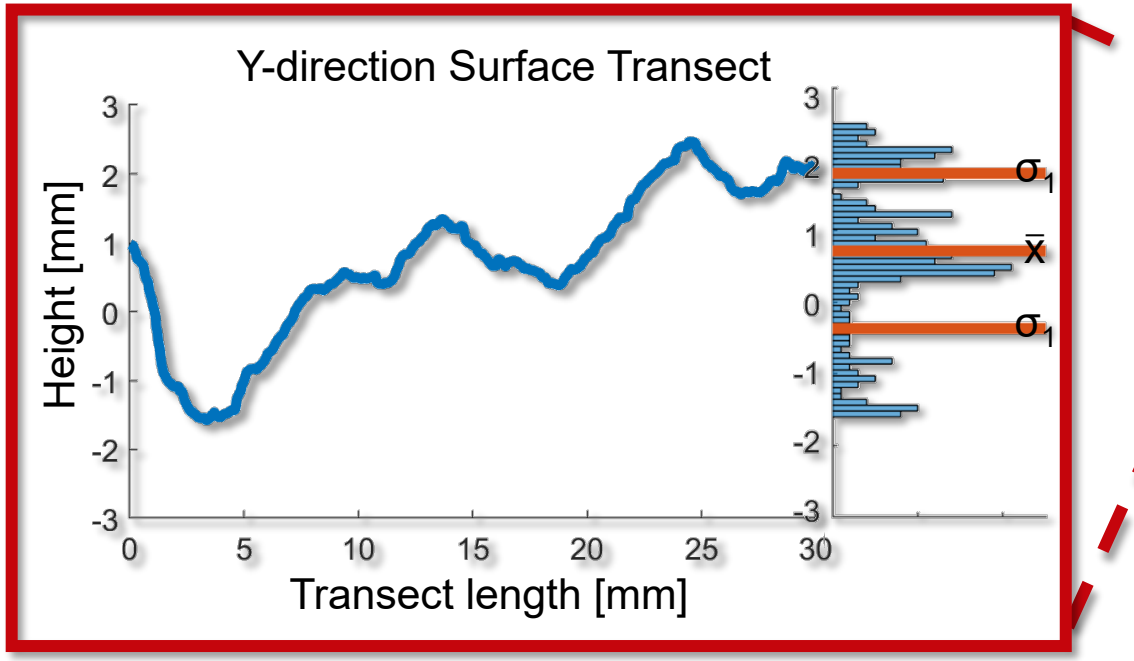

Figure. 1-D RMS roughness calculation.

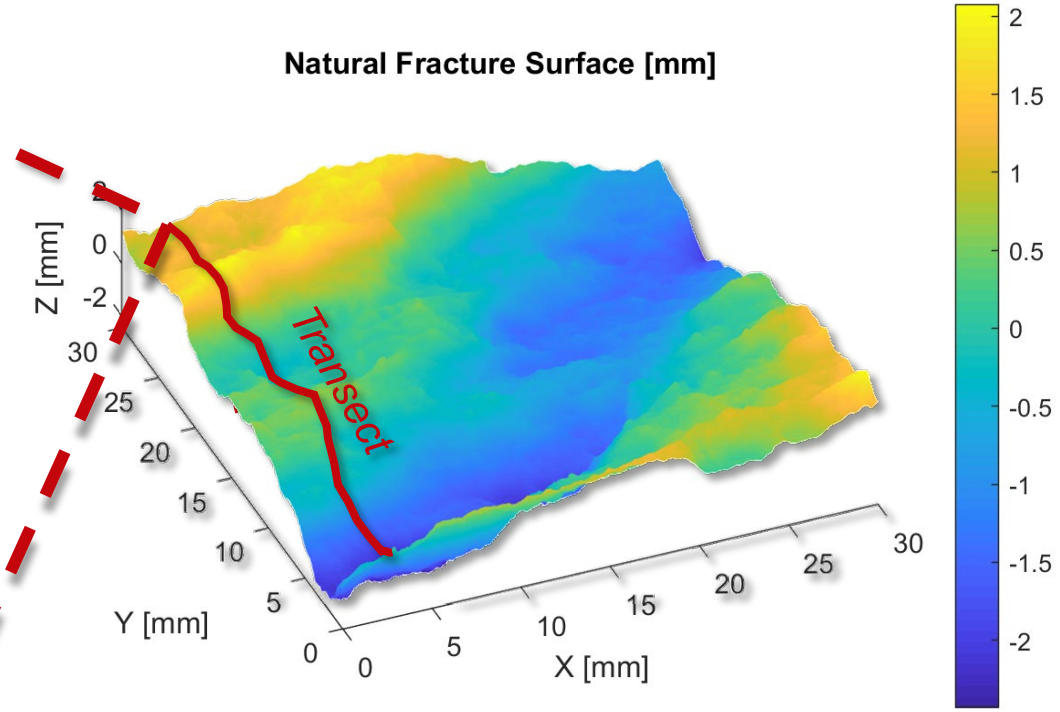

Figure. Fracture surface from WLI scan with selected transect.

II. Natural Surface Roughness Measurement

RMS height (*Rq*) → waviness measurement

$$R_q = \sqrt{\frac{1}{n}\sum_{i=1}^{n} z(x_i)^2} \approx 1.1\ mm$$

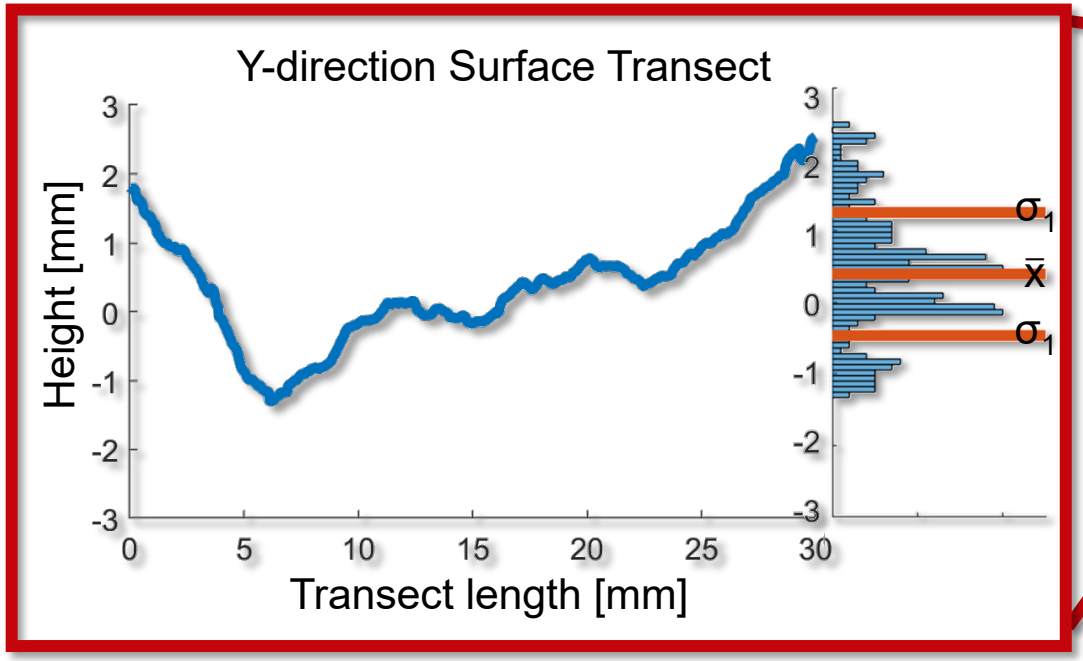

Figure. 1-D RMS roughness calculation.

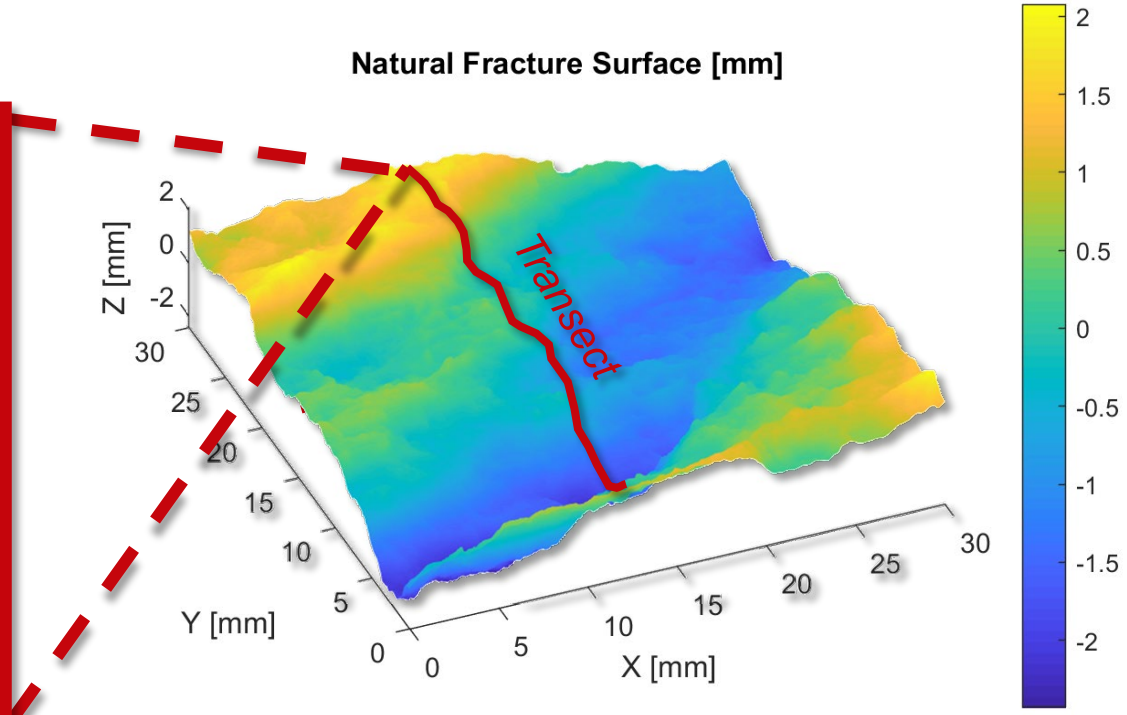

Figure. Fracture surface from WLI scan with selected transect.

II. Natural Surface Roughness Measurement

RMS height (*Rq*) → waviness measurement

$$R_q = \sqrt{\frac{1}{n}\sum_{i=1}^{n} z(x_i)^2} \approx 1.1\ mm$$

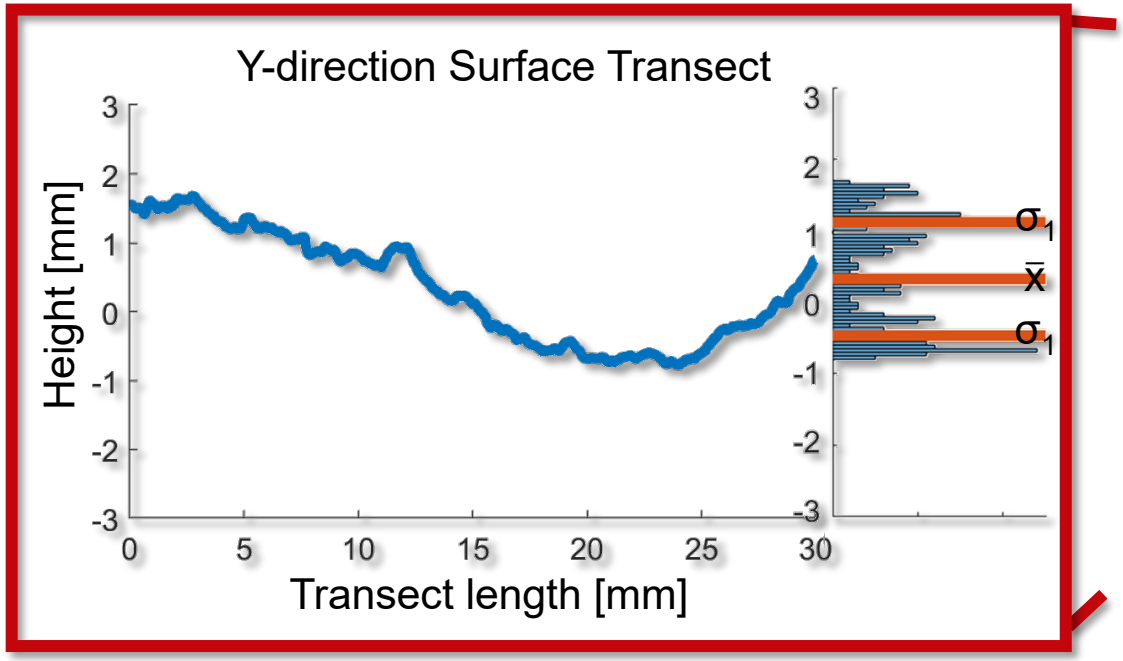

Figure. 1-D RMS roughness calculation.

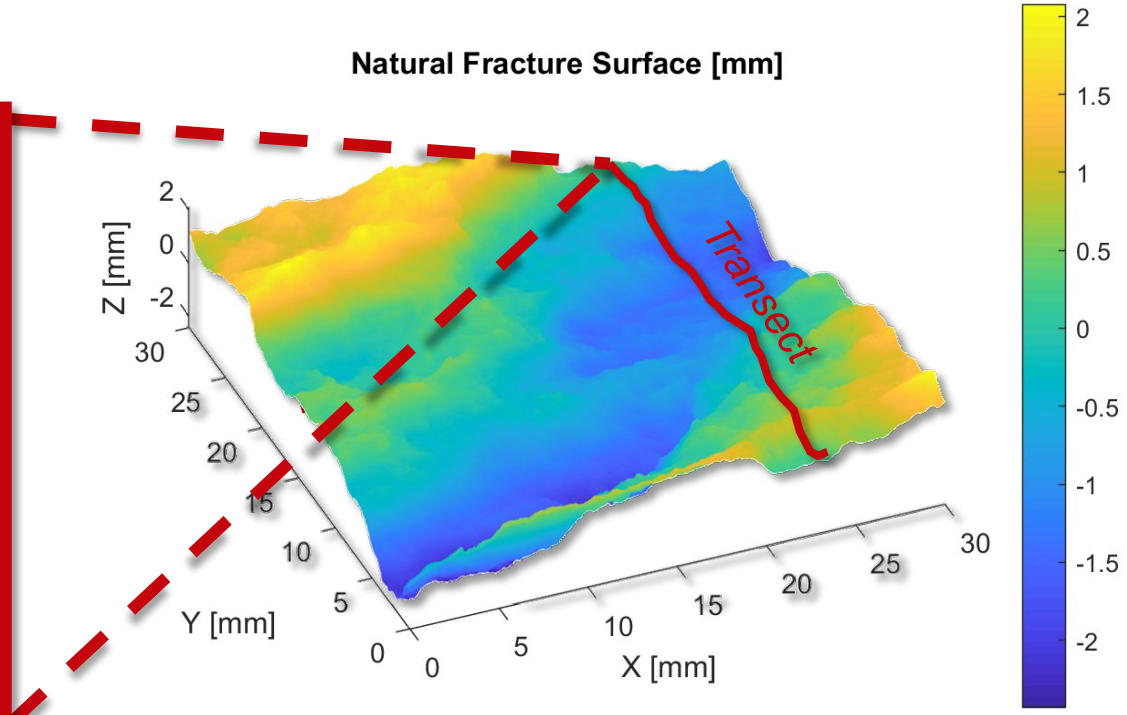

Figure. Fracture surface from WLI scan with selected transect.

II. Natural Surface Roughness Measurement

Hurst Exponent *(H)* → roughness measurement

$$P(k) = Ck^{-\alpha} \qquad H = \frac{\alpha - 1}{2}$$

$$H_x \approx 0.915$$

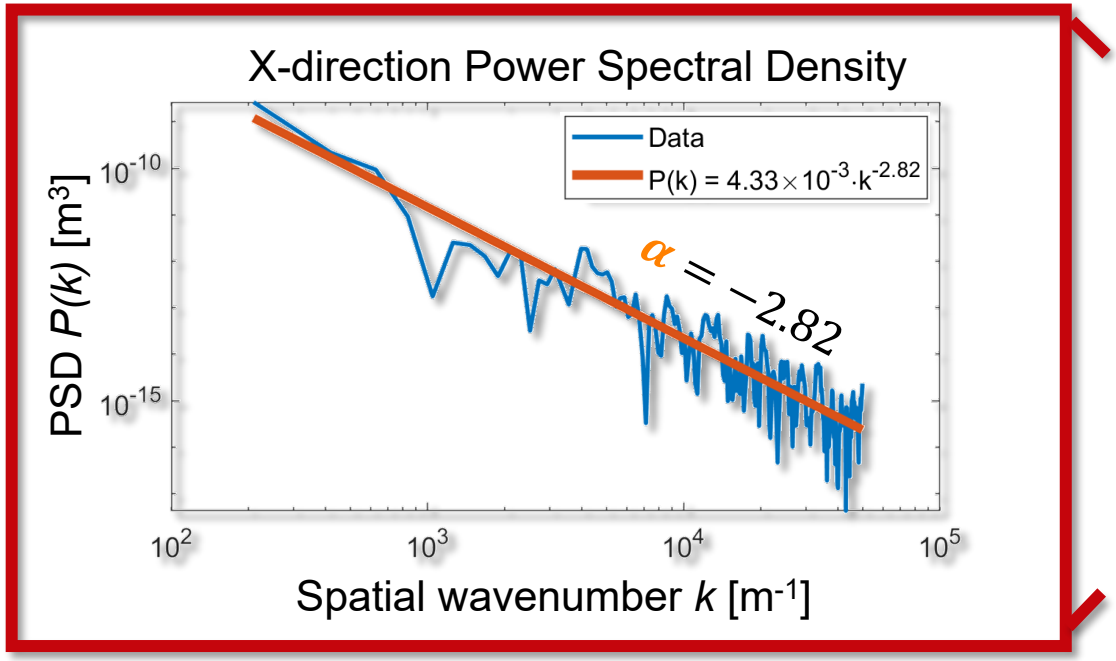

Figure. 1-D Hurst exponent roughness calculation.

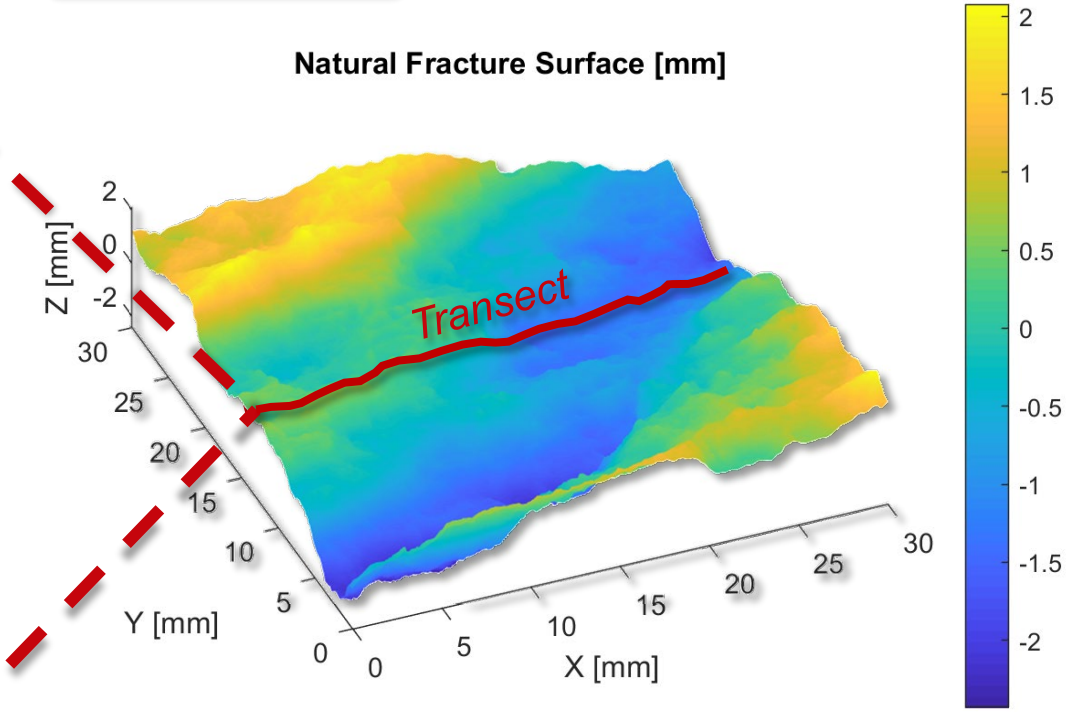

Figure. Fracture surface from WLI scan with selected transect.

II. Natural Surface Roughness Measurement

Hurst Exponent *(H)* → roughness measurement

$$P(k) = Ck^{-\alpha} \qquad H = \frac{\alpha - 1}{2}$$

$H_x \approx 0.915$ $H_y \approx 0.952$

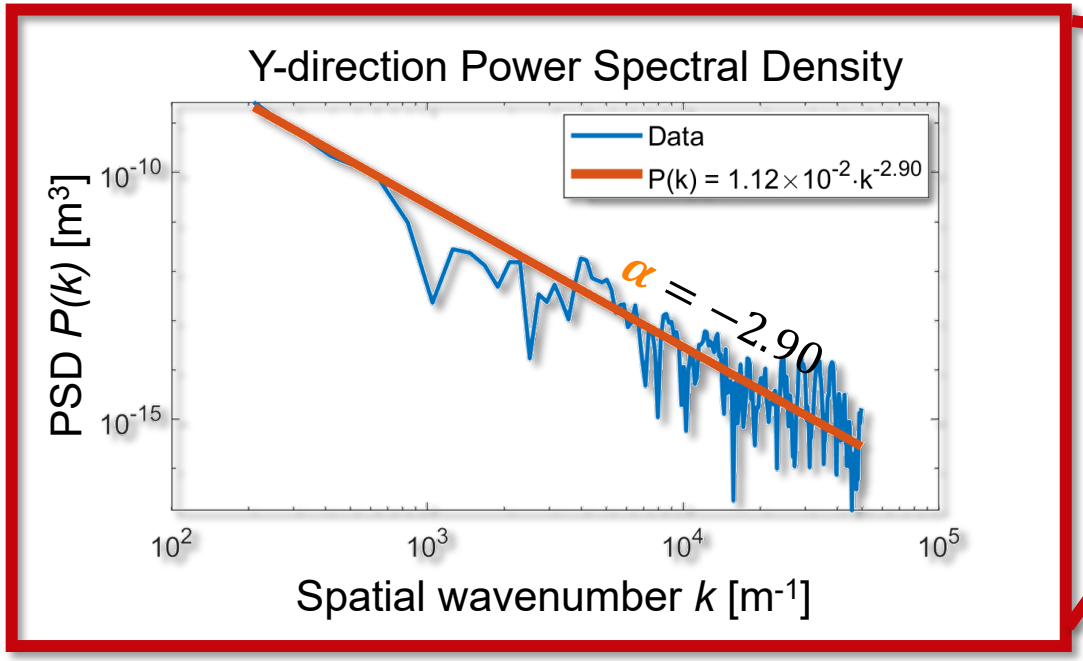

Figure. 1-D Hurst exponent roughness calculation.

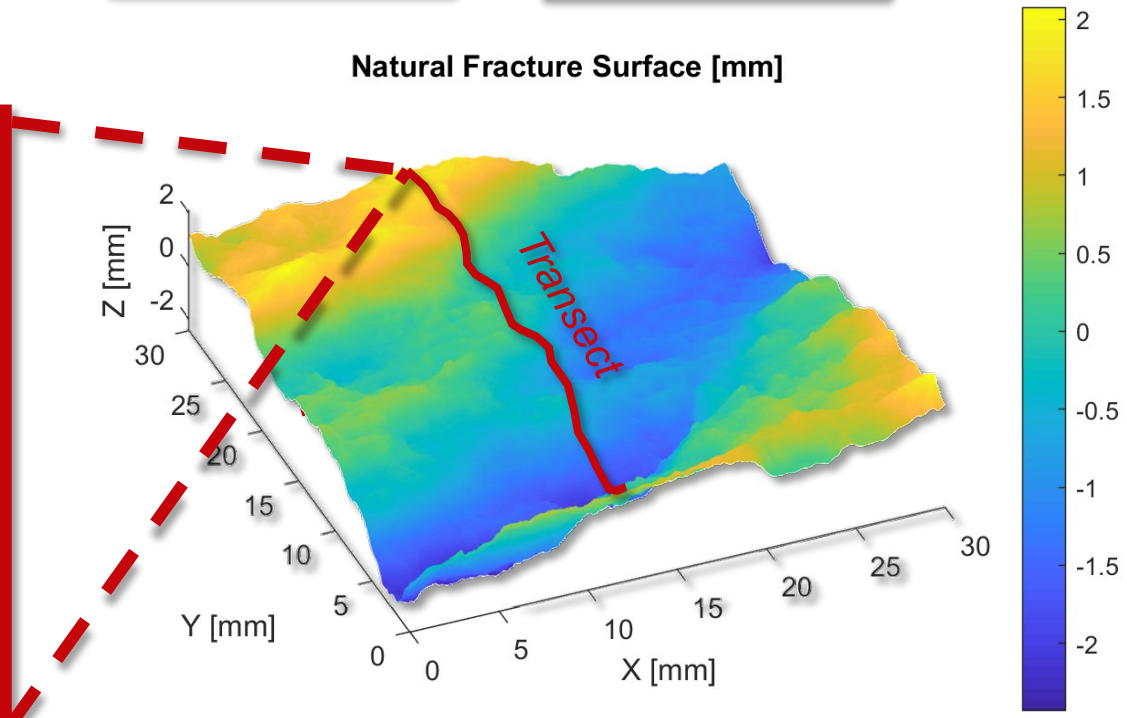

Figure. Fracture surface from WLI scan with selected transect.

II. Methods: Synthetic Surface Generation

- Synthetic fracture surfaces are generated from measured natural roughness parameters to test effects of variable surface roughness

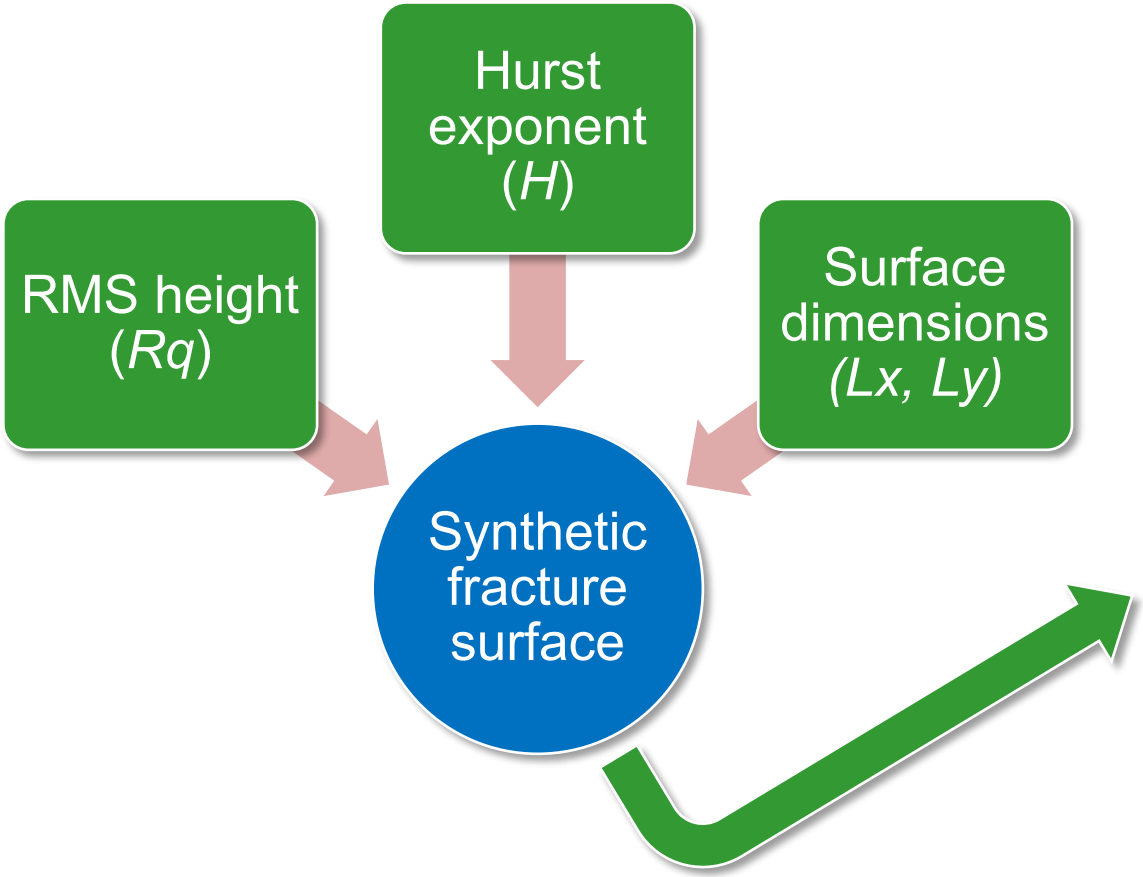

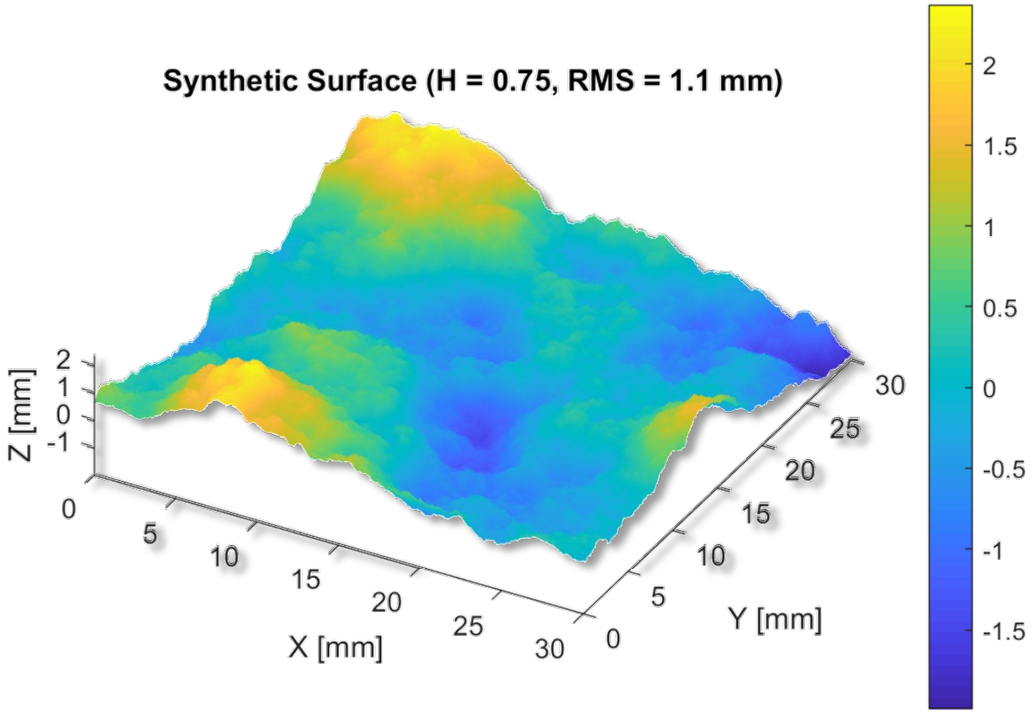

Figure. Generated synthetic fracture surface (MATLAB).

II. Methods: Synthetic Surface Generation

- Generated synthetic surfaces possess variable Hurst exponent *H = 0.75, 0.90*
- Used to make apertures of varying roughness

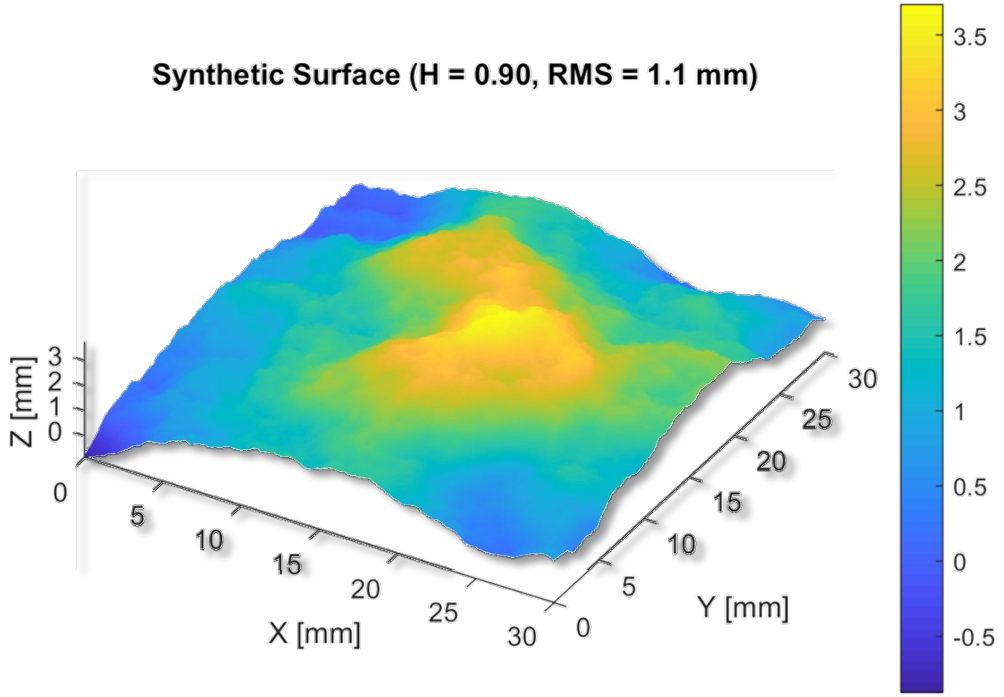

Figure. Generated synthetic fracture surface H = 0.90 (MATLAB).

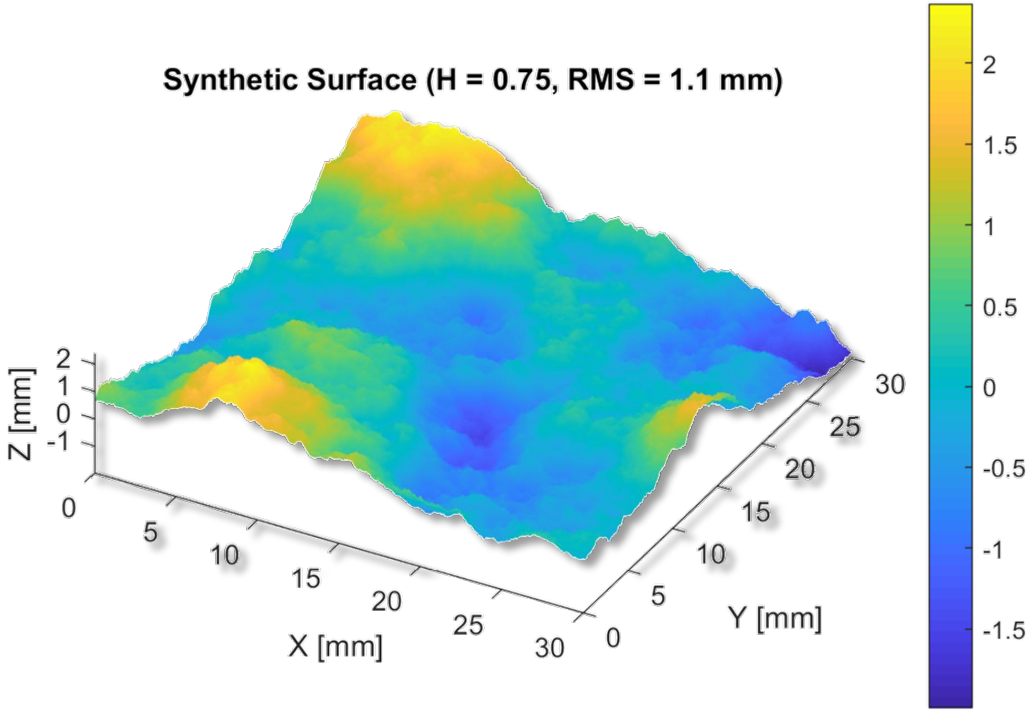

Figure. Generated synthetic fracture surface H = 0.75 (MATLAB).

Overview

I. Introduction

II. Methods

   I. Experimental design
   II. Fracture surface acquisition for model input
   III. Aperture composition & analysis

III. Modeling

IV. Results & Discussion

V. Conclusions

II. Aperture Composition

- Fracture apertures (6) generated from natural & synthetic surfaces in MATLAB

- Operations:
  1. 2-D slope trend removal
  2. Surface separation (*0.5 mm*)
  3. Lateral displacement (*0 – 1.5 mm*)
  4. Asperity corrections (*0.2 mm minimum*)
  5. STL aperture geometry file created

Table 1. Aperture Geometries (6 total)

	Synthetic		*Natural*
Hurst exponent *(H)*	0.75	0.90	0.935
Displacement [*mm*]	0, 1.5	0, 1.5	0, 1.5

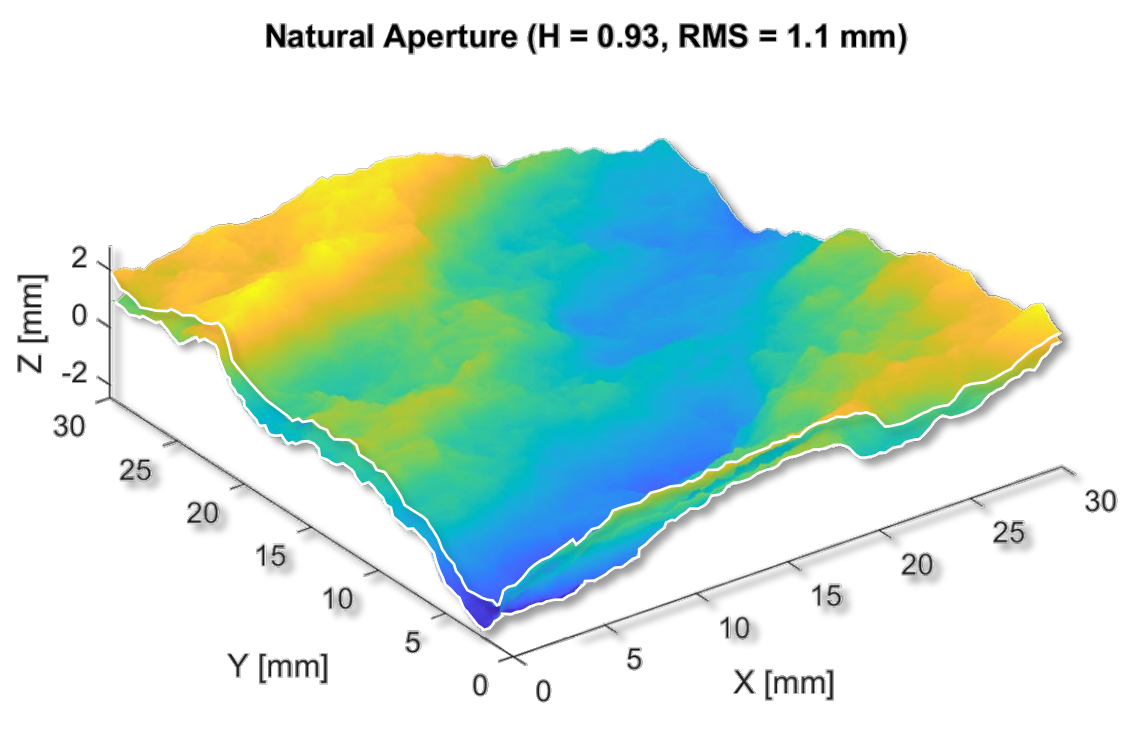

Figure. Natural fracture aperture perspective plot.

II. Aperture Heterogeneity Characterization

- Variogram used to estimate correlation length of aperture width at variable orientations
- Correlation length gives variability in a direction

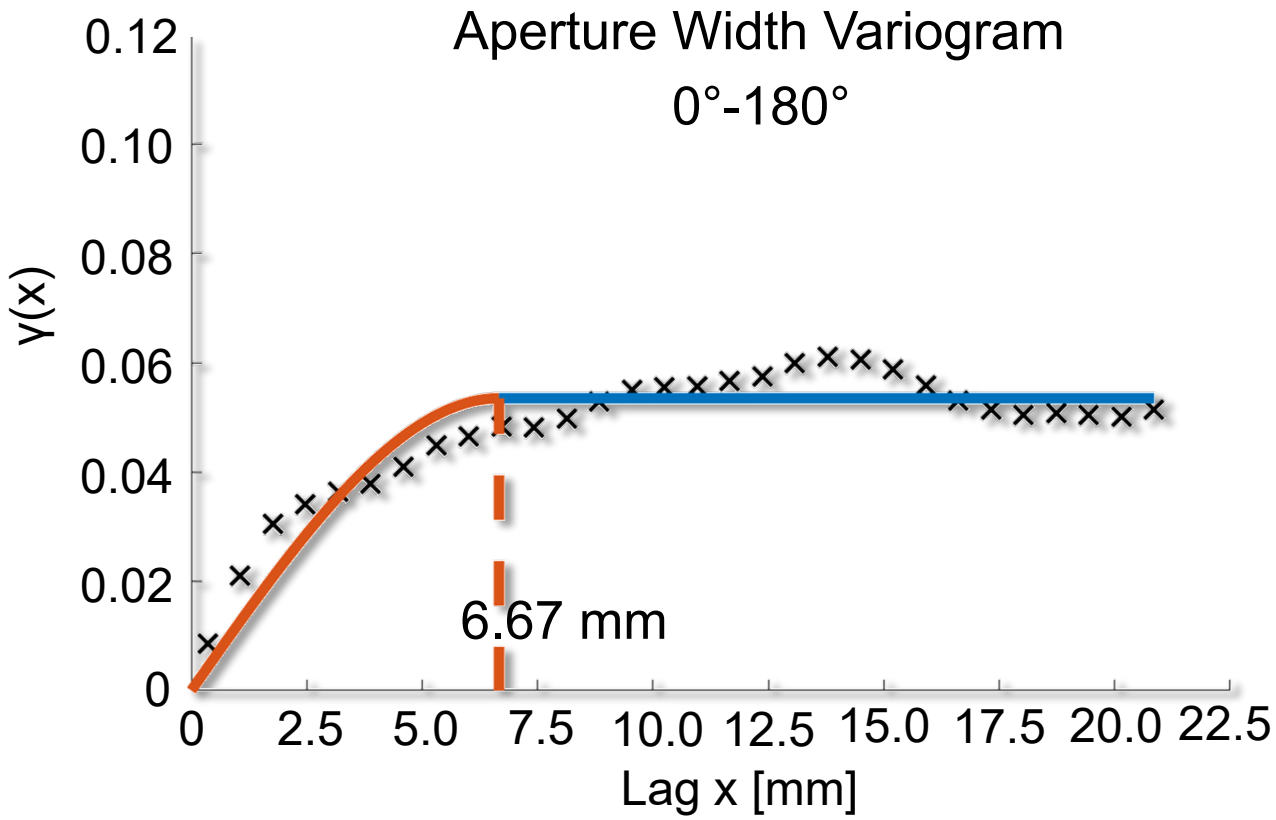

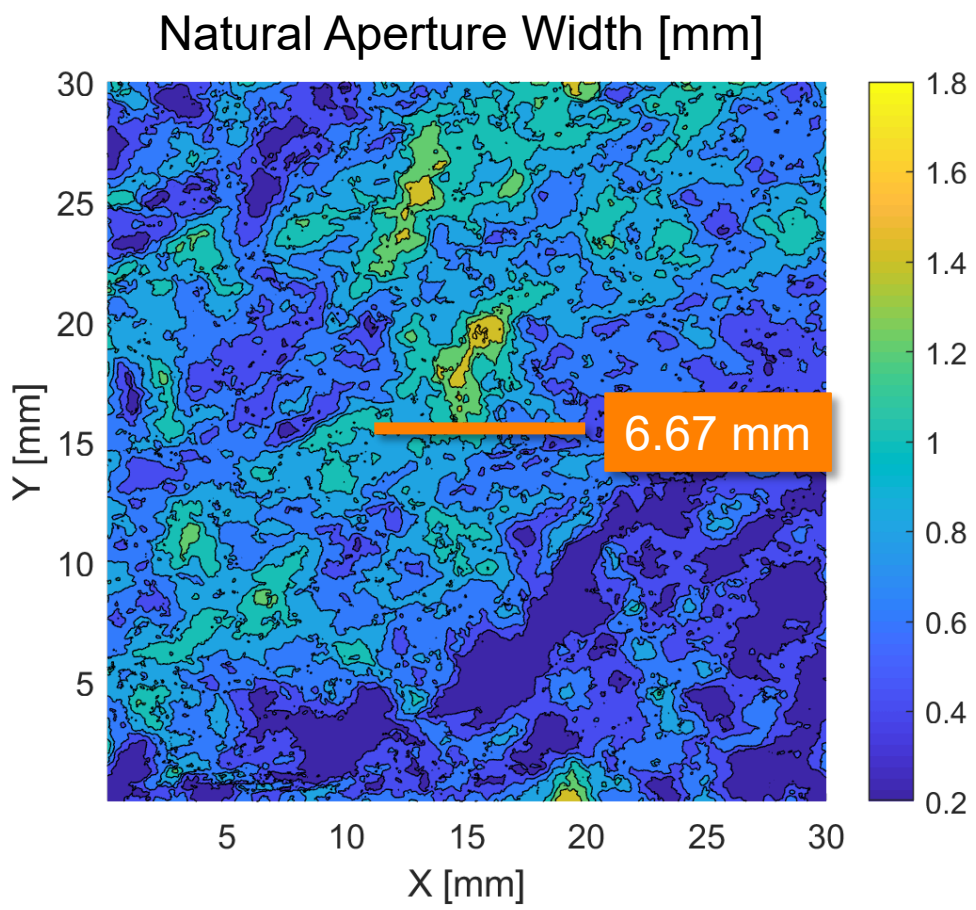

Figure. Natural fracture aperture distribution with measured transect(s).

II. Aperture Heterogeneity Characterization

- Variogram used to estimate correlation length of aperture width at variable orientations
- Correlation length gives variability in a direction

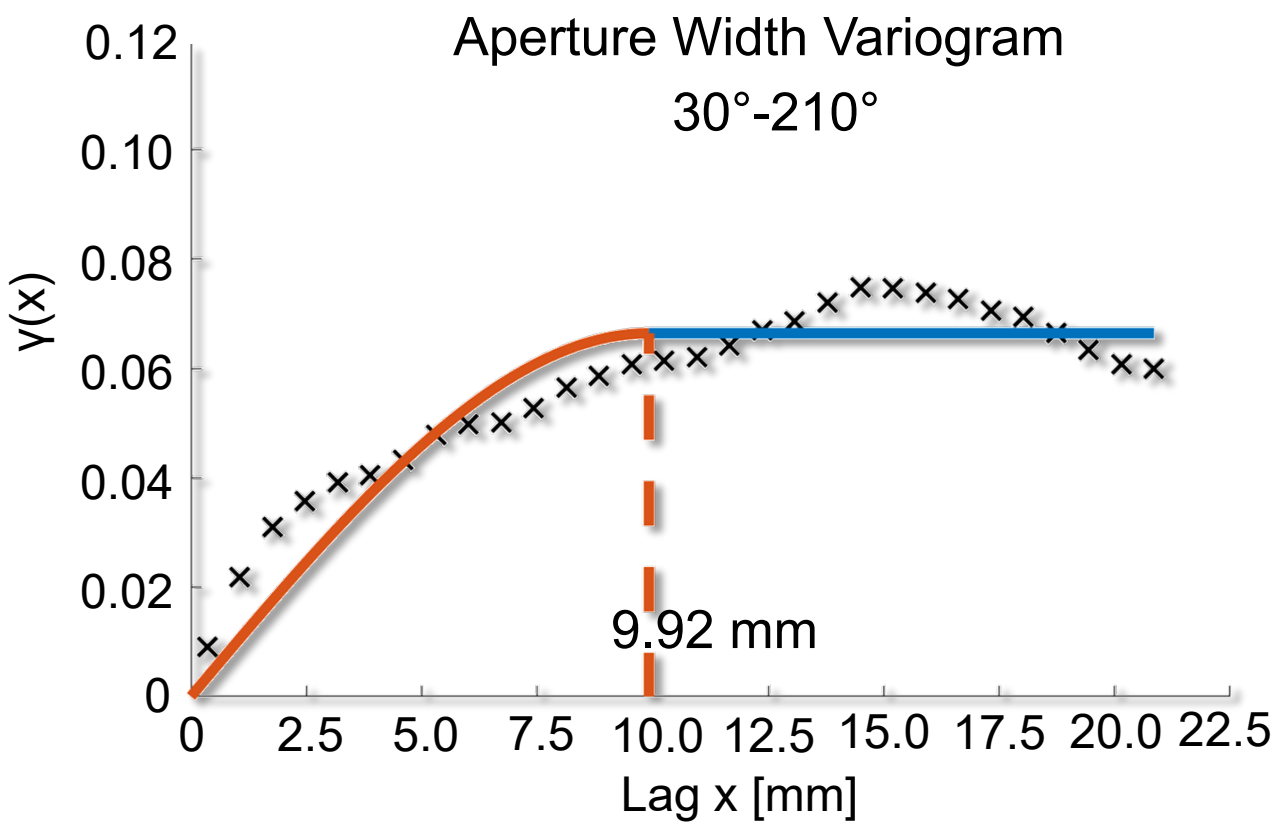

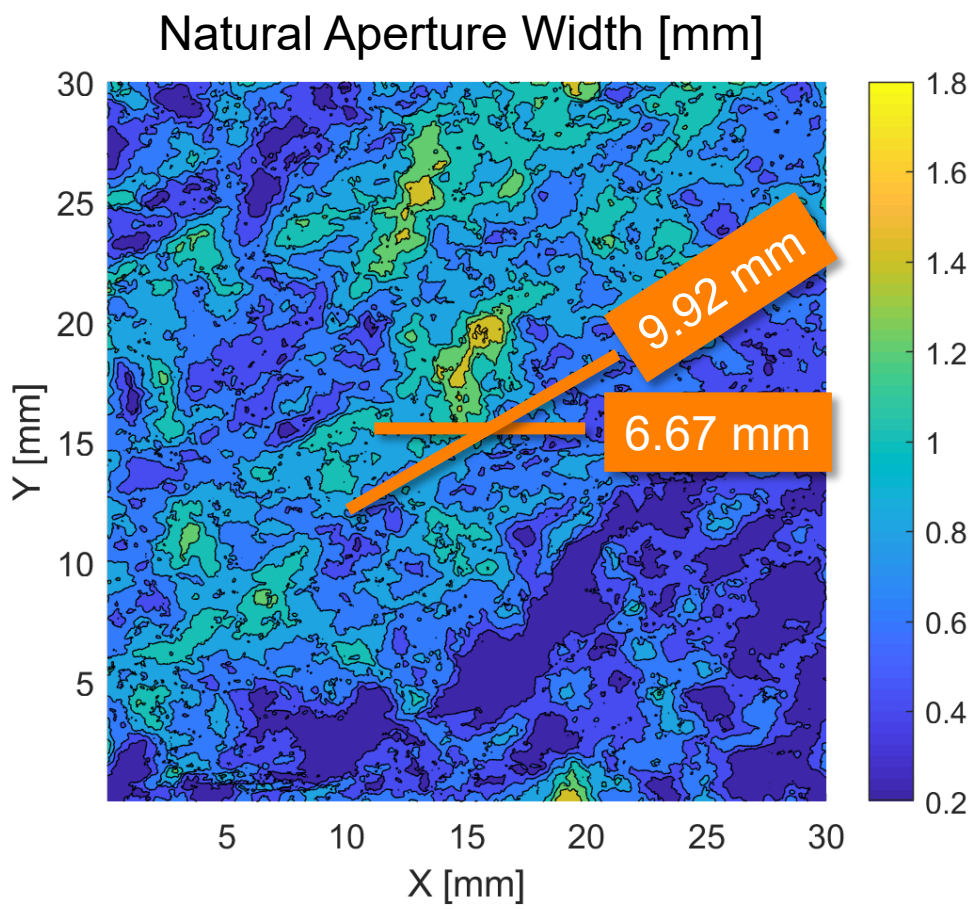

Figure. Natural fracture aperture distribution with measured transect(s).

II. Aperture Heterogeneity Characterization

- Variogram used to estimate correlation length of aperture width at variable orientations
- Correlation length gives variability in a direction

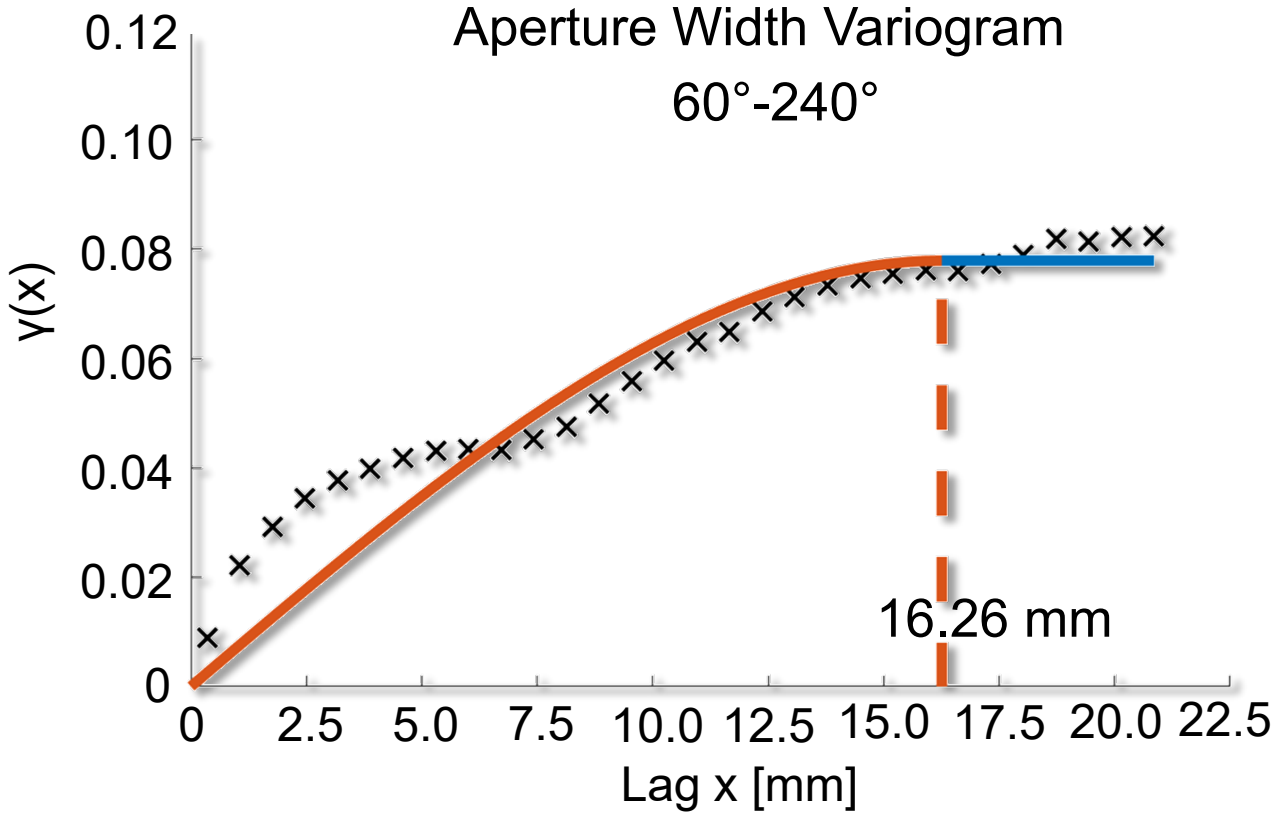

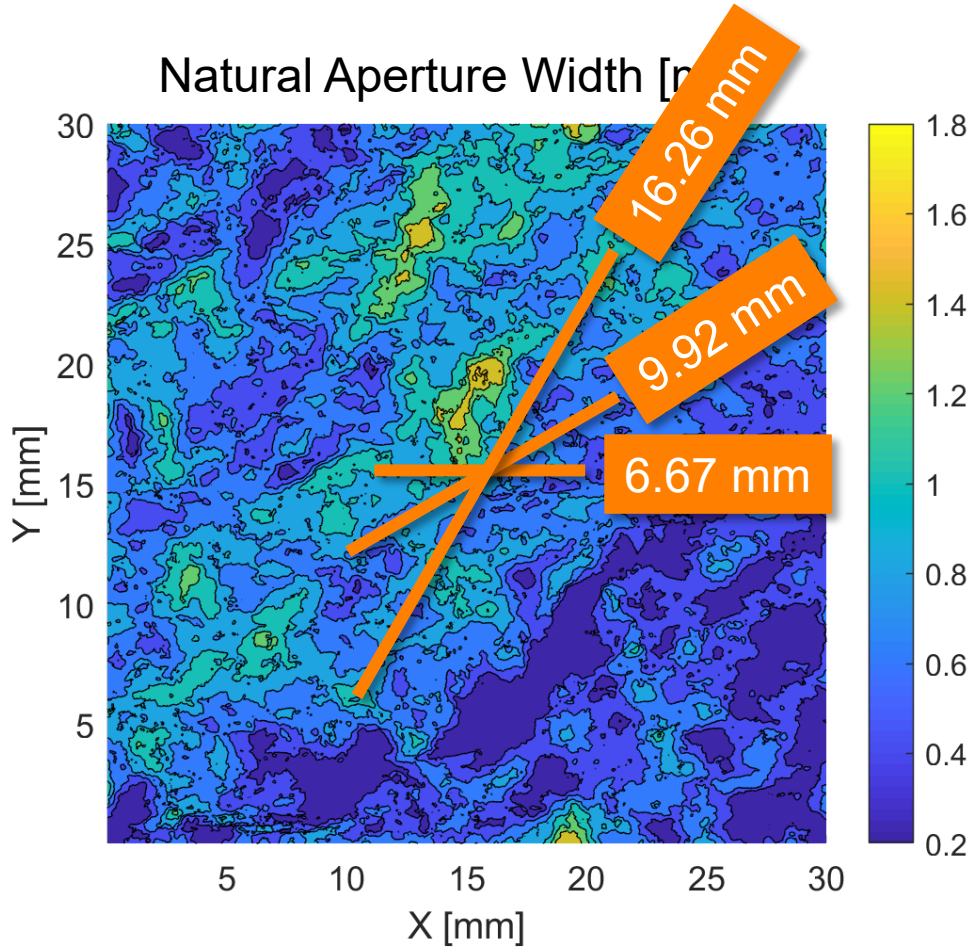

Figure. Natural fracture aperture distribution with measured transect(s).

II. Aperture Heterogeneity Characterization

- Variogram used to estimate correlation length of aperture width at variable orientations
- Correlation length gives variability in a direction

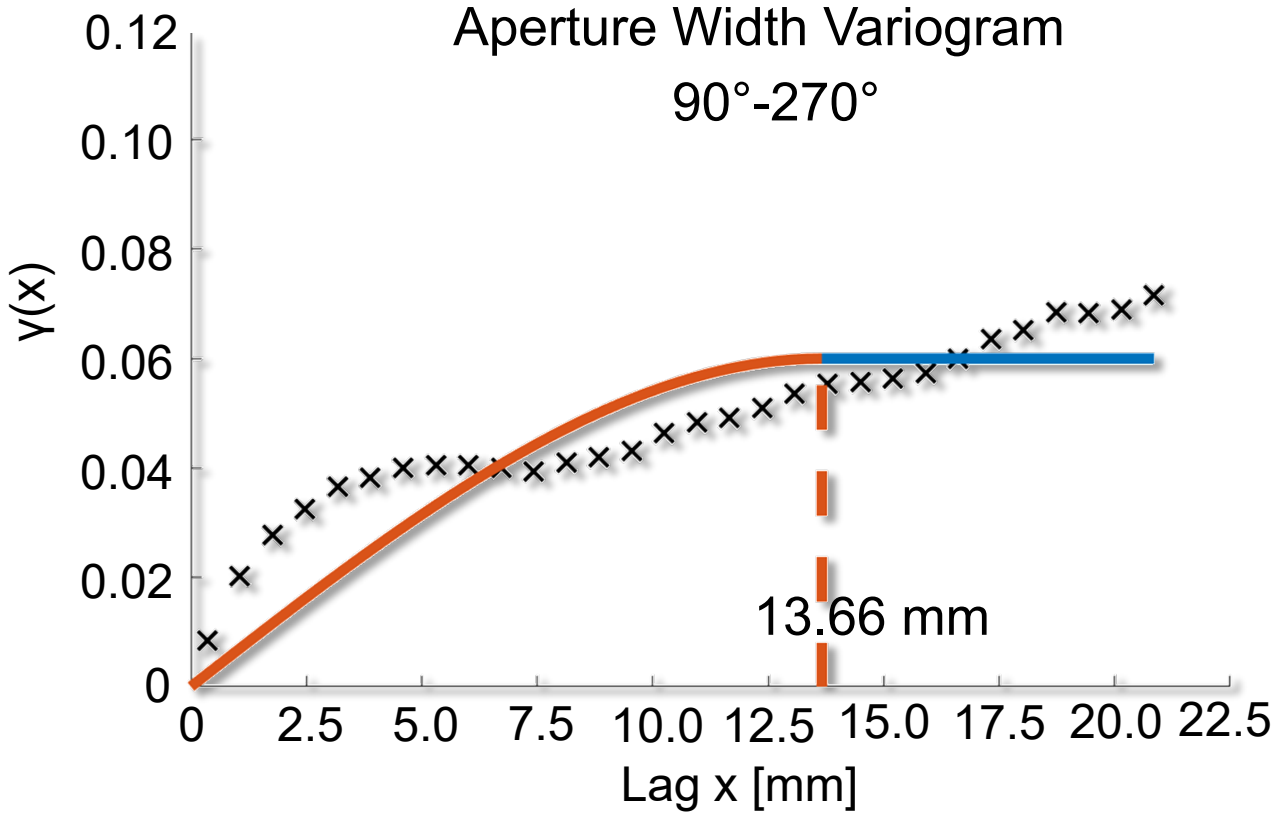

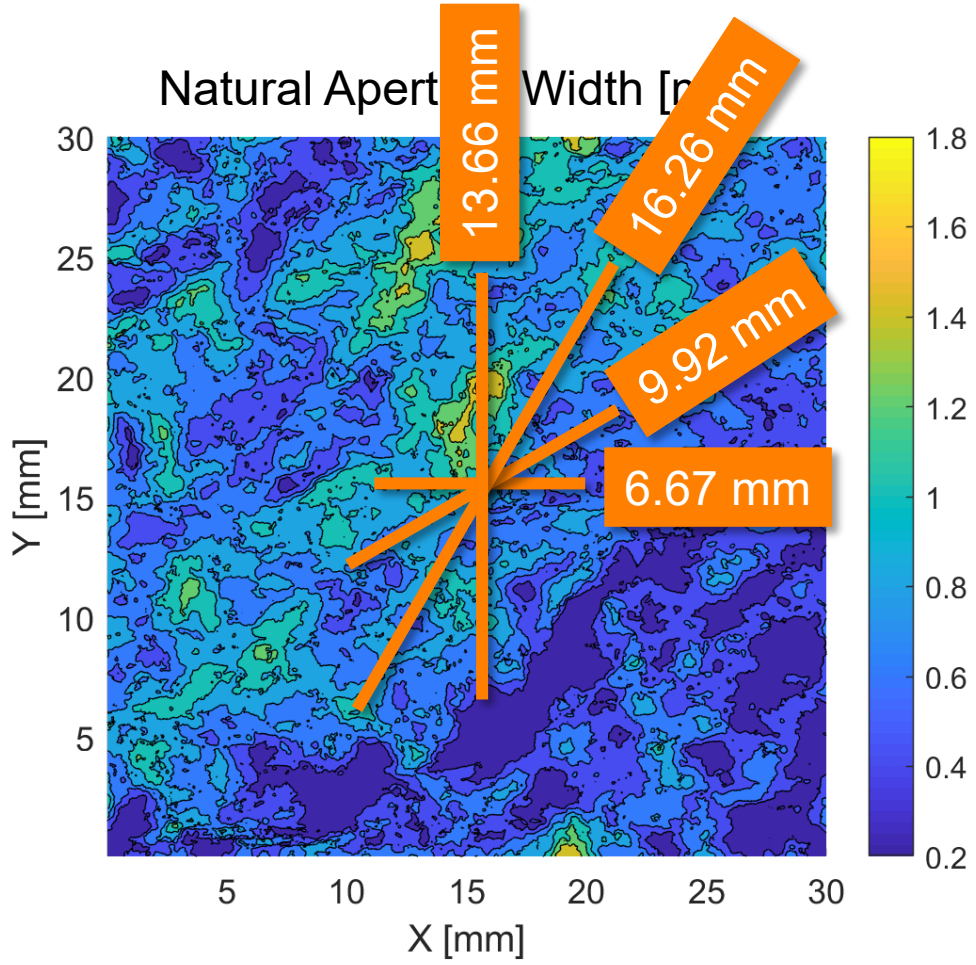

Figure. Natural fracture aperture distribution with measured transect(s).

II. Aperture Heterogeneity Characterization

- Variogram used to estimate correlation length of aperture width at variable orientations
- Correlation length gives variability in a direction

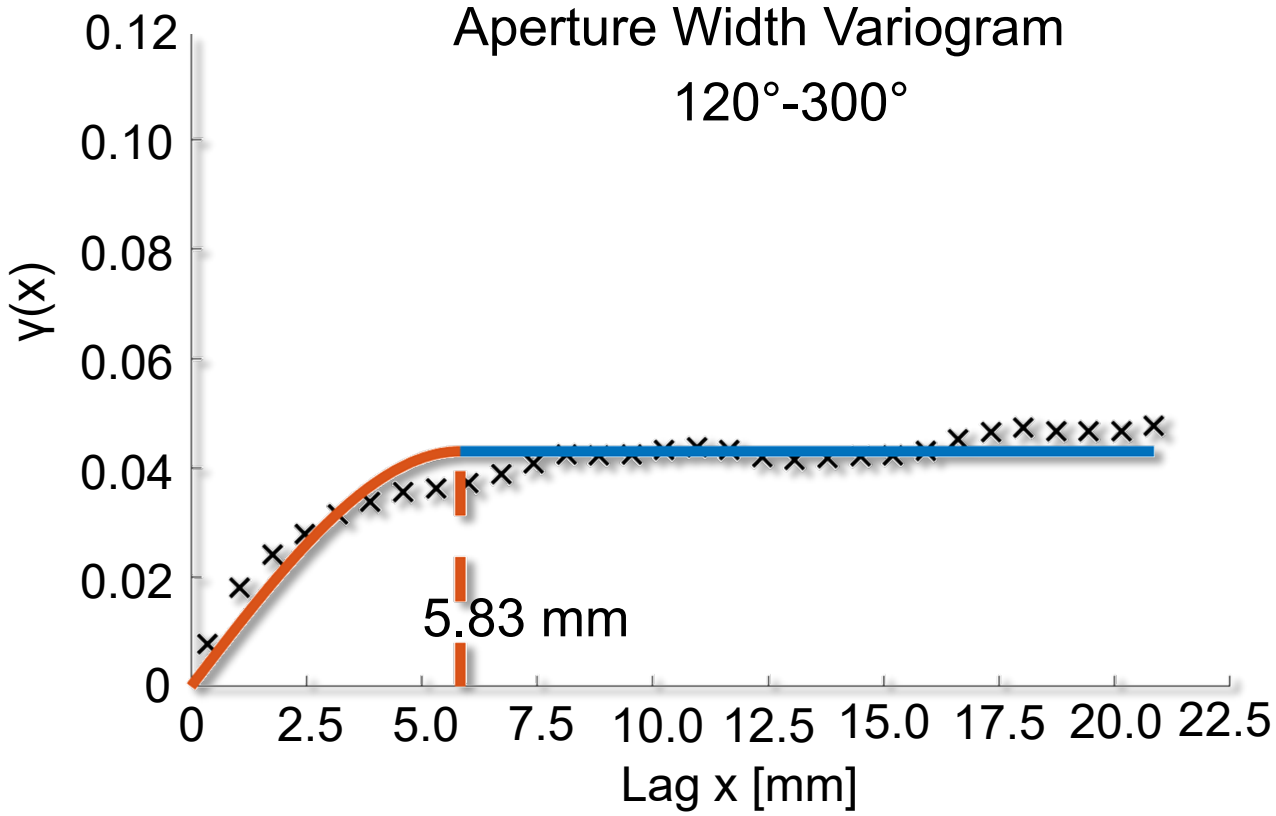

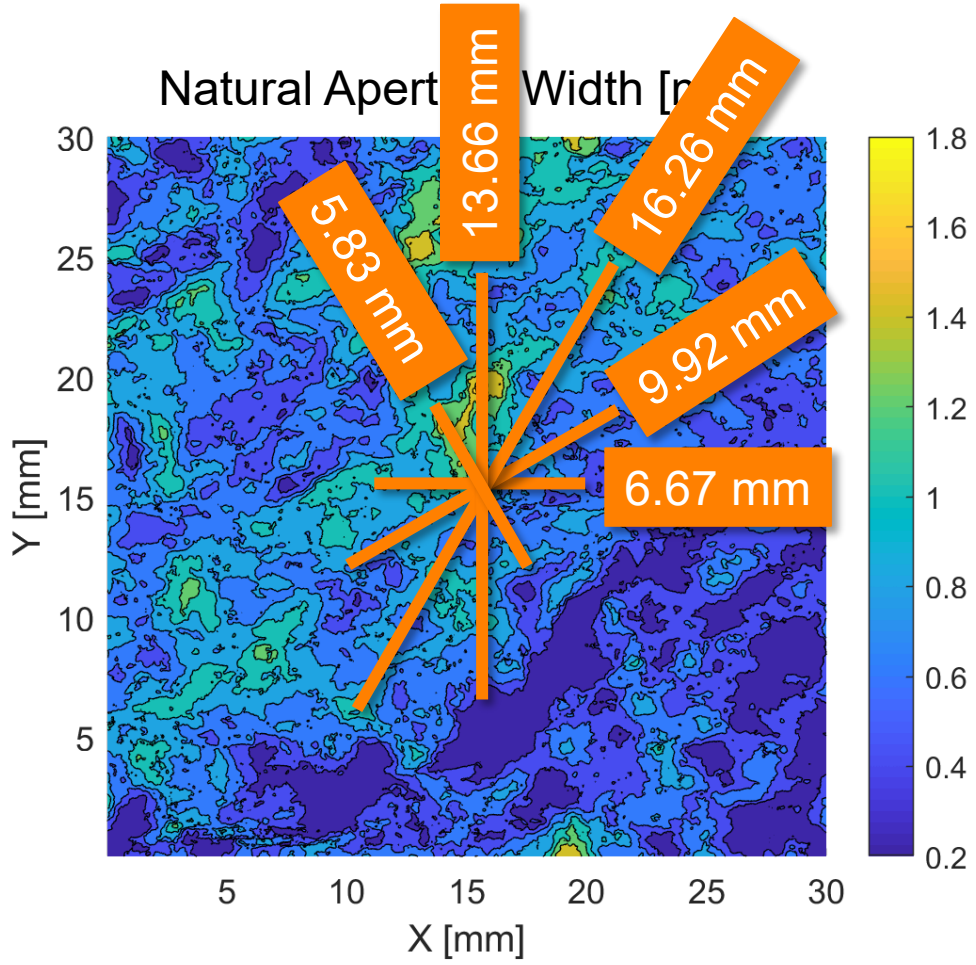

Figure. Natural fracture aperture distribution with measured transect(s).

II. Aperture Heterogeneity Characterization

- Variogram used to estimate correlation length of aperture width at variable orientations
- Correlation length gives variability in a direction

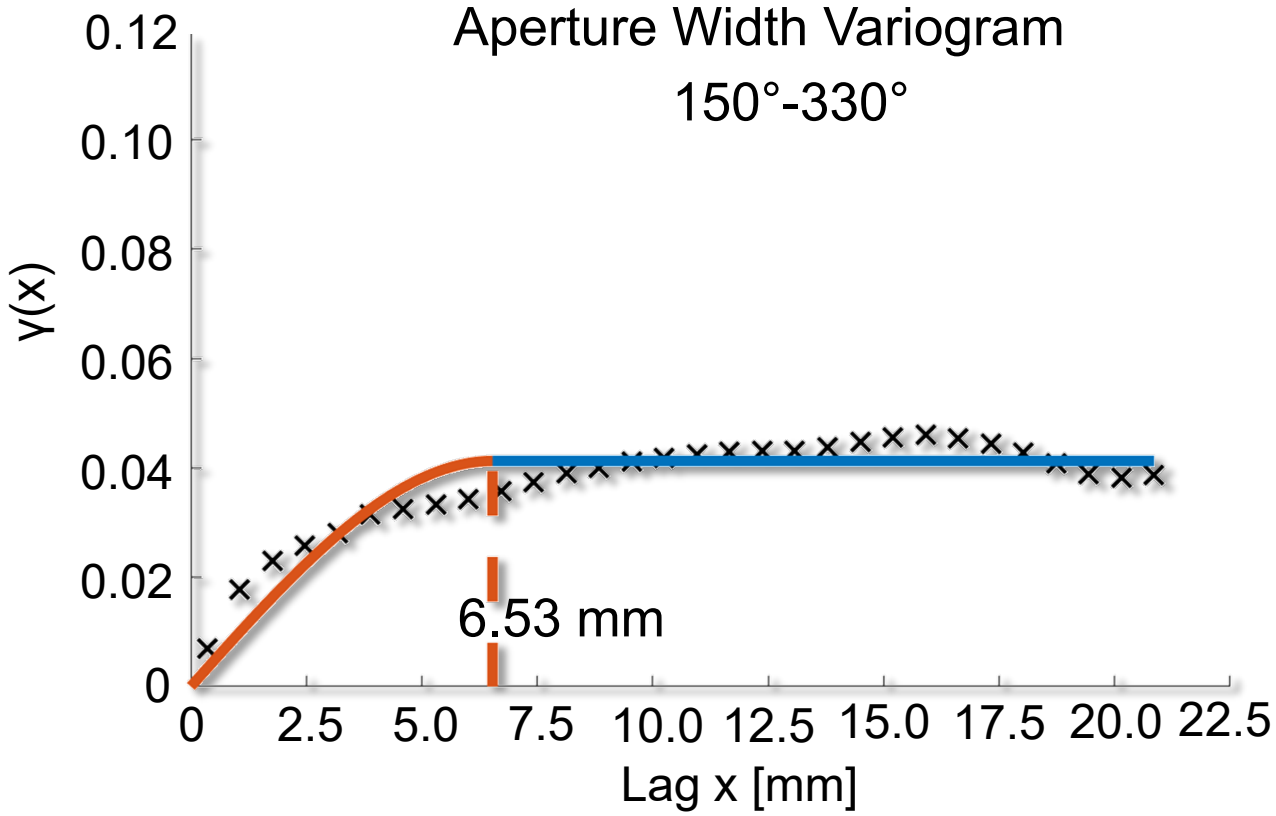

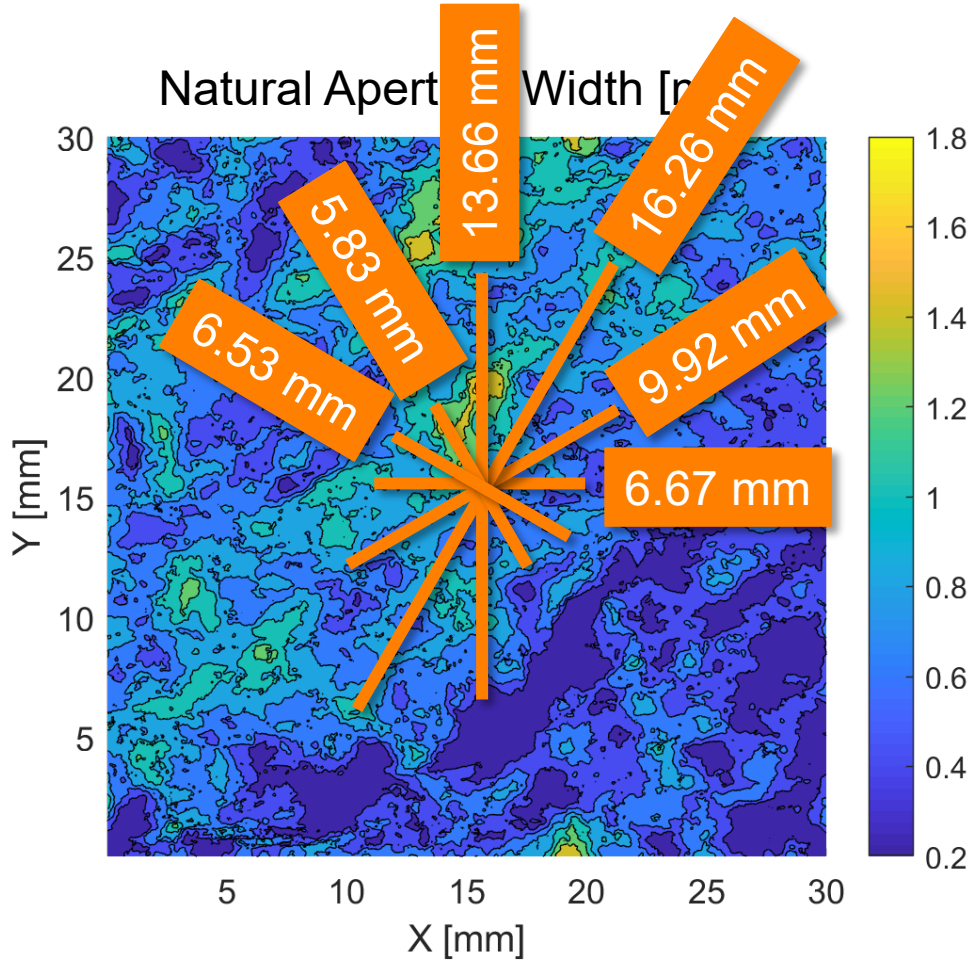

Figure. Natural fracture aperture distribution with measured transect(s).

II. Correlation Length Anisotropy

- **Aperture width heterogeneity** causes **anisotropy** in correlation lengths
- How will this affect **flow** behavior?
- How will this affect **heat flux** behavior?
- Numerical flow modeling conducted to investigate

Sampling Direction	Mean Correlation Length
X (↔)	7.70 mm
Y (↕)	11.92 mm

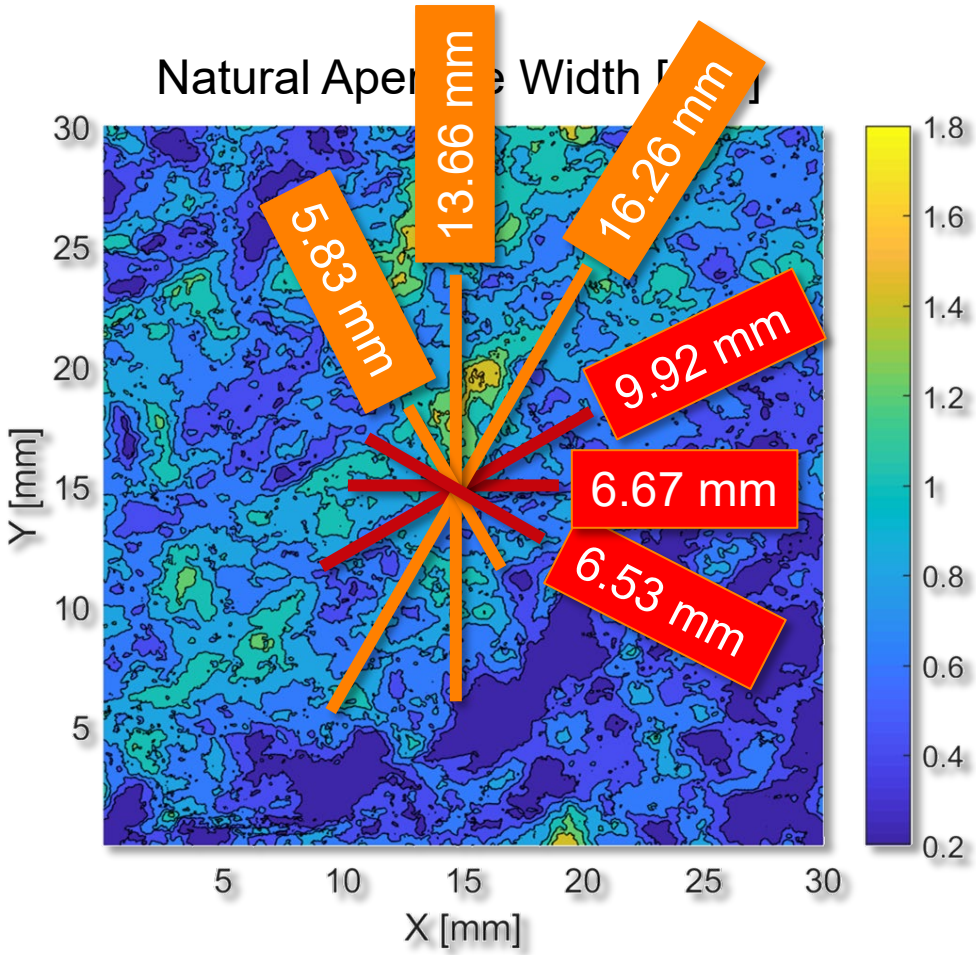

Figure. Variogram range [mm] as a function of sampling direction.

Overview

I. Introduction

II. Methods

III. Flow Modeling

  I. Model configuration & boundary conditions

  II. Parameters of interest

IV. Results & Discussion

V. Conclusions

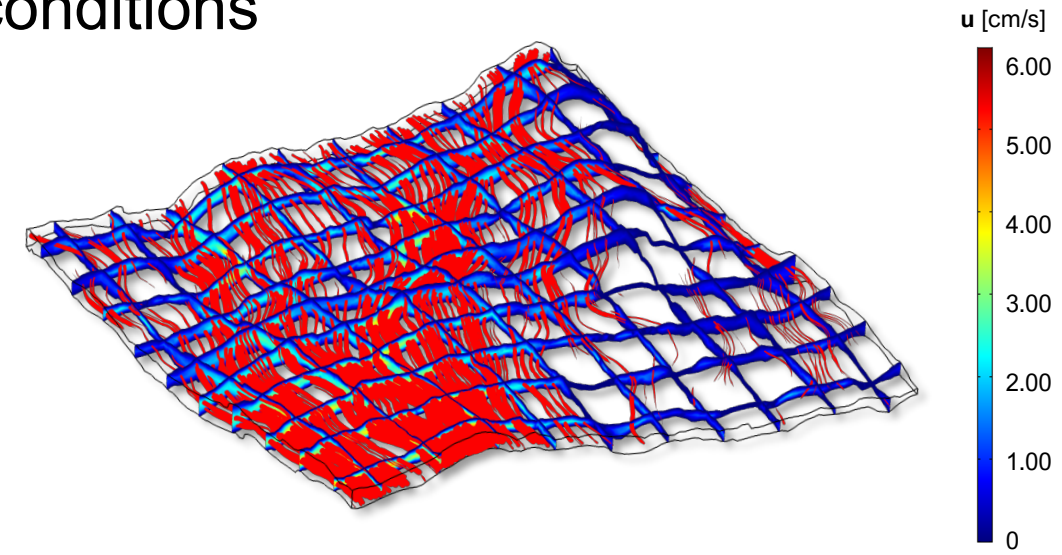

Figure. Stokes flow solution within natural fracture geometry.

Overview

I. Introduction

II. Methods

III. Flow Modeling

  I. Model configuration & boundary conditions

  II. Parameters of interest

IV. Results & Discussion

V. Conclusions

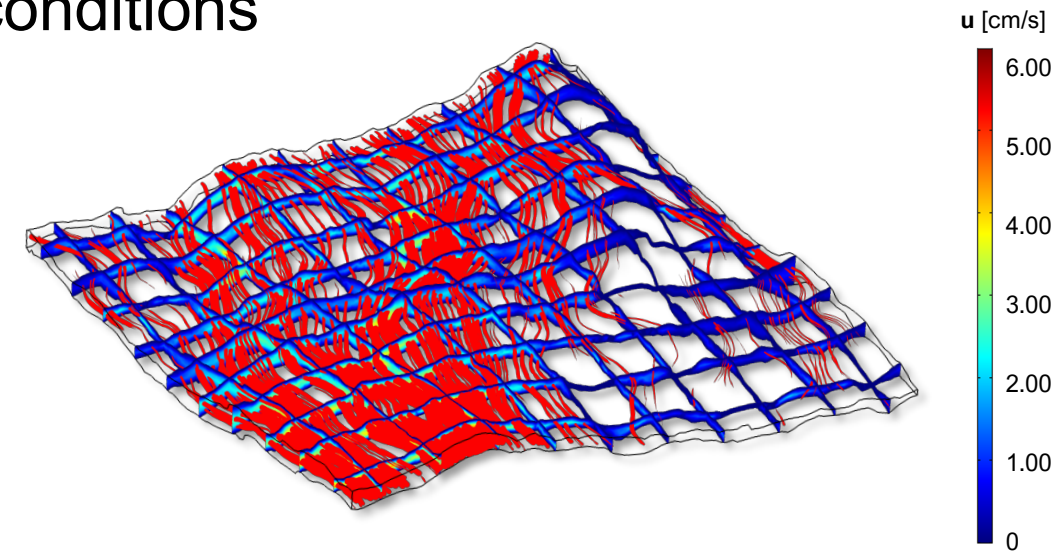

Figure. Stokes flow solution within natural fracture geometry.

III. COMSOL FEM Flow Model Configuration

- Aperture domain STL imported to COMSOL

Table 2. Geometry Size Parameters

Domain	Host Granite	Fracture Aperture
H x W x L	33 x 33 x 60.5 mm	30 x 30 x 0.5 mm

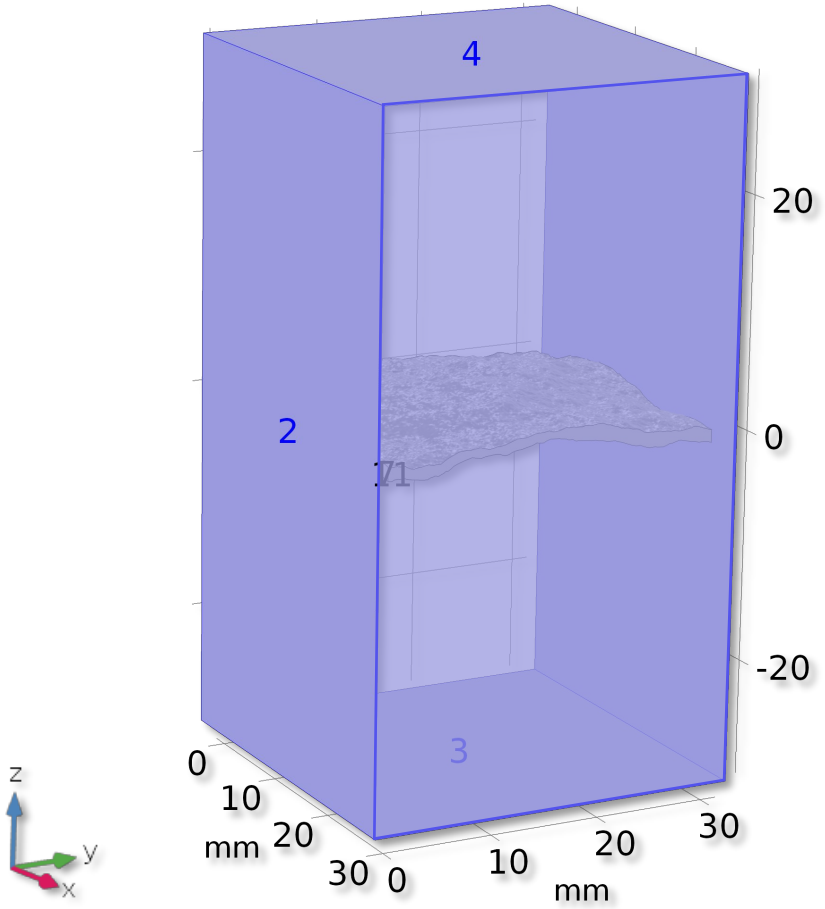

Figure. CAD model geometry with rock matrix selection highlighted (granite).

III. COMSOL FEM Flow Model Configuration

- Aperture domain STL imported to COMSOL

Table 2. Geometry Size Parameters

Domain	Host Granite	Fracture Aperture
H x W x L	33 x 33 x 60.5 mm	30 x 30 x 0.5 mm

- Physics used in model:
  1. Laminar Flow
     - Stokes flow
  2. Conjugate Heat Transfer
     - Heat conduction & advection
- Multiphysics coupling:
  1. Nonisothermal Flow
- Steady-state computation

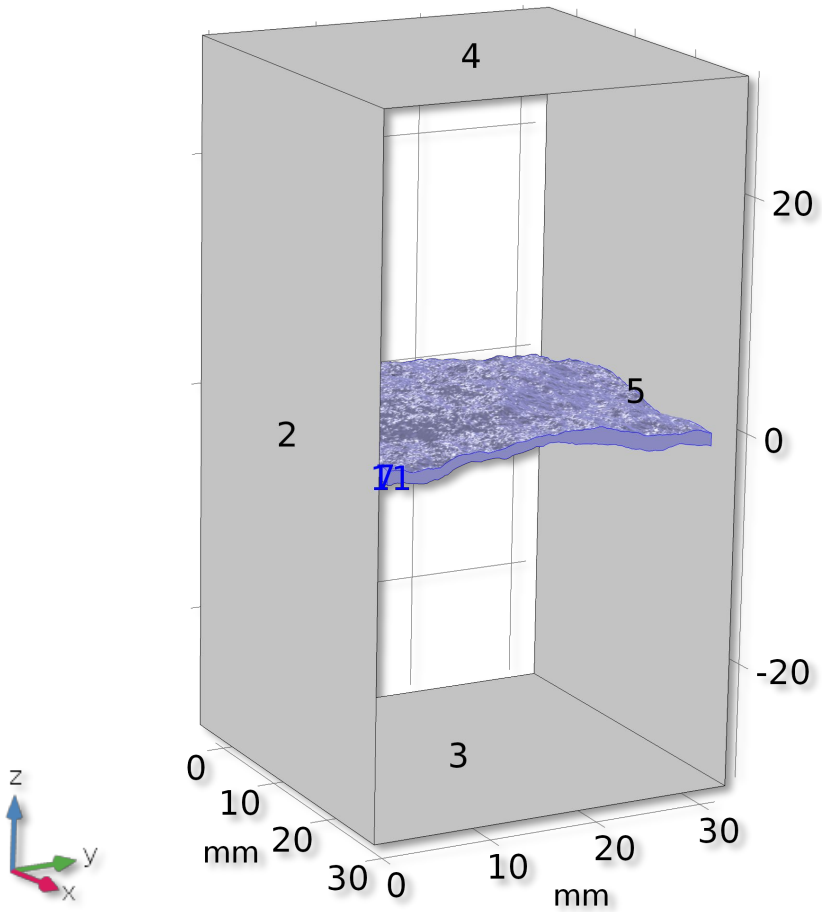

Figure. CAD model geometry with aperture selection highlighted (water).

III. Boundary Conditions: Flow

Fluid flow boundary conditions:

1. No slip
2. Specified pressure outlet (0 Pa)
3. Specified velocity inlet (variable)

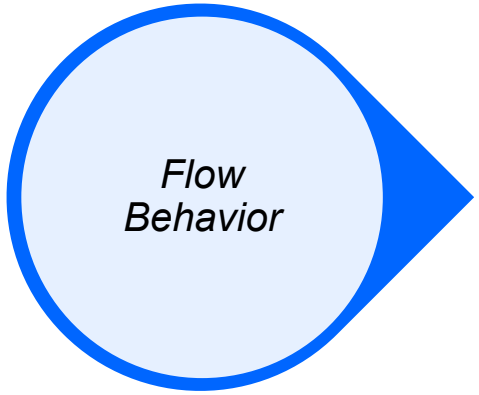

Thermal boundary conditions:

1. Constant temperature (92.5°C)
2. Thermal inflow (25.0°C)
3. Thermal outflow

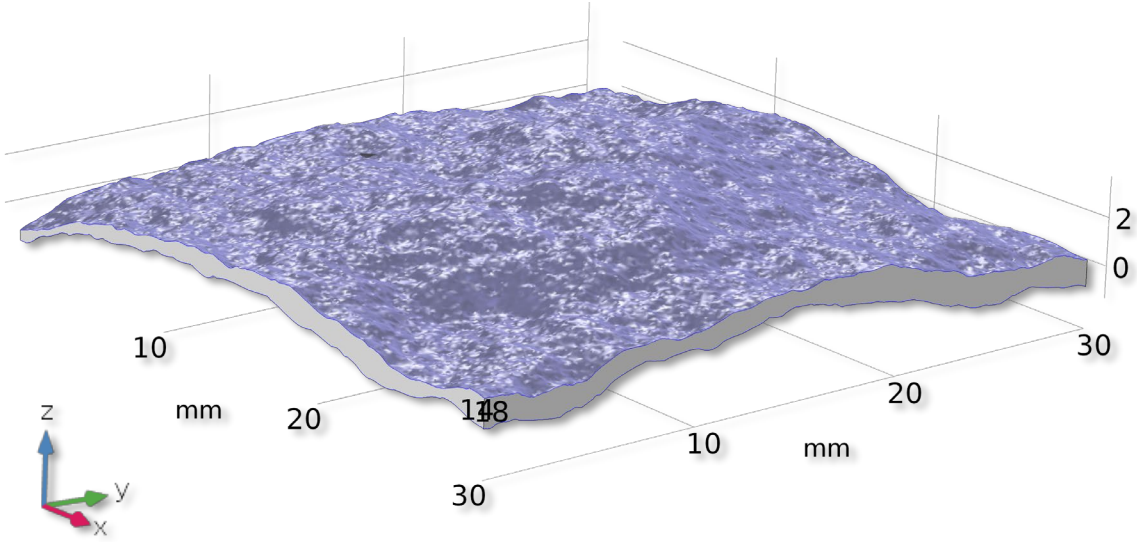

Figure. Model aperture geometry with no-slip boundaries highlighted.

III. Boundary Conditions: Flow

Fluid flow boundary conditions:

1. No slip
2. Specified pressure outlet (0 Pa)
3. Specified velocity inlet (variable)

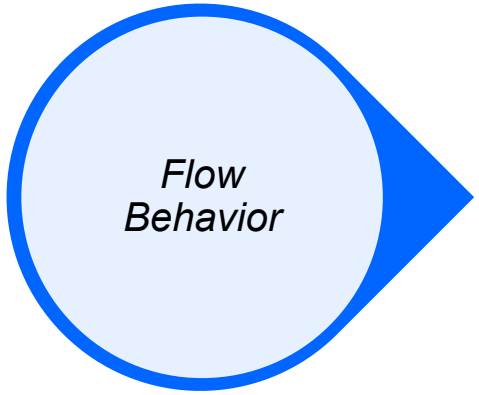

Thermal boundary conditions:

1. Constant temperature (92.5°C)
2. Thermal inflow (25.0°C)
3. Thermal outflow

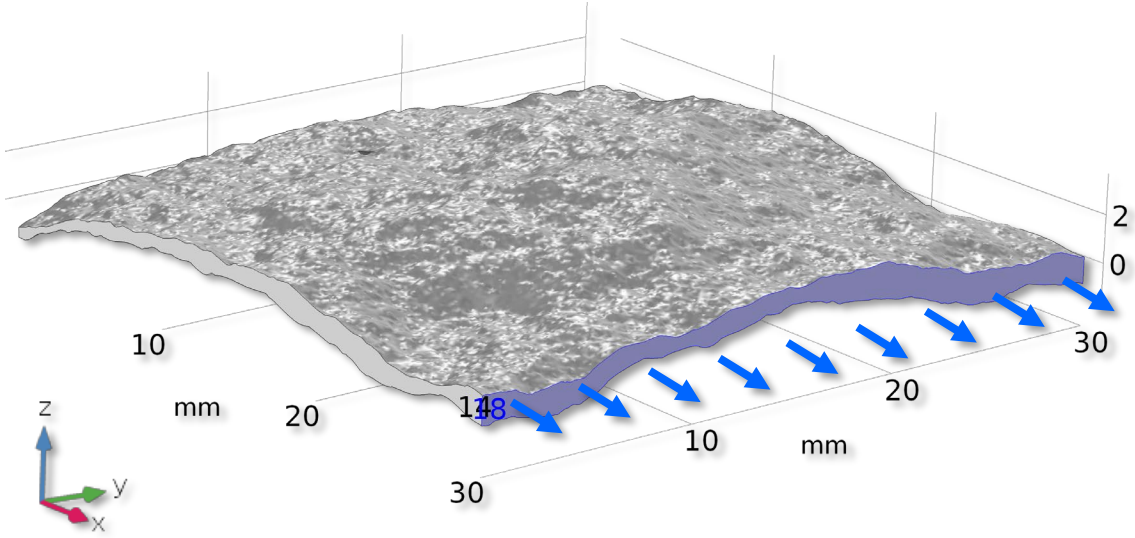

Figure. Model aperture geometry with flow outlet boundary highlighted.

III. Boundary Conditions: Flow

Fluid flow boundary conditions:

1. No slip
2. Specified pressure outlet (0 Pa)
3. Specified velocity inlet (variable)

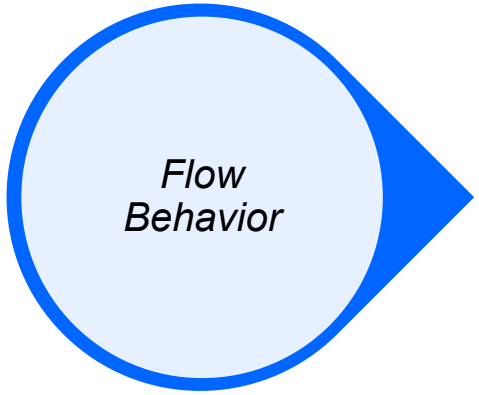

Thermal boundary conditions:

1. Constant temperature (92.5°C)
2. Thermal inflow (25.0°C)
3. Thermal outflow

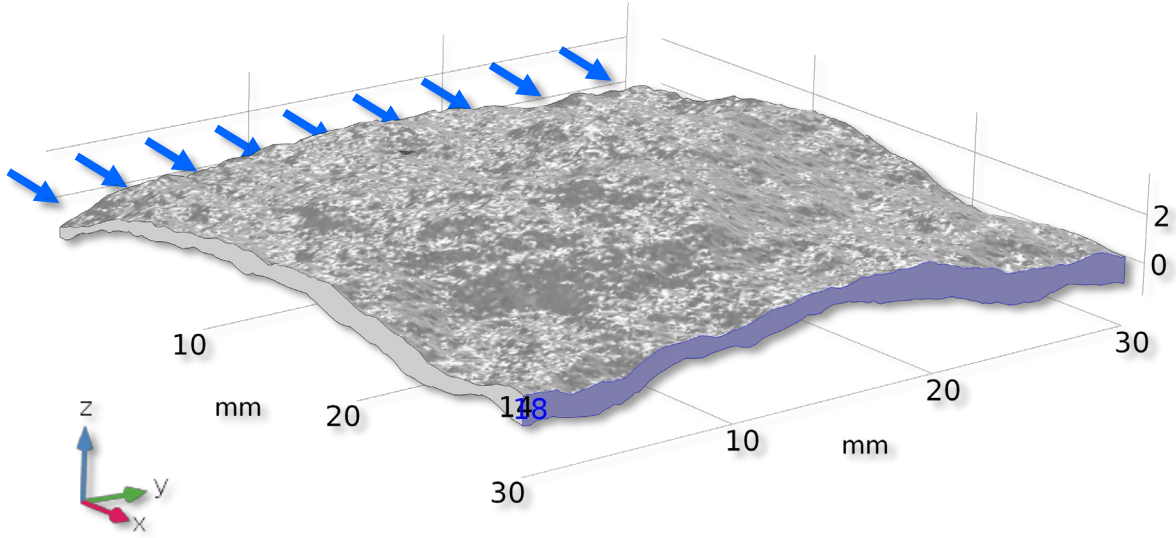

Figure. Model aperture geometry with flow inlet boundary denoted.

III. Boundary Conditions: Heat Flow

Fluid flow boundary conditions:

1. No slip
2. Specified pressure outlet (0 Pa)
3. Specified velocity inlet (variable)

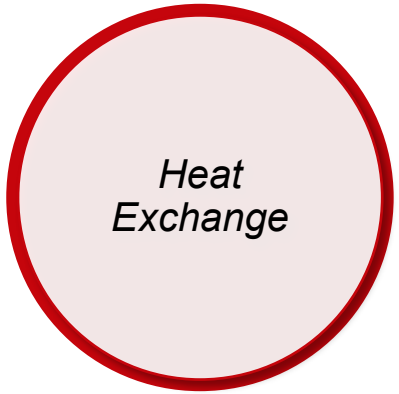

Thermal boundary conditions:

1. Constant temperature (92.5°C)
2. Thermal inflow (25.0°C)
3. Thermal outflow

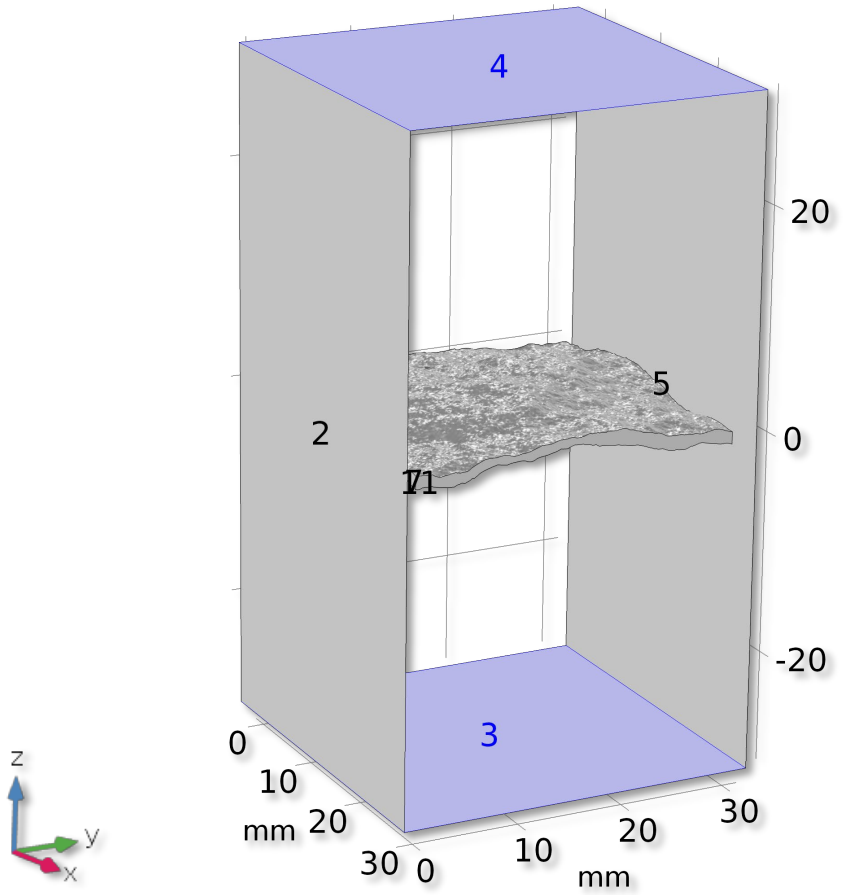

Figure. Model geometry with constant temperature boundaries highlighted.

III. Boundary Conditions: Heat Flow

Fluid flow boundary conditions:

1. No slip
2. Specified pressure outlet (0 Pa)
3. Specified velocity inlet (variable)

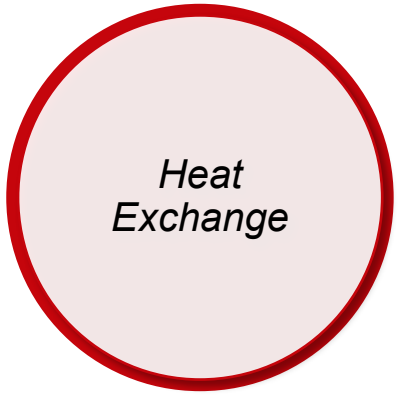

Thermal boundary conditions:

1. Constant temperature (92.5°C)
2. Thermal inflow (25.0°C)
3. Thermal outflow

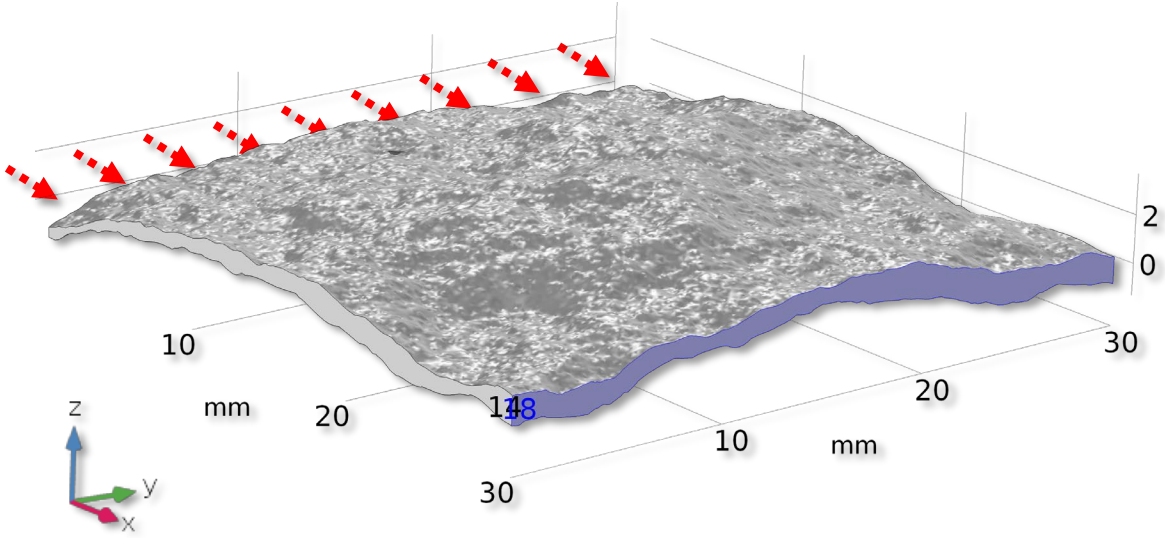

Figure. Model aperture geometry with thermal inflow boundary denoted.

III. Boundary Conditions

Fluid flow boundary conditions:

1. No slip
2. Specified pressure outlet (0 Pa)
3. Specified velocity inlet (variable)

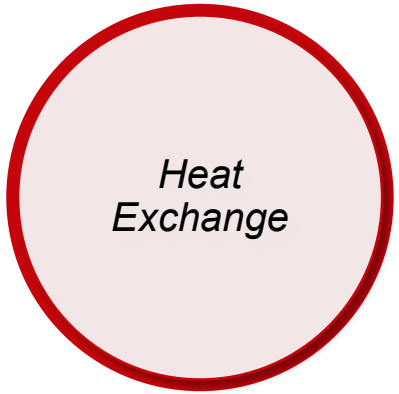

Thermal boundary conditions:

1. Constant temperature (92.5°C)
2. Thermal inflow (25.0°C)
3. Thermal outflow

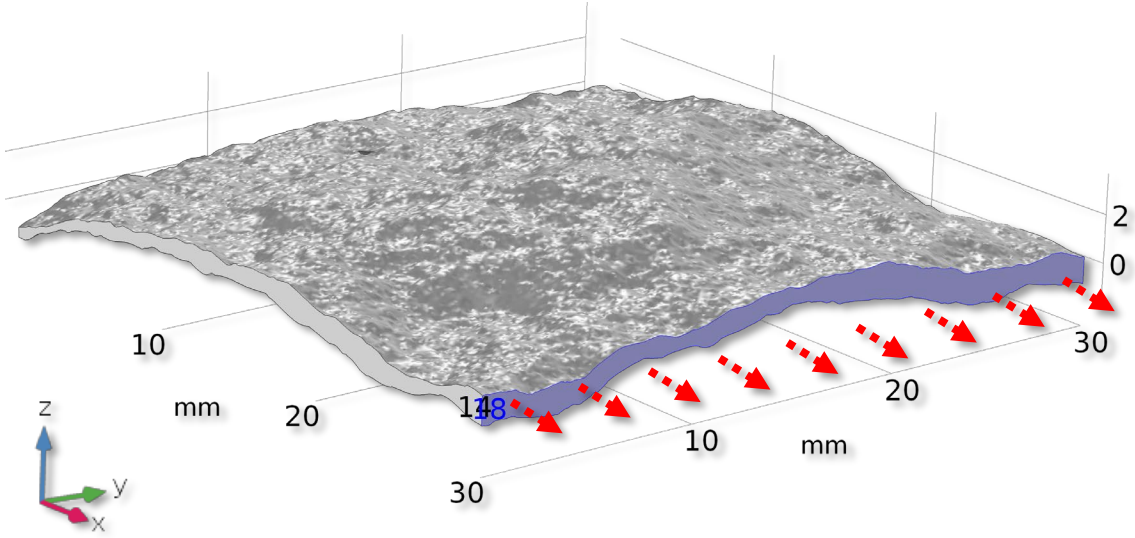

Figure. Model aperture geometry with thermal outflow boundary highlighted.

III. Parameters of Interest

Model Inputs

Independent Variable	*Unit*	*Value(s) Used*
Inlet velocity	[m/s]	1E-4,1E-3, 1E-2, 0.3, 0.5, 0.1
Hurst exponent *(H)*	[-]	0.75, 0.90, 0.935
Fracture surface slip	[mm]	0, 1.5

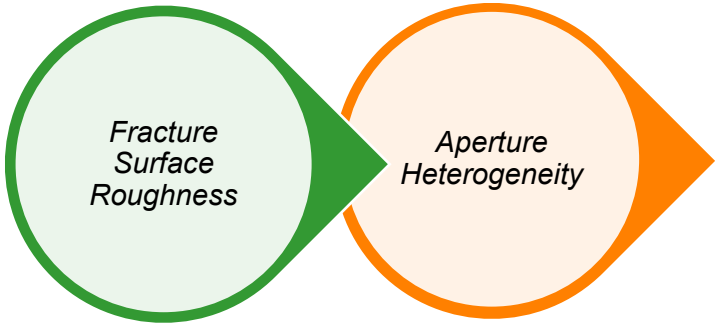

COMSOL Flow & Heat Transfer Model

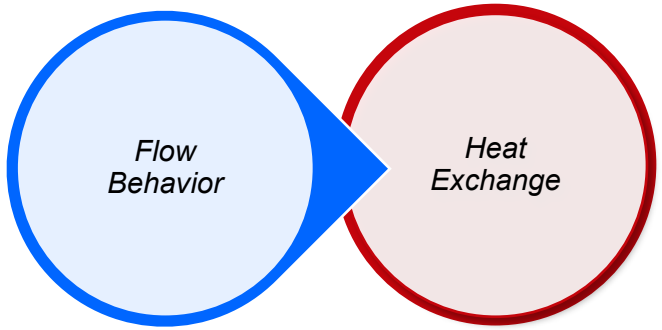

Model Outputs

Dependent Variable	*Unit*
Volumetric flow rate	[m^3/s]
Fracture surface heat flow	[W]

III. Model Run Scheme

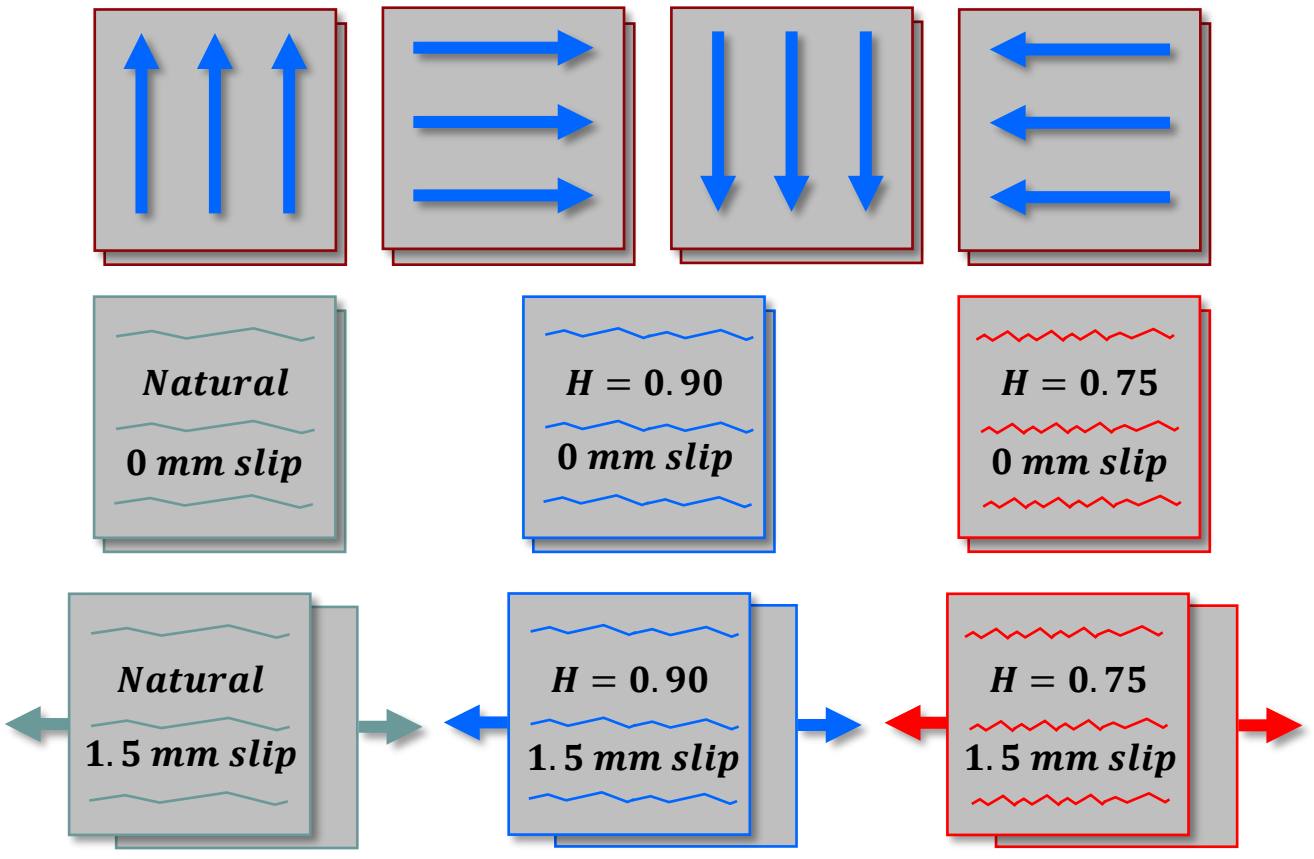

4 Flow orientations

Directional dependence

6 Fracture apertures

Fracture surface roughness

Aperture heterogeneity

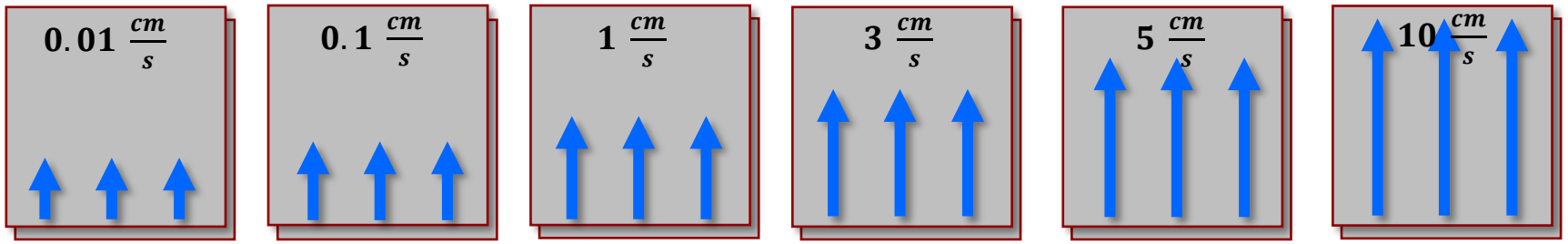

6 Inlet velocities

Overview

I. Introduction

II. Methods

III. Flow Modeling

IV. Results & Discussion

  I. Working backwards to link processes

V. Conclusions

IV. Results & Discussion: Working Backwards

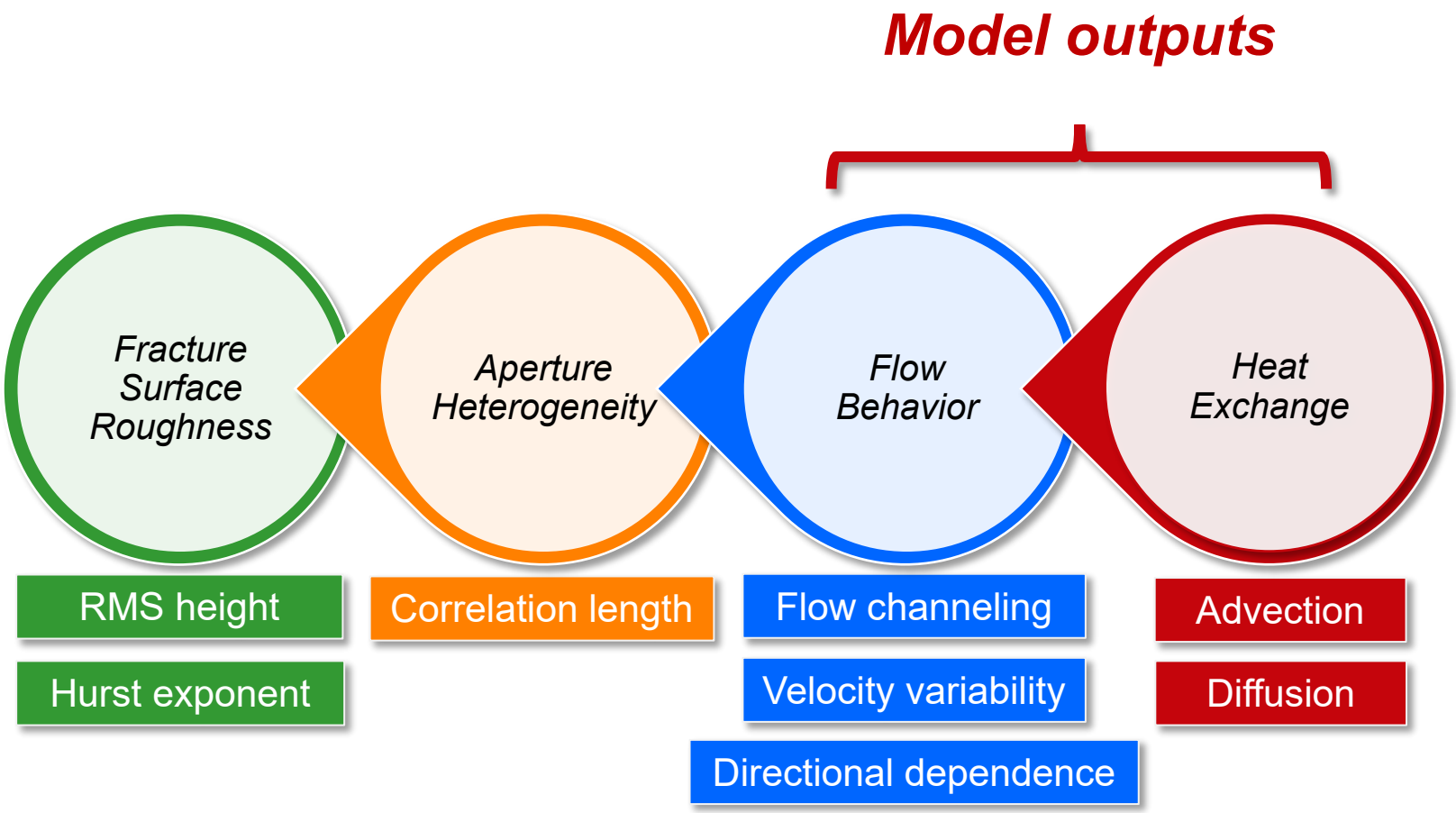

IV. Linking Flow and Heat Exchange

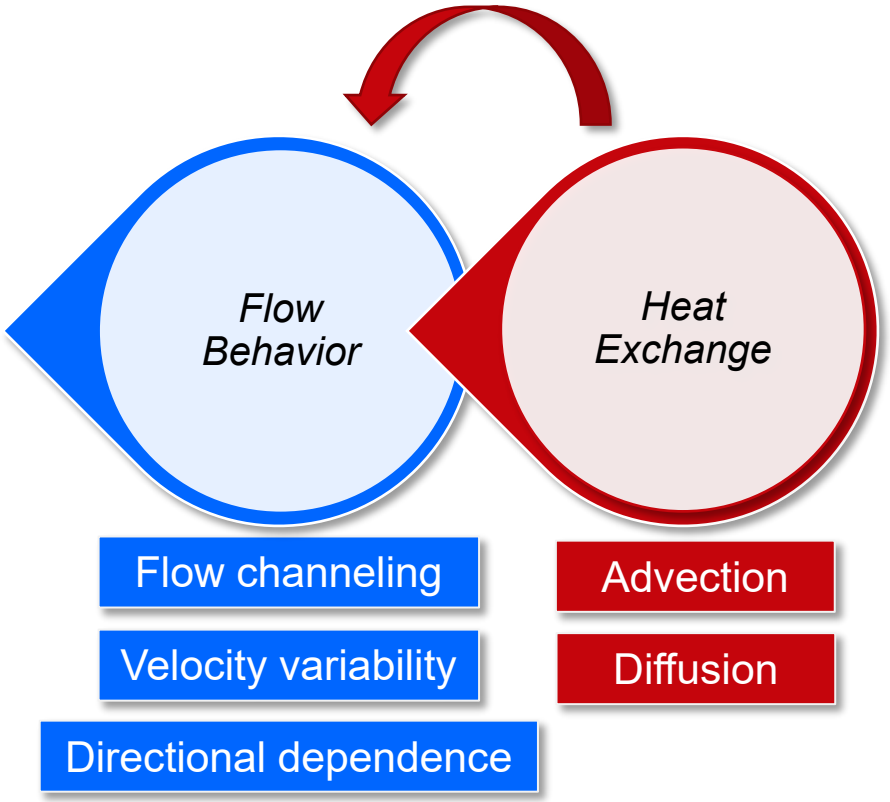

IV. L1: Flow Channeling & Advective Heat Flux

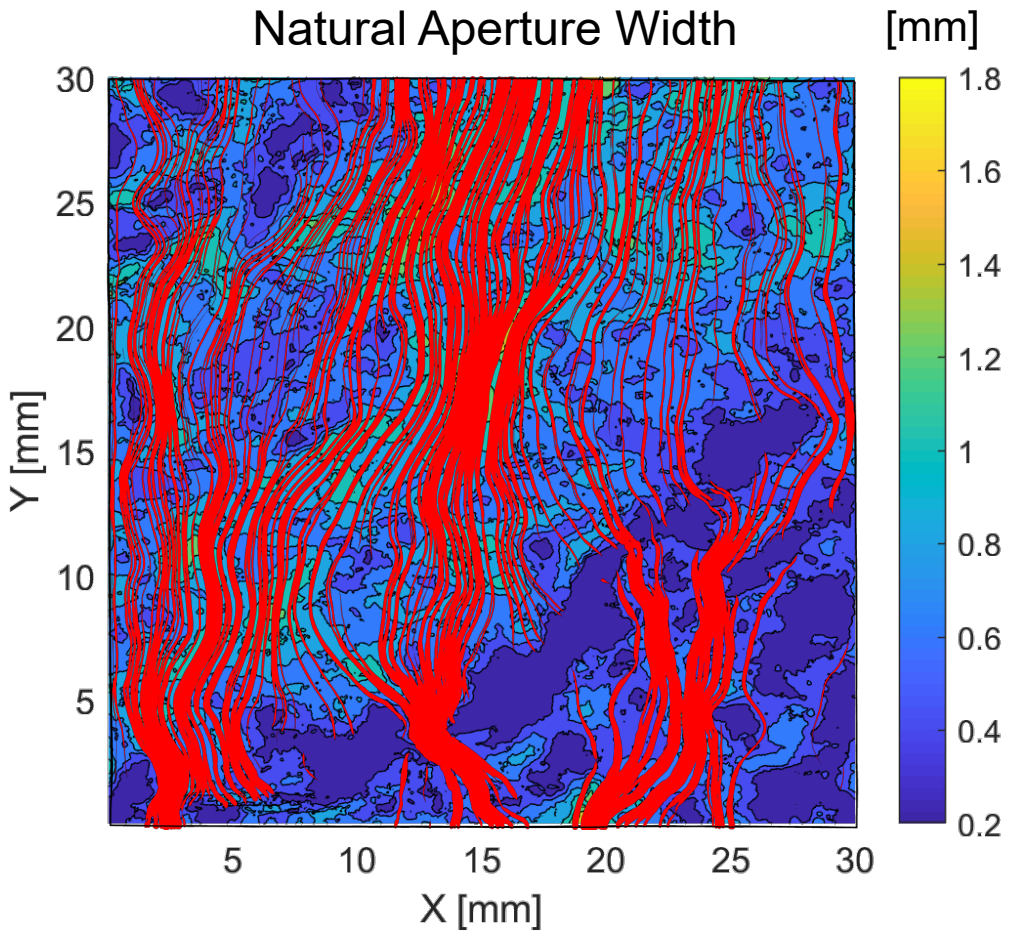

Figure. Y-direction streamlines from steady state Stokes flow solution superimposed on aperture width distribution.

Flow direction

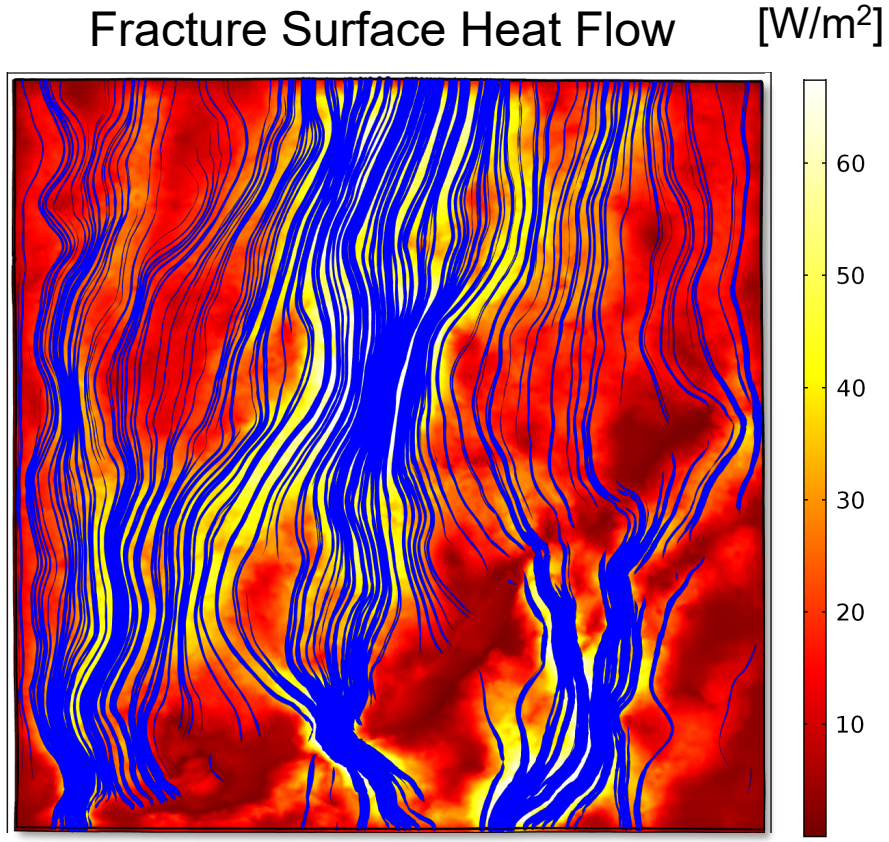

Mean heat flux = 26.2 [W/m^2]

Figure. Fracture surface heat flux magnitude from coupled steady state Stokes flow and heat ADE solution.

IV. Results: Linking Flow & Heat Exchange

IV. L1: Flow Channeling & Advective Heat Flux

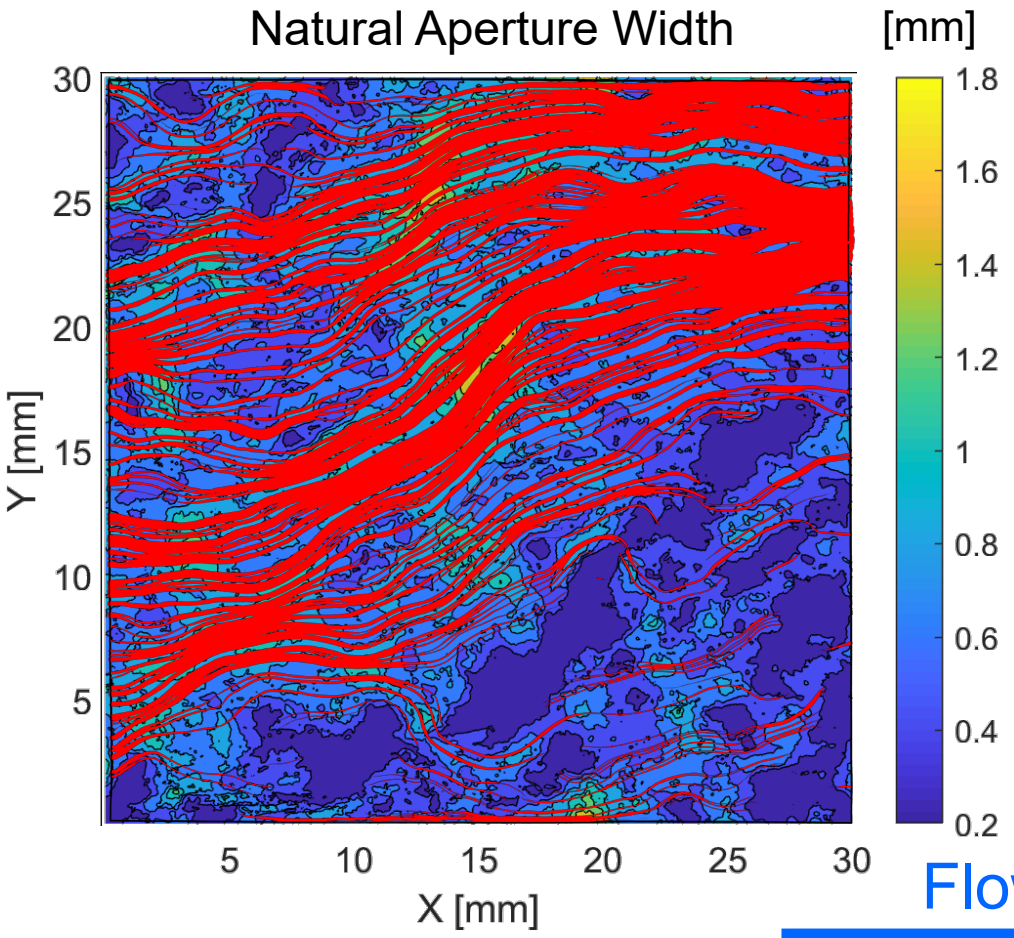

Figure. Y-direction streamlines from steady state Stokes flow solution superimposed on aperture width distribution.

Flow direction

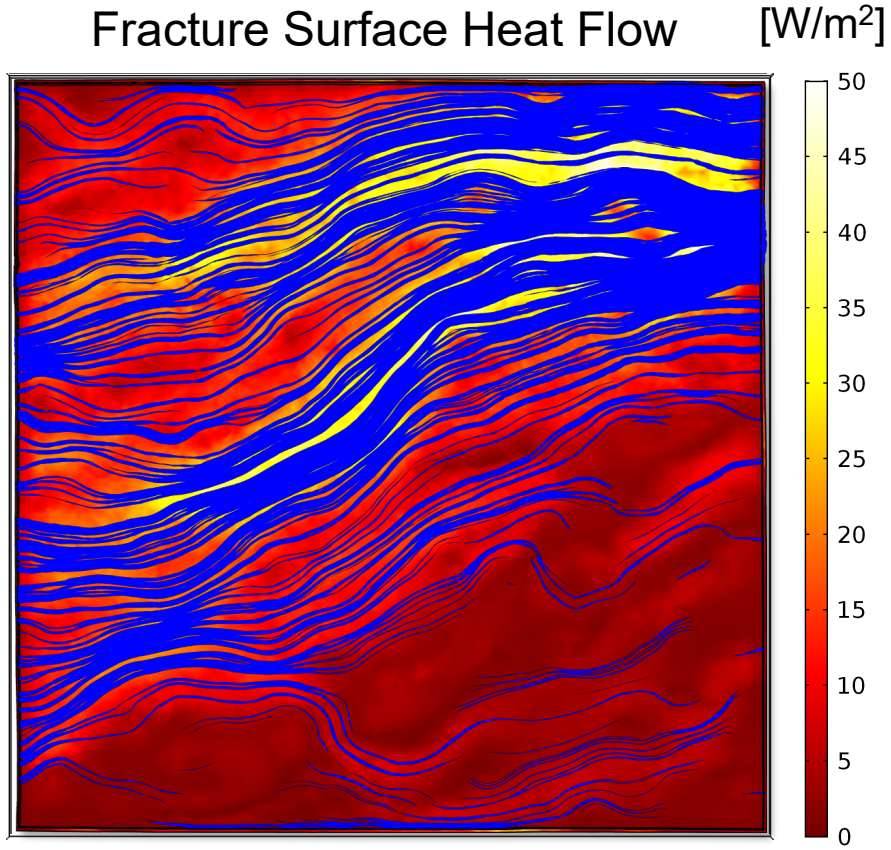

Mean heat flux = 21.4 [W/m^2]

Figure. Fracture surface heat flux magnitude from coupled steady state Stokes flow and heat ADE solution.

IV. Results: Linking Flow & Heat Exchange

IV. Linking Heat Exchange to Flow Behaivors

Heat exchange exhibits anisotropy which is dependent upon flow channel strength and distribution

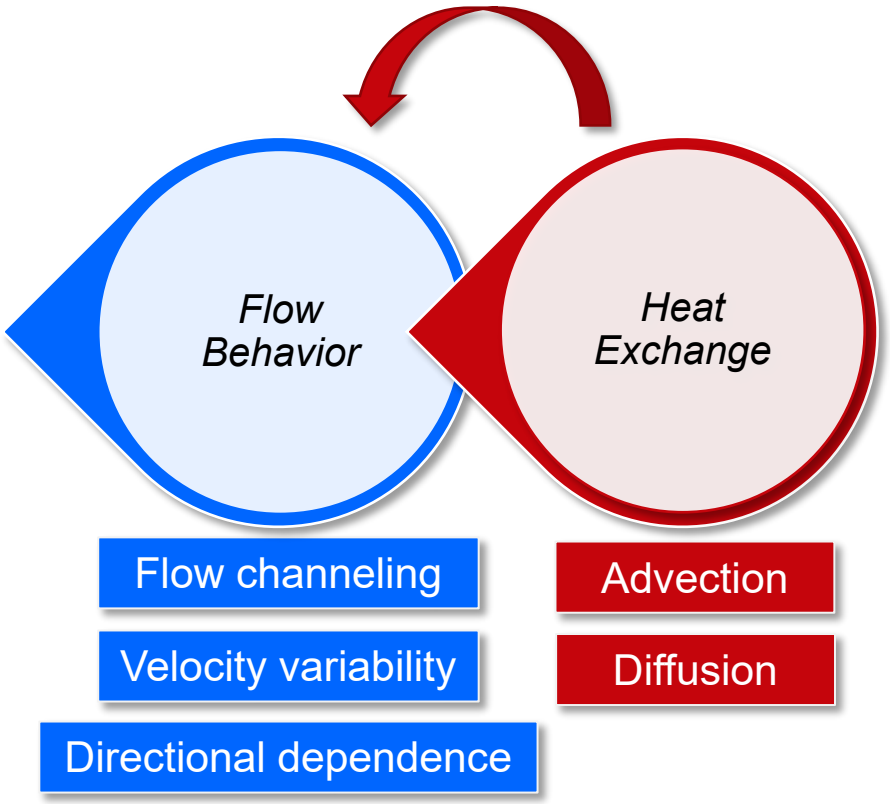

IV. Linking Flow to Aperture Heterogeneity

Heat exchange exhibits anisotropy which is dependent upon flow channel strength and distribution

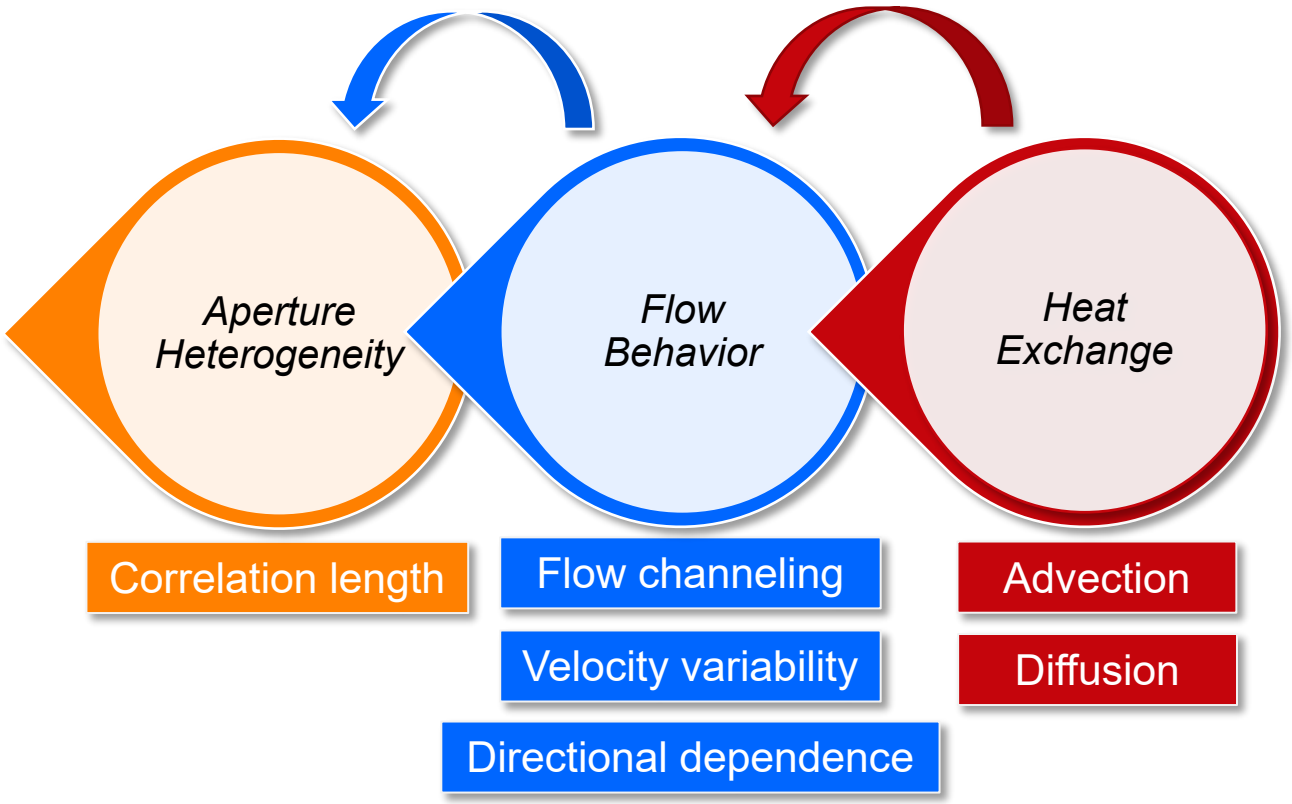

IV. L2: Correlation Length & Flow Channeling

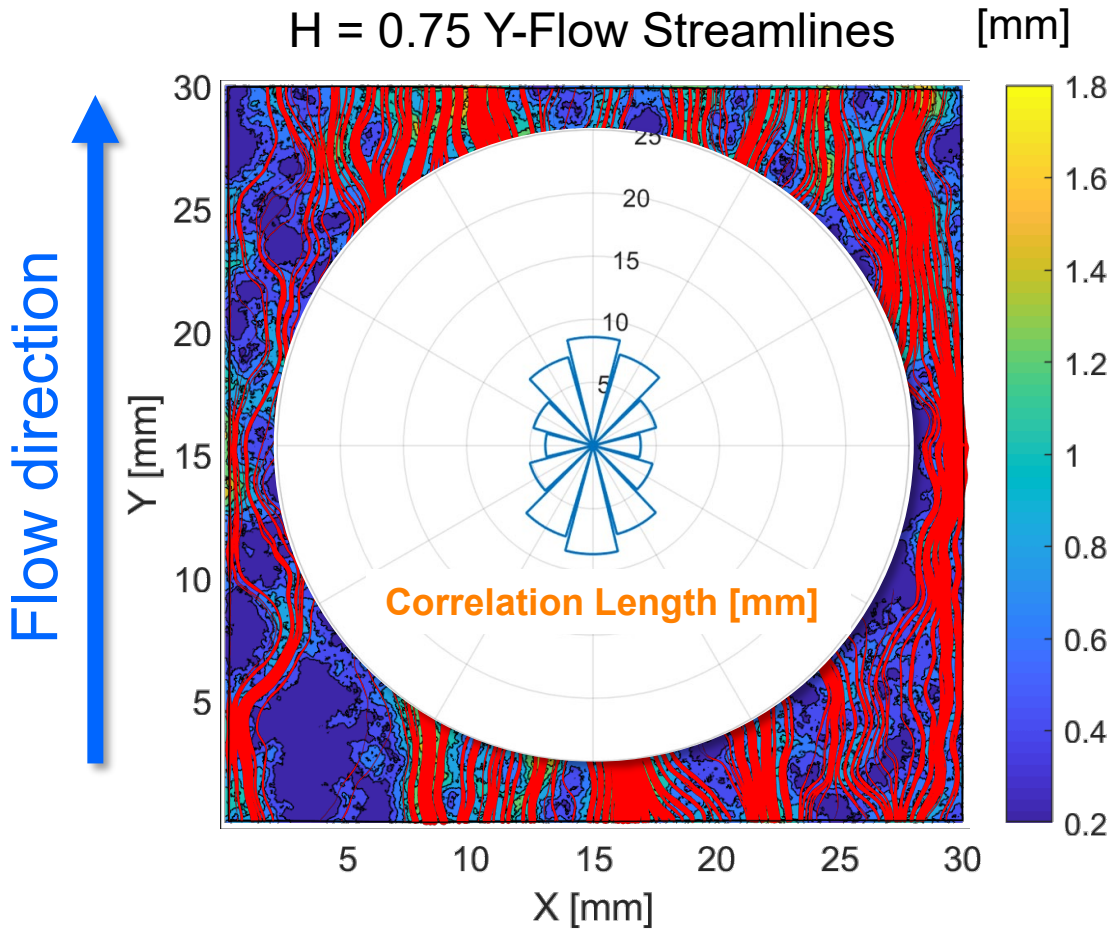

Figure. Y-direction streamlines from steady state 1 cm/s inlet Stokes flow solution superimposed on aperture width distribution.

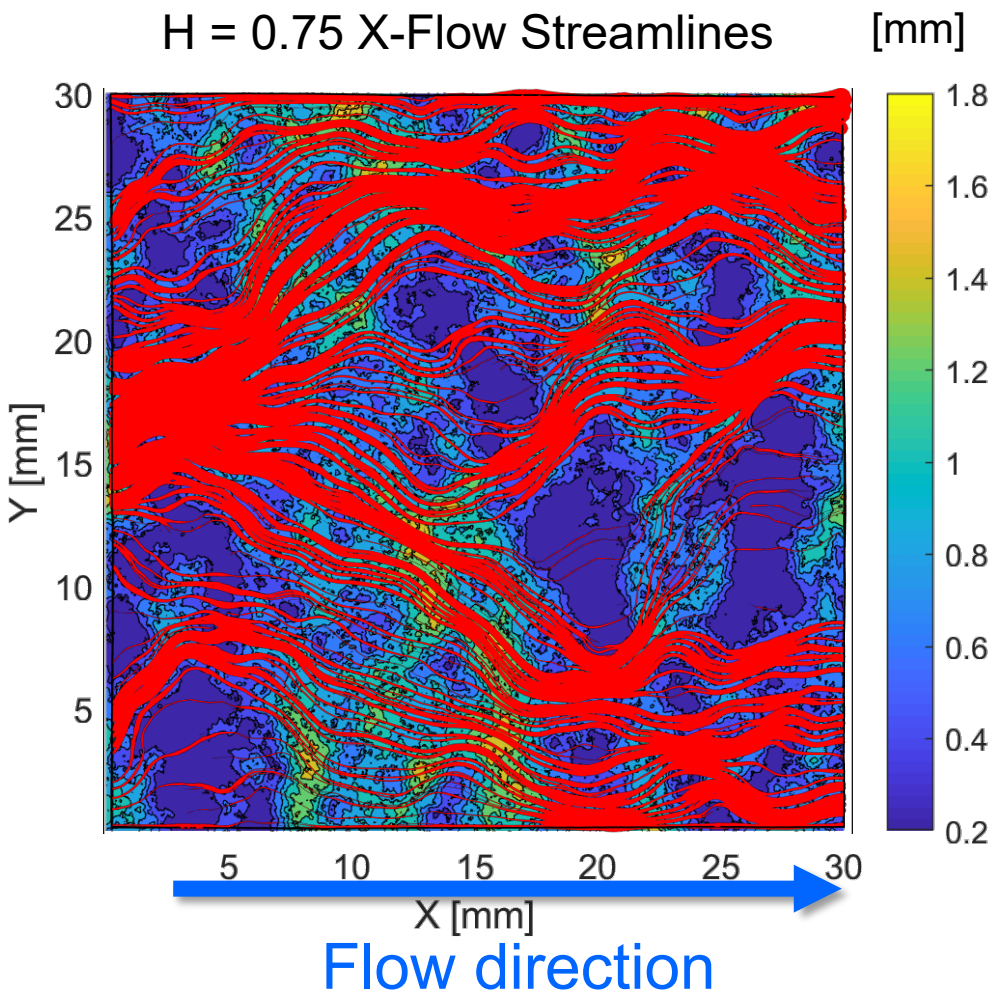

Figure. X-direction streamlines from steady state 1 cm/s inlet Stokes flow solution superimposed on aperture width distribution.

IV. L2: Correlation Length & Flow Channeling

Y-Flow Surface Heat Flow [W/m^2]

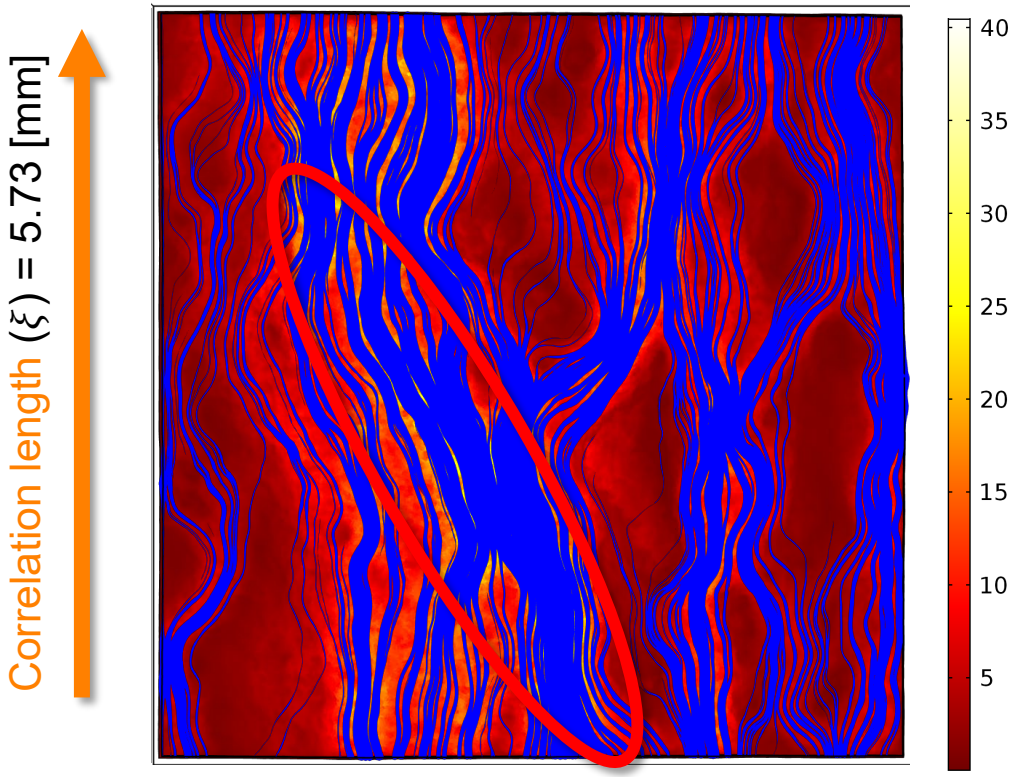

Figure. Y-Flow fracture surface heat flux magnitude from coupled steady state Stokes flow and heat ADE solution.

Mean heat flux = 14.8 [W/m^2]

X-Flow Surface Heat Flow [W/m^2]

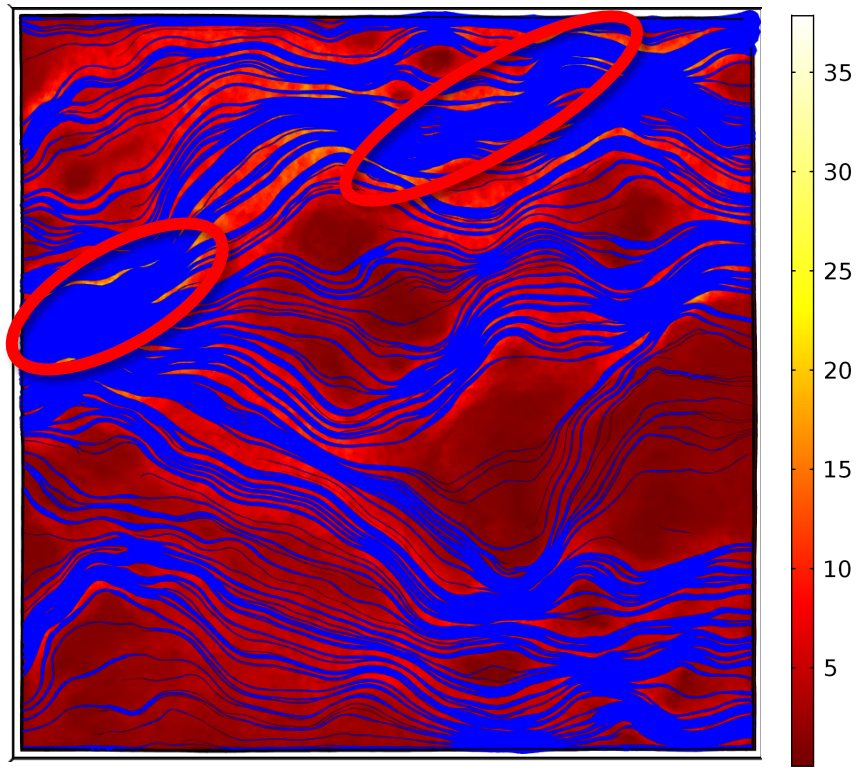

Figure. X-Flow fracture surface heat flux magnitude from coupled steady state Stokes flow and heat ADE solution.

Mean heat flux = 12.1 [W/m^2]

Correlation length (ξ) = 3.09 [mm]

IV. Linking Flow to Aperture Heterogeneity

Flow channel strength and distribution is dependent upon aperture width correlation length

Heat exchange exhibits anisotropy which is dependent upon flow channel strength and distribution

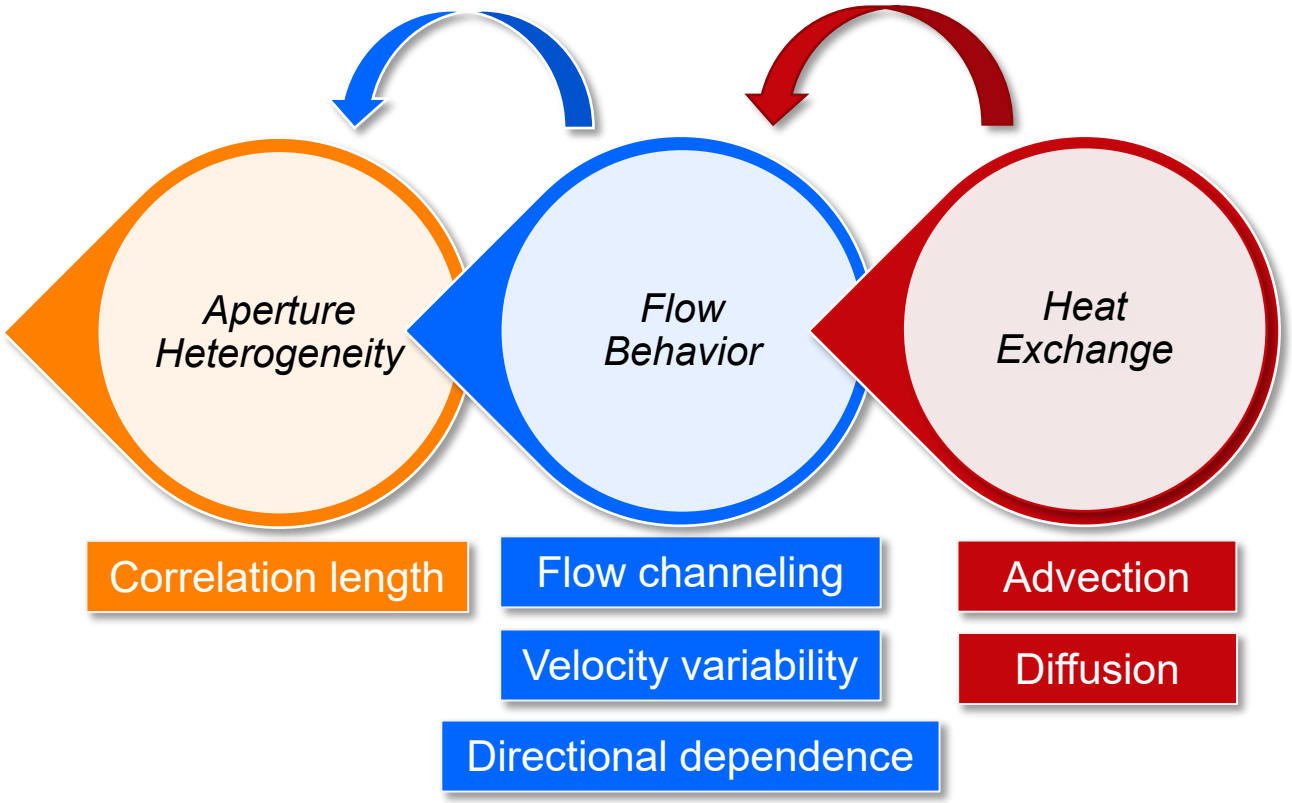

IV. Linking Aperture Heterogeneity to Roughness

Flow channel strength and distribution is dependent upon aperture width correlation length

Heat exchange exhibits anisotropy which is dependent upon flow channel strength and distribution

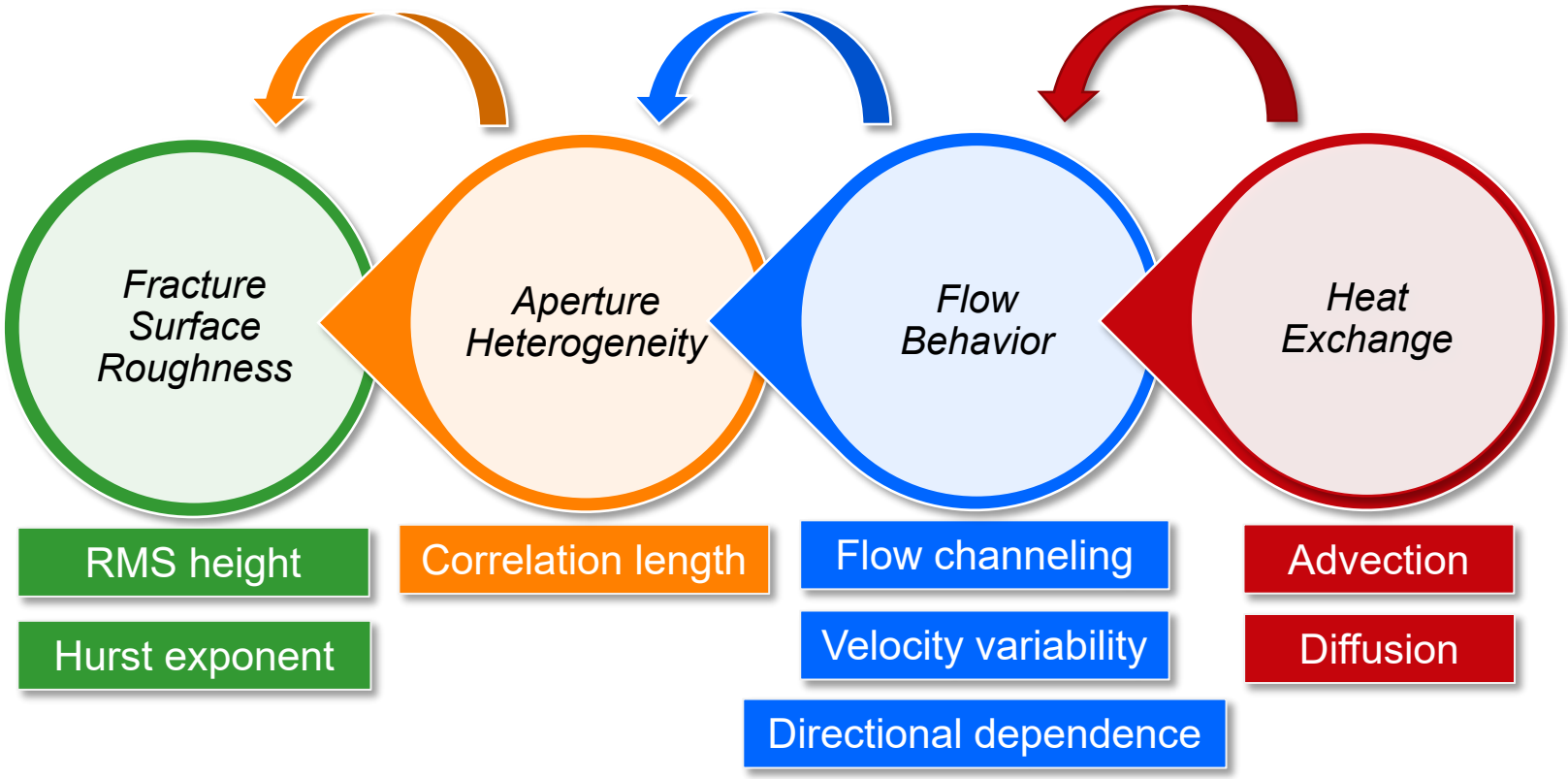

IV. L3: Surface Roughness & Correlation Length

Roughest Surface roughness used to create aperture **Smoothest**

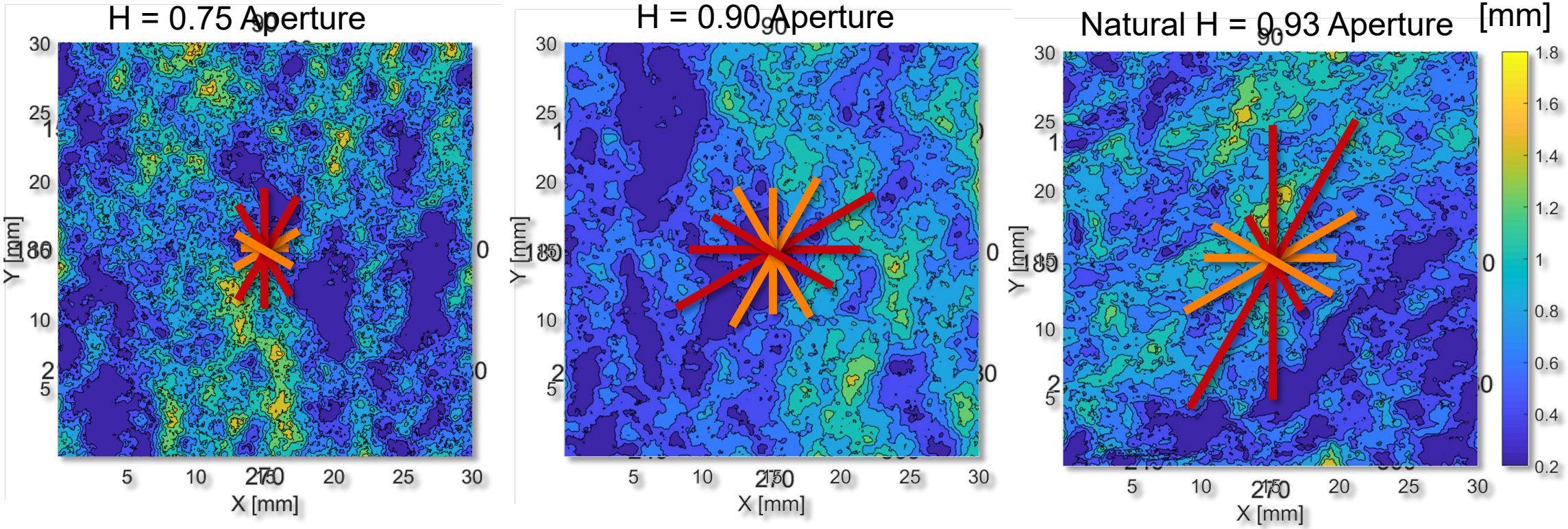

Shortest Average correlation length (variability) **Longest**

IV. From Surface Roughness to Heat Exchange

Aperture width correlation length decreases with increased fracture surface roughness

Flow channel strength and distribution is dependent upon aperture width correlation length

Heat exchange exhibits anisotropy which is dependent upon flow channel strength and distribution

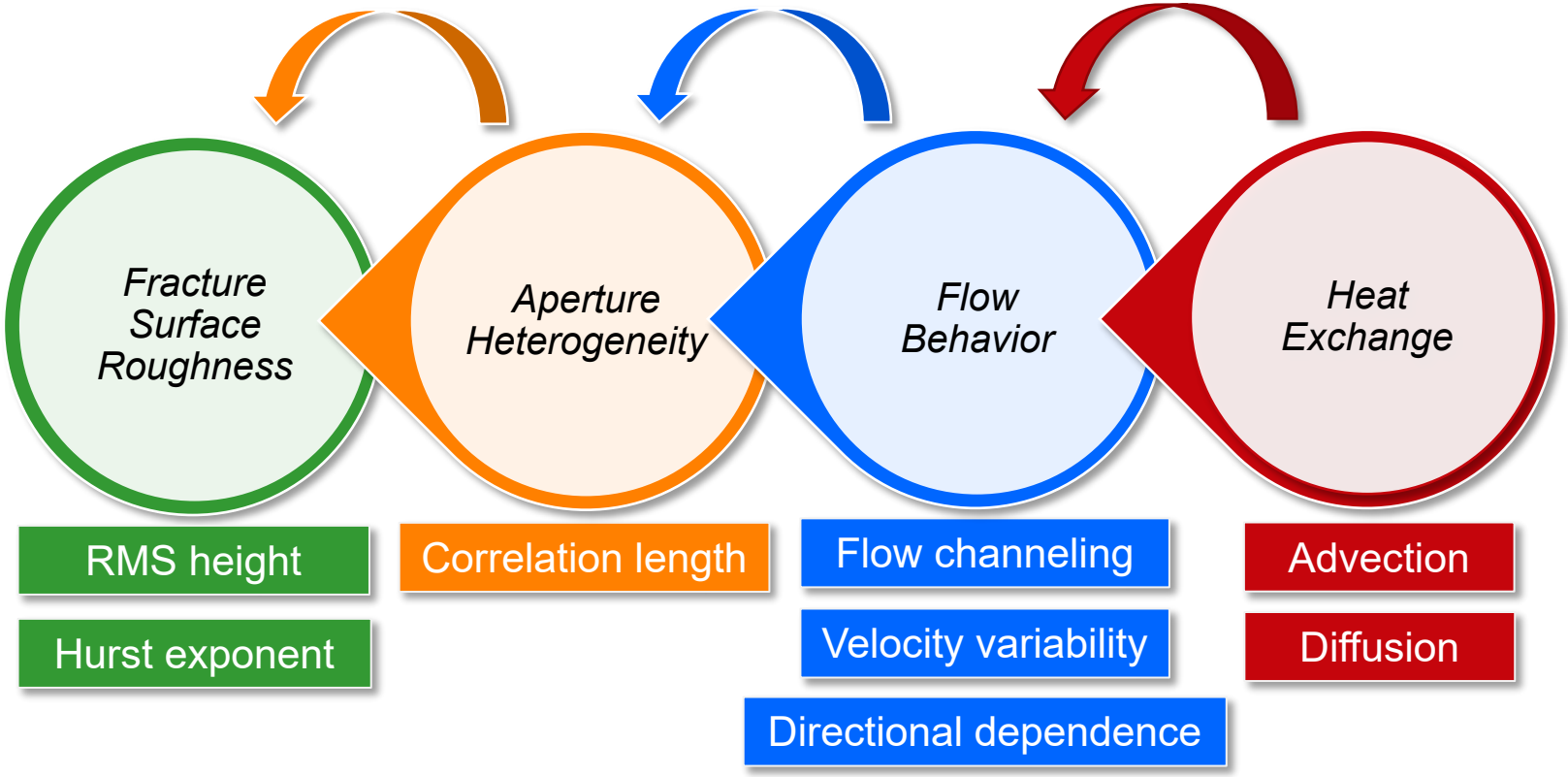

IV. Quick Aside: Peclet Number & Upscaling

- Dimensionless Peclet number Pe may be used to simulate results within a larger domain:

$$Pe = \frac{advective\ transport\ rate}{diffusive\ transport\ rate} = \frac{U * l}{\alpha}$$

$$Where \begin{cases} U = Fluid\ velocity & [m/s] \\ l = Characteristic\ length & [m] \\ \alpha = Thermal\ diffusivity & [m^2/s] \end{cases}$$

- Characteristic length l (aperture) & thermal diffusivity α are held constant.

- Increasing inlet flow velocity *U* in **small model domain** results in Pe consistent with **larger *model domain*** with upscaled roughness features.

IV. Heat Flux & Surface Roughness

- **Non-sheared** aperture models possess **uniform apertures** but variable surface roughness
- The effect of surface roughness on heat flux may be evaluated directly for each model
- Viscous sublayer thickness (δ) provides a plausible explanation for result

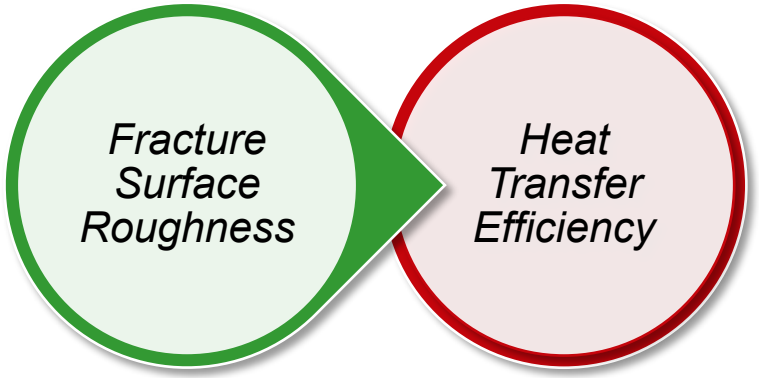

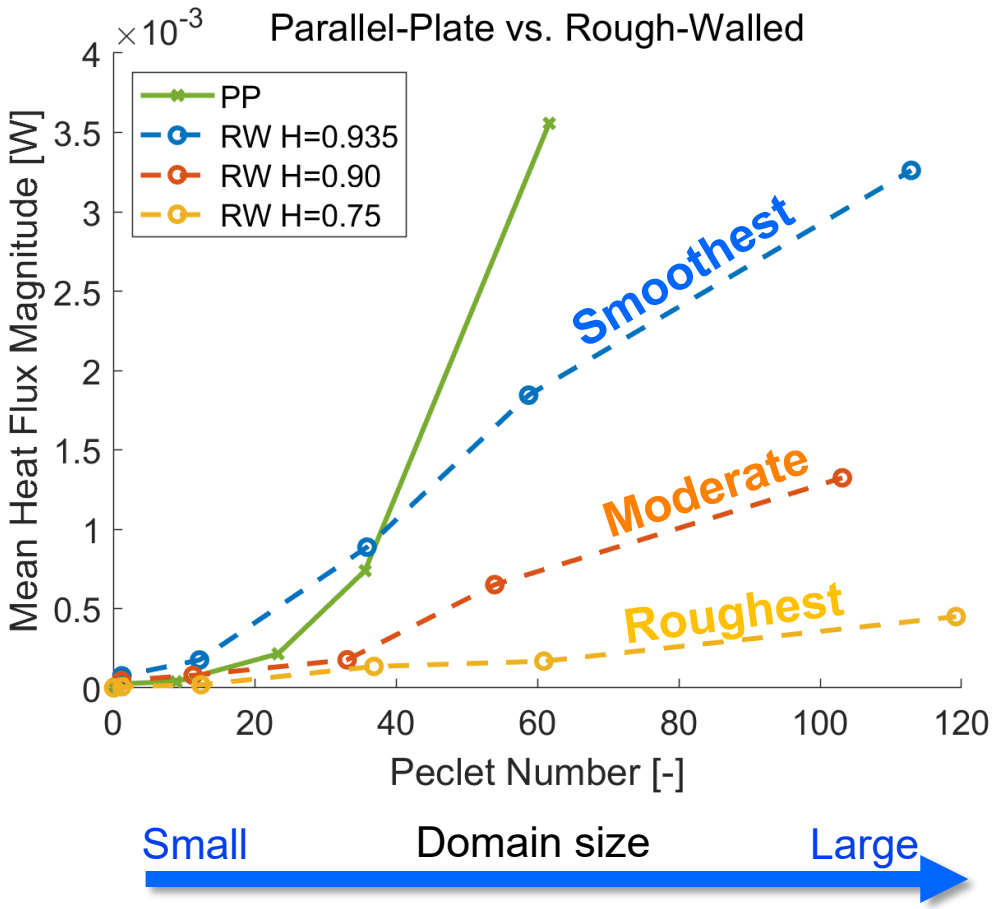

Figure. Parallel plate vs. rough-walled aperture heat output.

IV. Heat Flux & Surface Roughness

- **Non-sheared** aperture models possess **uniform apertures** but variable surface roughness
- The effect of surface roughness on heat flux may be evaluated directly for each model
- Viscous sublayer thickness (δ) provides a plausible explanation for result

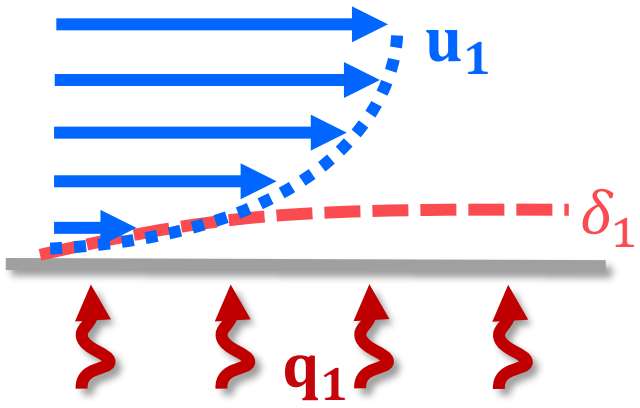

Figure. Boundary layer thinning at high H.

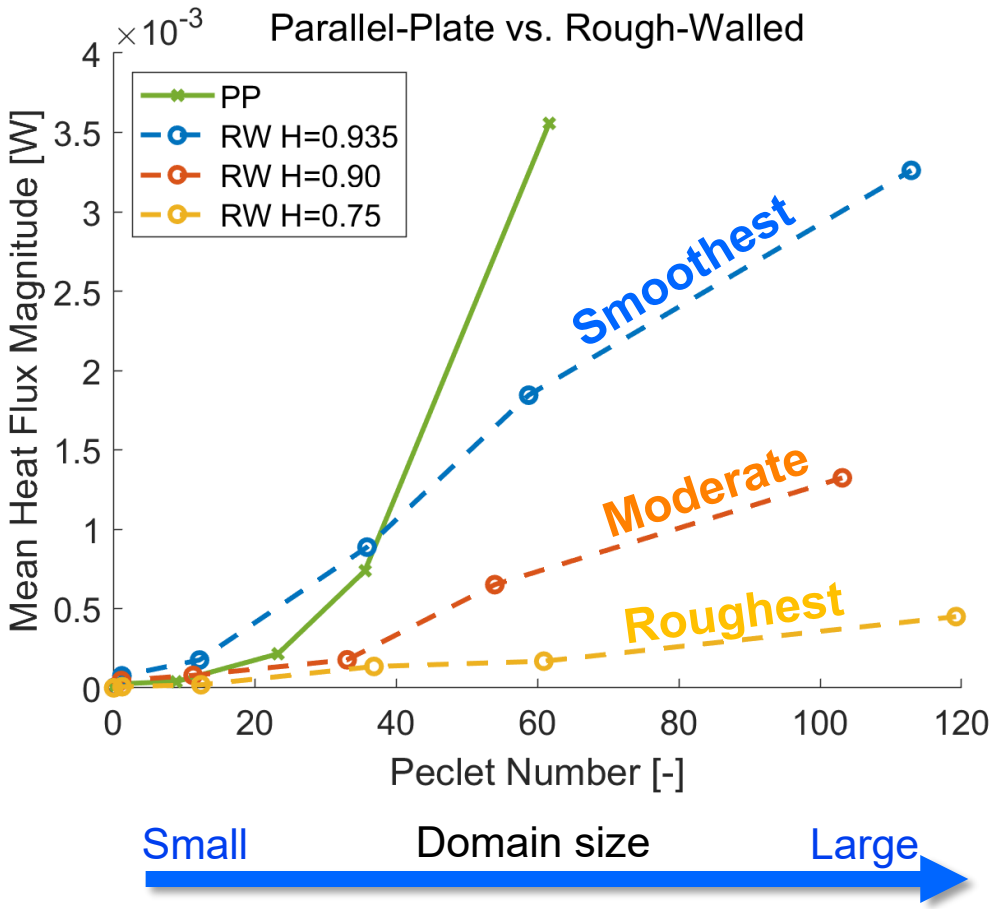

Figure. Parallel plate vs. rough-walled aperture heat output.

IV. Heat Flux & Surface Roughness

- **Non-sheared** aperture models possess **uniform apertures** but variable surface roughness
- The effect of surface roughness on heat flux may be evaluated directly for each model
- Viscous sublayer thickness (δ) provides a plausible explanation for result

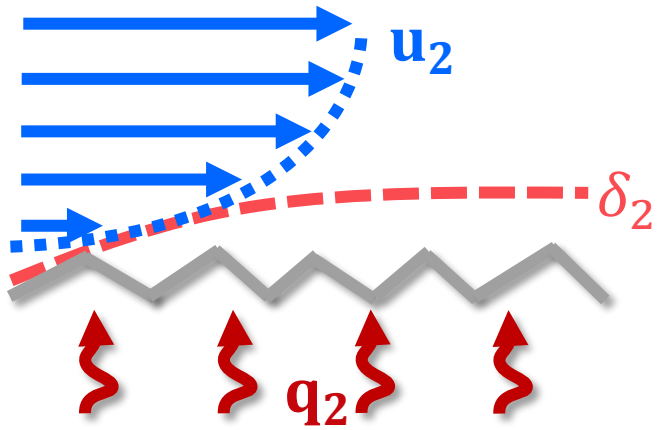

Figure. Boundary layer thickening at low H.

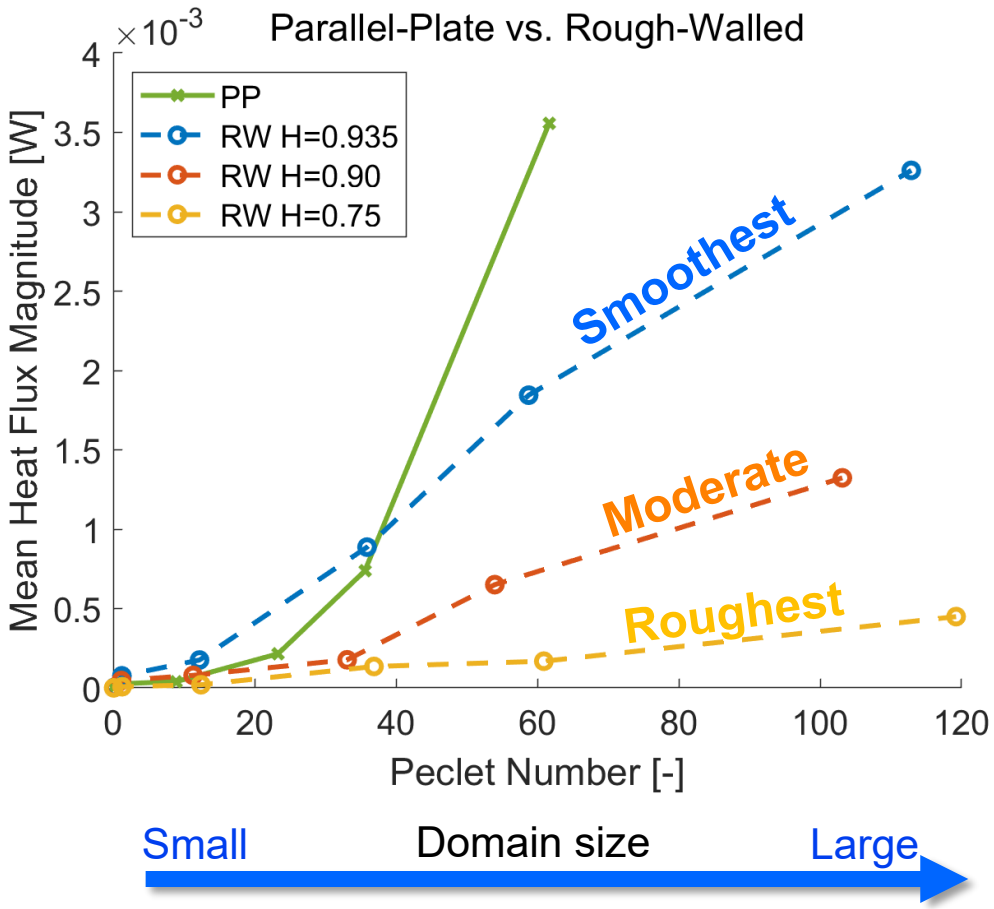

Figure. Parallel plate vs. rough-walled aperture heat output.

IV. Correlation Anisotropy → Heat Flow Anisotropy

- Longer aperture width correlation lengths in the direction of flow yield greater heat flux
- This effect is observed across all models

Surface roughness used to create aperture

Roughest → **Smoothest**

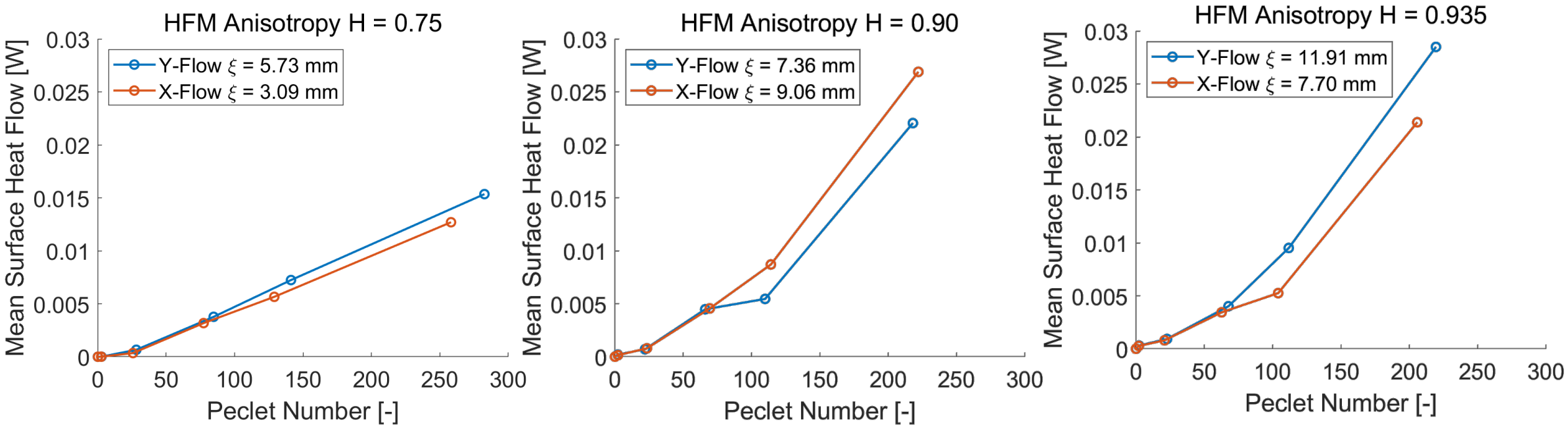

Figure. Aperture width correlation length effect on heat output.

Overview

I. Introduction

II. Methods

III. Flow Modeling

IV. Results & Discussion

V. Conclusions

V. Conclusions

Primary findings of work:

1. Fracture surface roughness increases heterogeneity and reduces aperture width correlation length
2. Aperture width correlation length has a controlling effect on flow channel strength and distribution
3. Heat exchange exhibits anisotropy which is dependent upon flow channel strength and distribution
4. Under laminar flow conditions, fracture surface roughness reduces heat transfer efficiency

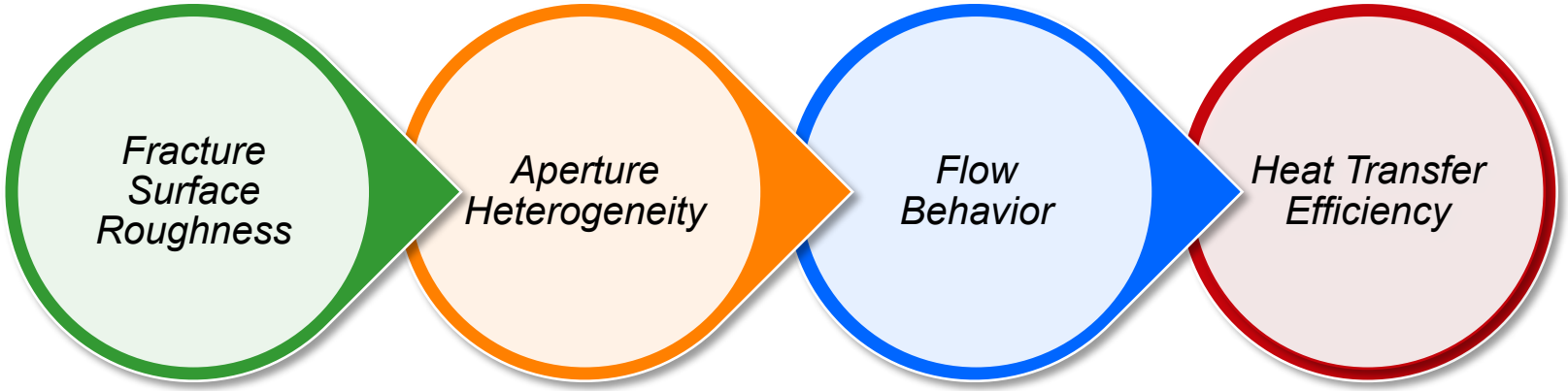

Acknowledgements

Technical support

- Ben Abernathy
- Dougal Hansen
- TEAM Lab
  - Mike Hughes
  - Joel Ballweg
- Rock mechanics group
  - Kate Condon
  - Ryan O'Connell

Family, Friends, Colleagues

- My family
- Monica Garcia
- Andrew Walters
- Shlomo Honig
- Geoscience grad students
- Many others

Funding

- UW Dept. of Geoscience
- National Science Foundation

Committee

- Michael Cardiff
- Hiroki Sone
- Luke Zoet

Hydrogeology Group

- Jeremy Patterson
- Collin Roland
- Catherine Christenson
- Laura Schachter

VI. Appendix

Additional Content

A) Asperity orientation & fracture permeability

B) Conservative solute transport & dispersivity estimation

C) Solutions to flow in a single fracture

D) Geostatistical fracture surface evaluation

E) Numerical model validation

VI-A. Asperities & Fracture Permeability

- The normalized hydraulic aperture (b_{eff}/b_{mech}) quantifies the reduction in fracture permeability relative to a parallel plate aperture due to aperture heterogeneity.

$$b_{eff} = \sqrt[3]{\frac{Q_{out}}{W}\frac{12\mu}{\rho g}\frac{L}{\Delta h}} = C\sqrt[3]{\frac{Q_{out}}{\Delta h}}$$

- Permeability in heterogeneous fractures is strongly dependent upon asperity orientation

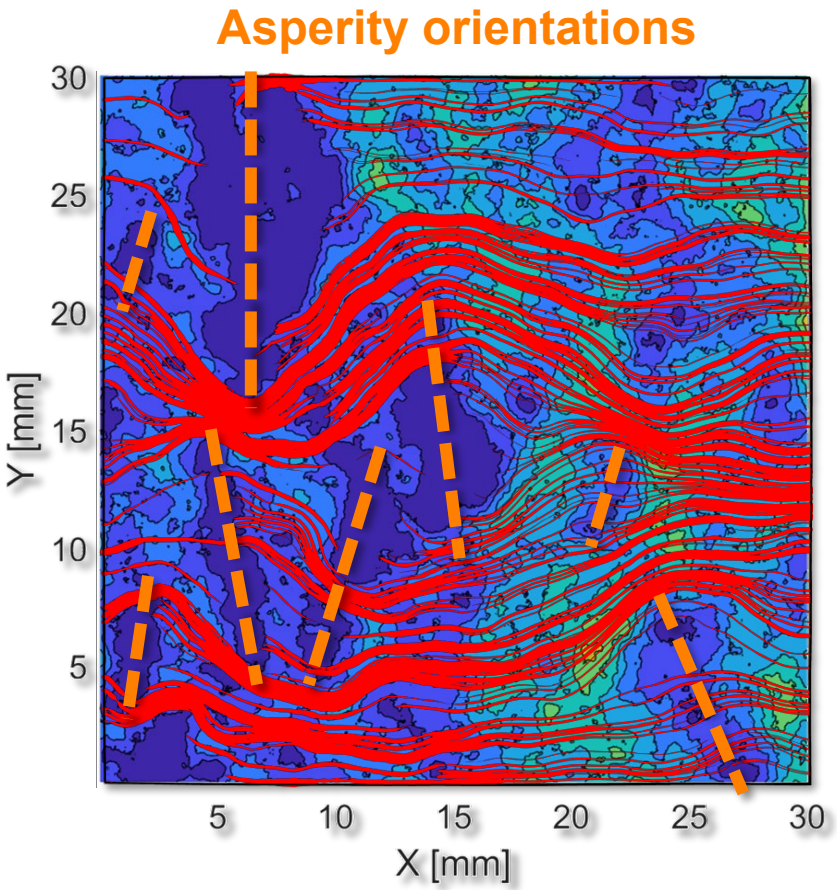

Figure. H = 0.90 aperture width distribution with long axis of major asperities denoted.

VI-A. Asperities & Fracture Permeability

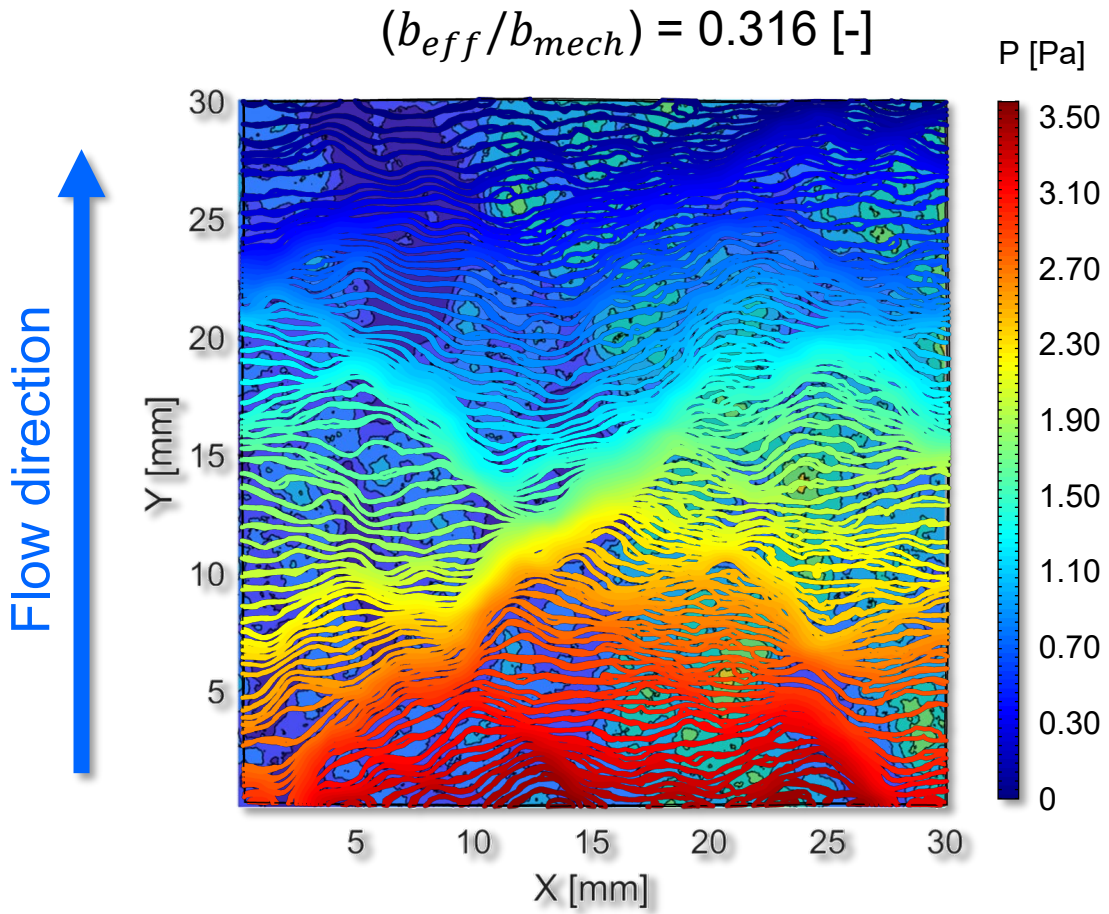

Figure. H = 0.90 aperture width distribution with pressure isobars from Y-direction Stokes flow solution superimposed.

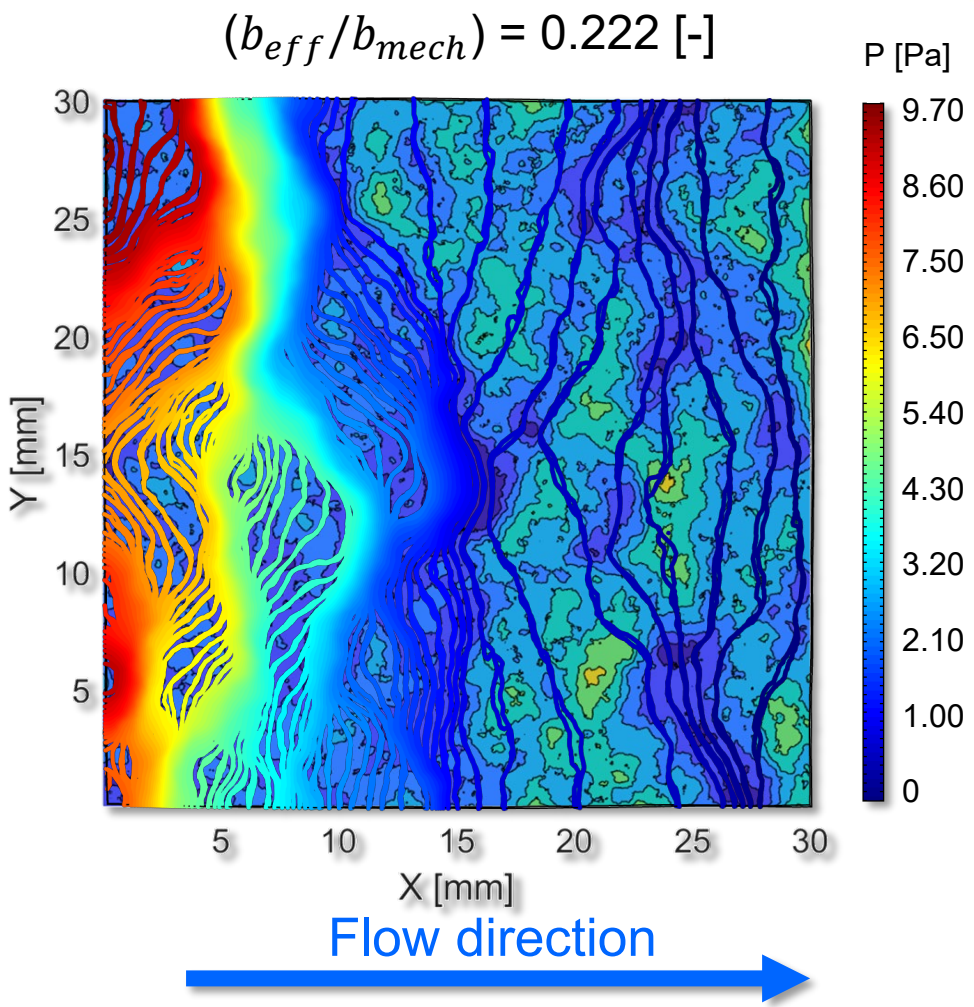

Figure. H = 0.90 aperture width distribution with pressure isobars from X-direction Stokes flow solution superimposed.

VI-B. Conservative Solute Transport Modeling

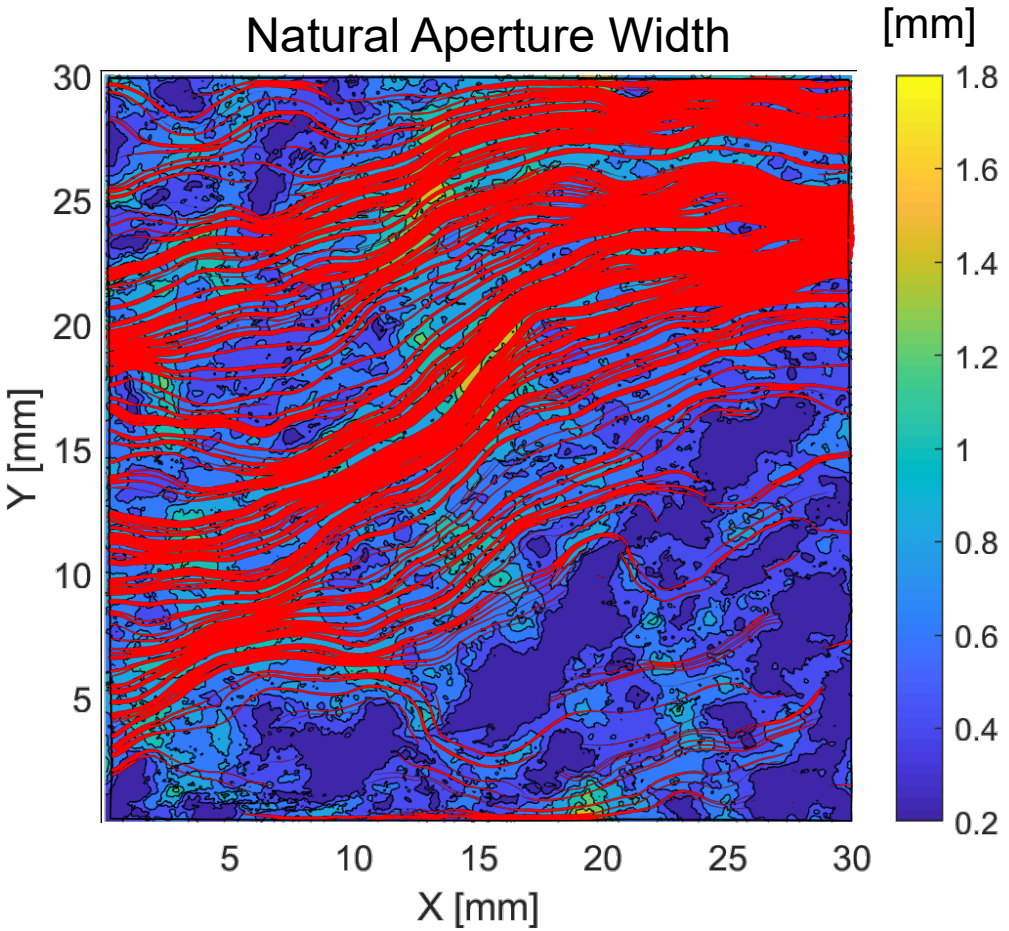

Correlation length (ξ) = 0.77 [cm]

Figure. Aperture width distribution & Stokes flow streamlines.

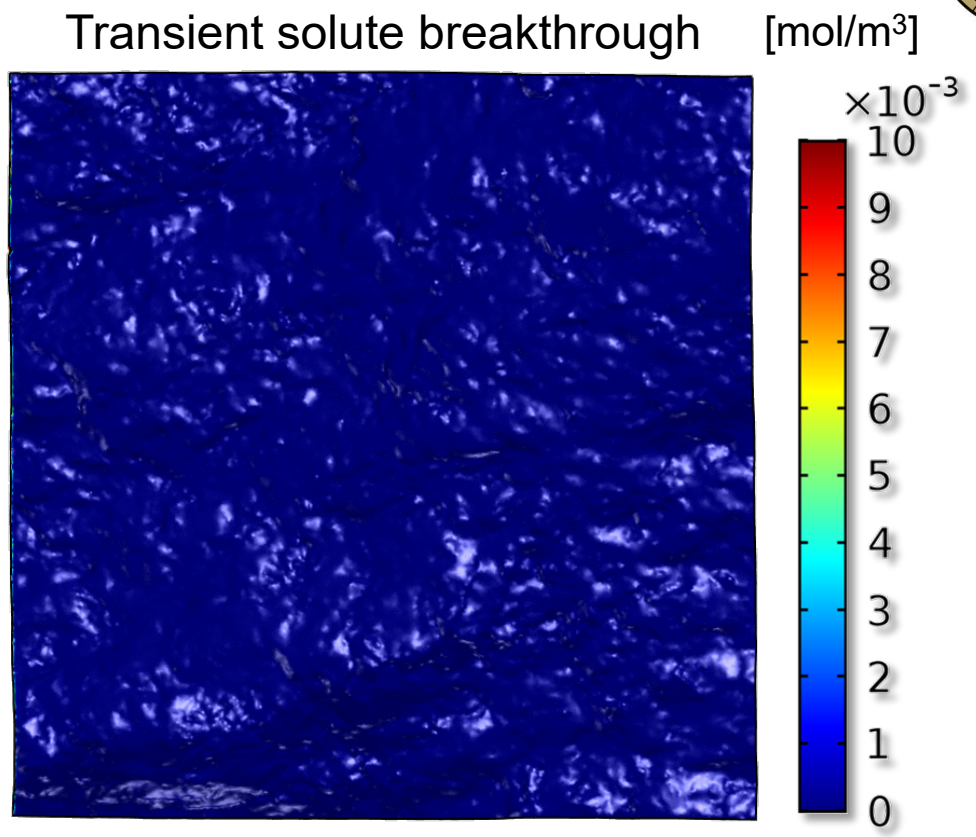

Effective dispersivity (α_{eff}) = 0.87 [cm]

Figure. Transient solute breakthrough concentration [mol/m^3] in natural fracture aperture.

VI-B. Conservative Solute Transport Modeling

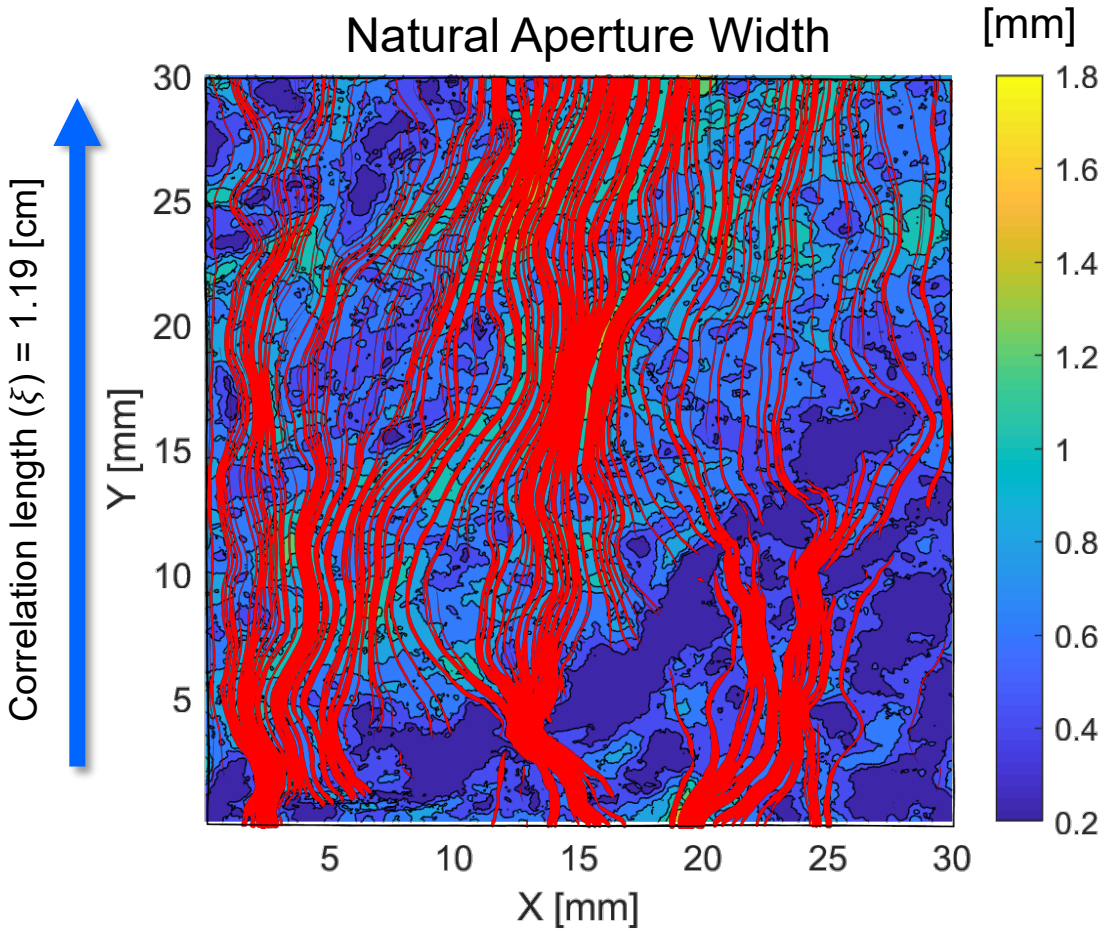

Figure. Aperture width distribution & Stokes flow streamlines.

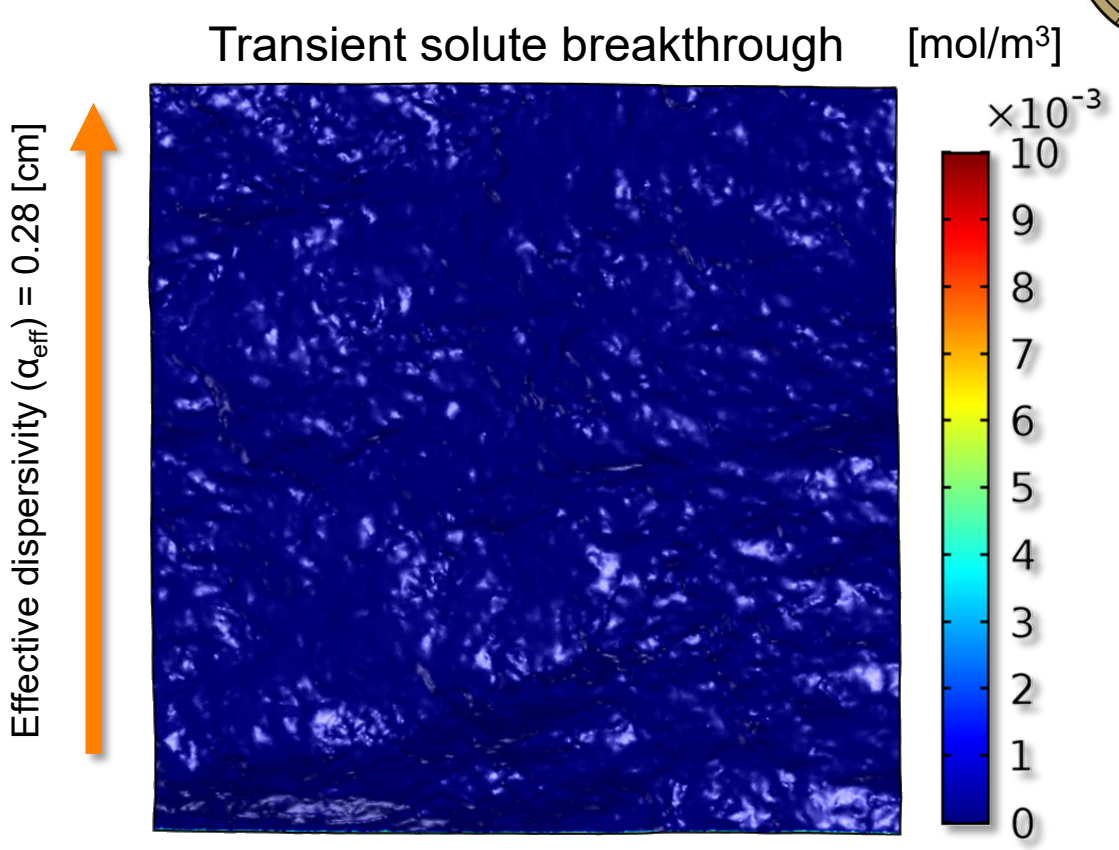

Figure. Transient solute breakthrough concentration [mol/m³] in natural fracture aperture.

VI-B. Conservative Solute Transport Modeling

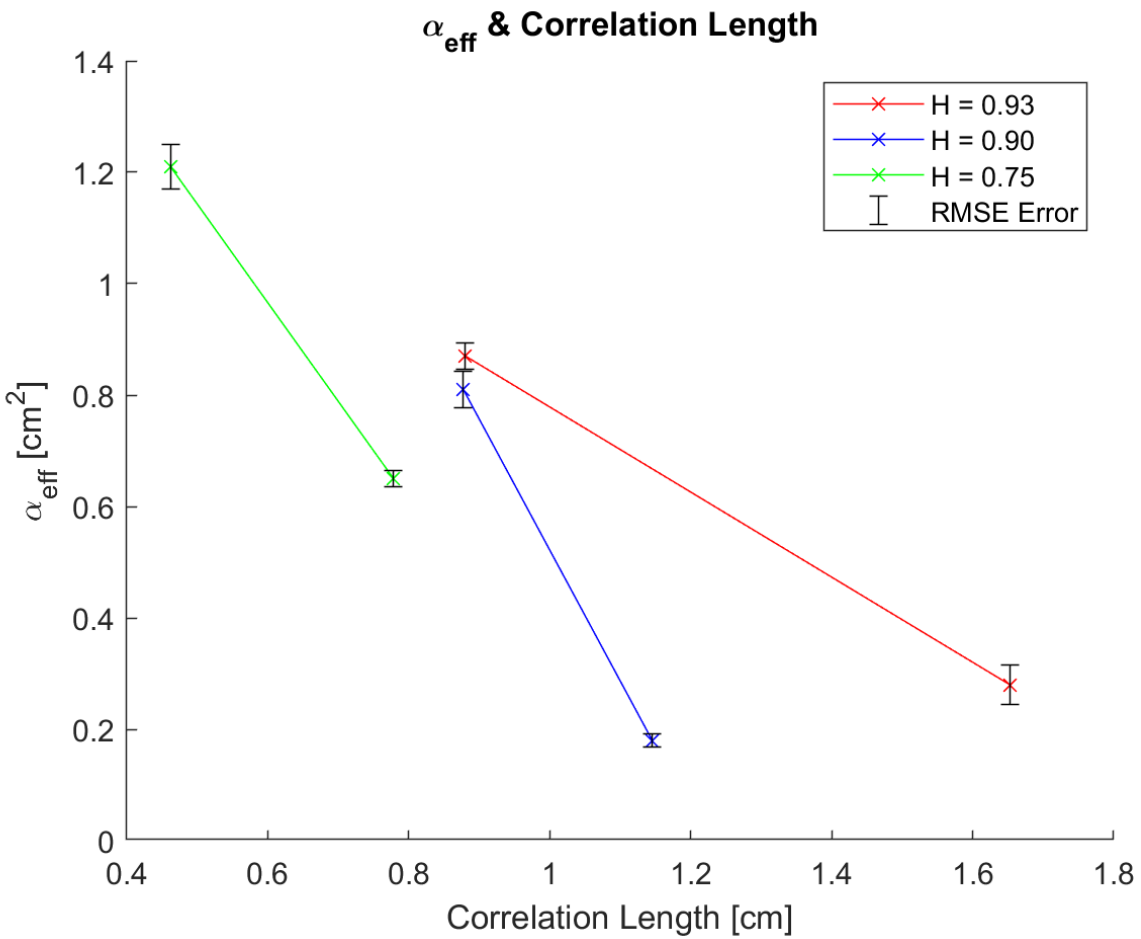

Figure. Effective dispersivity (α_{eff}) estimates plotted as a function of flow direction aperture width correlation length for all models. A negative correlation is generally observed.

VI-C. Flow in a Single Fracture

- Navier-Stokes equations for momentum balance describe the motion of viscous fluids

- Navier-Stokes equations (NSE) for an incompressible viscous fluid:

$$\frac{\partial \mathbf{u}}{\partial t} + (\mathbf{u} \cdot \nabla)\mathbf{u} = \nu \nabla^2 \mathbf{u} - \frac{1}{\rho}\nabla p \qquad \text{(momentum balance)}$$

convection viscous drag pressure

$$\nabla \cdot \mathbf{u} = 0 \qquad \text{(flow continuity)}$$

- The NSE are often used to describe fluid flow through a single fracture

VI-C. Parallel Plate Flow: The Cubic Law

- The most common solution to fracture flow approximates a parallel plate geometry.

- Solution to Navier-Stokes for parallel plate geometry:

$$Q = W \frac{\rho g}{12\mu} b^3 \frac{\nabla h}{L} \qquad \text{(cubic law)}$$

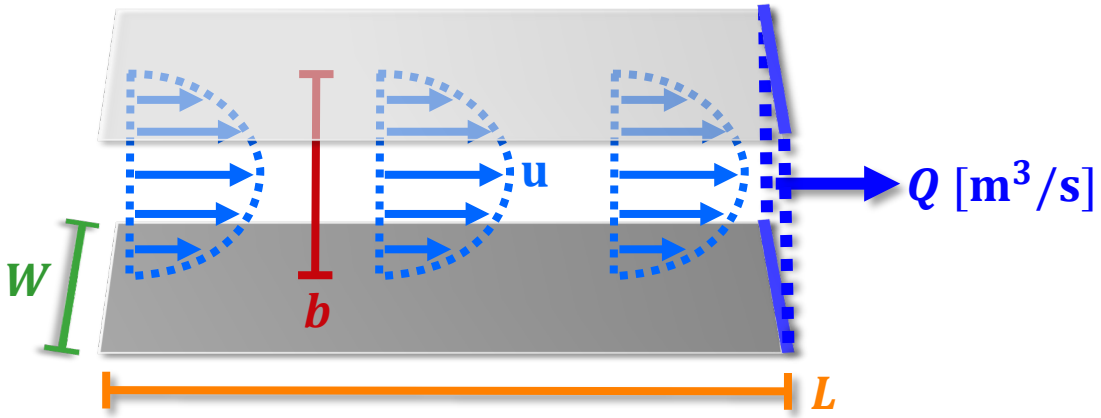

Figure. Parallel plate flow

- Assumptions:
  1. Constant aperture b throughout
  2. Flow tortuosity negligible (linear flow)
  3. Constant flow velocity

VI-C. The Local Cubic Law

- Local cubic law assumes *flow continuity* between *piecewise sections of fracture aperture*.

2-Dimensional analytical solution:

Local Cubic Law (LCL)

- Solution to Navier-Stokes for variable aperture:

$$Q = W \frac{\rho g}{12\mu} b^3 \frac{\nabla h}{L} \qquad \text{(local cubic law)}$$

$$\nabla \cdot \mathrm{Q} = 0 \qquad \text{(flow continuity)}$$

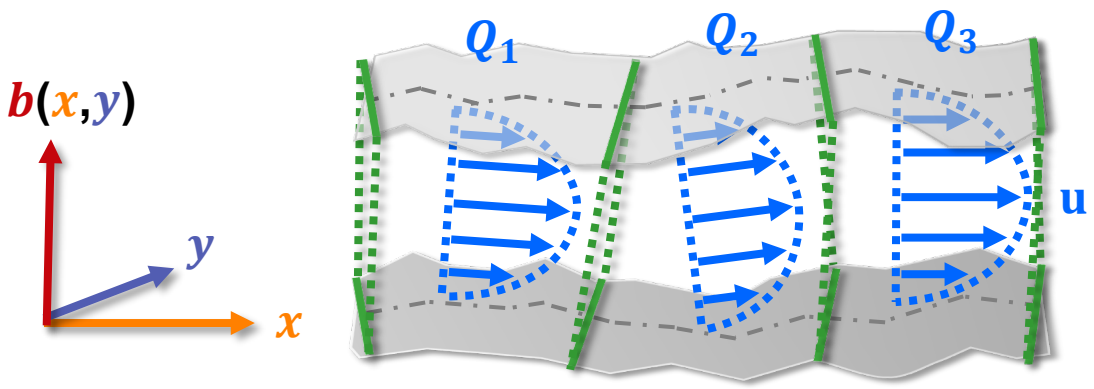

Figure. Local cubic law

- Assumptions:
  1. Solution validity limited to small roughness slopes
  2. Laminar flow assumed throughout (low Re)

VI-C. Stokes Flow in 3-Dimensions

- In 3-dimensions, fracture flow must be solved numerically.

3-Dimensional numerical solution:

Stokes Flow (creeping flow)

- Solution to Stokes flow equation in 3-dimensions:

$$\frac{\partial \mathbf{u}}{\partial t} = v\nabla^2\mathbf{u} - \frac{1}{\rho}\nabla p \qquad \text{(Stokes flow)}$$

$$\nabla \cdot \mathbf{u} = 0 \qquad \text{(flow continuity)}$$

- Assumptions:
  1. Laminar flow assumed throughout (low Re)

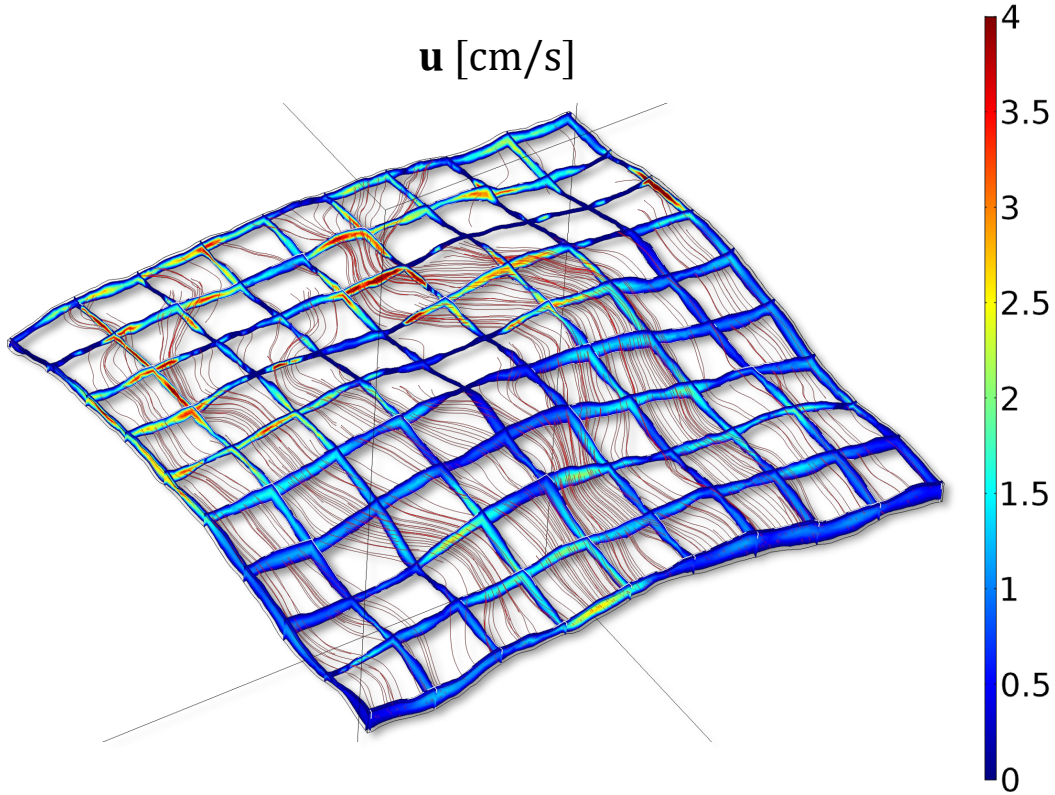

Figure. Stokes flow velocity solution in 3-D

VI-D. Fracture Surface Characterization

- Variogram used to estimate correlation length of granite surface at variable orientations
- Unbounded exponential model used to fit data

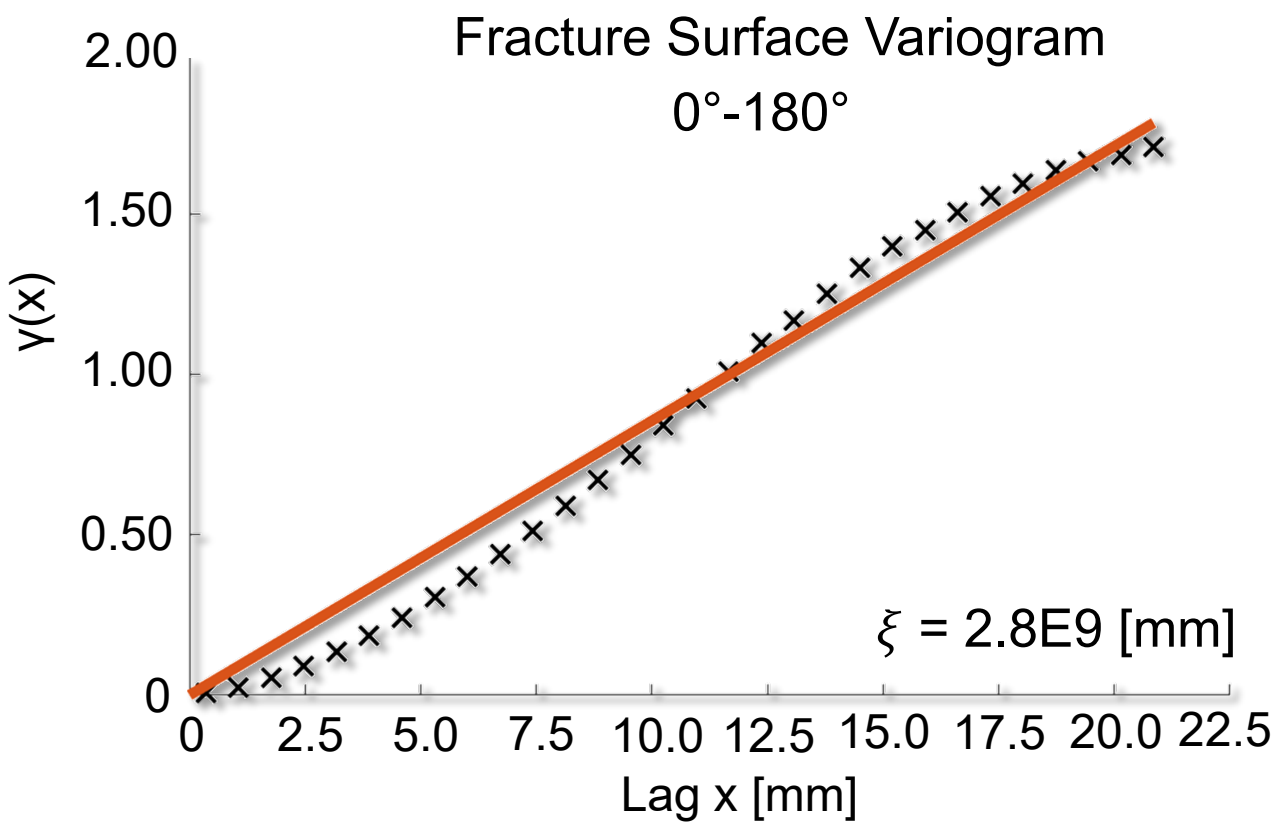

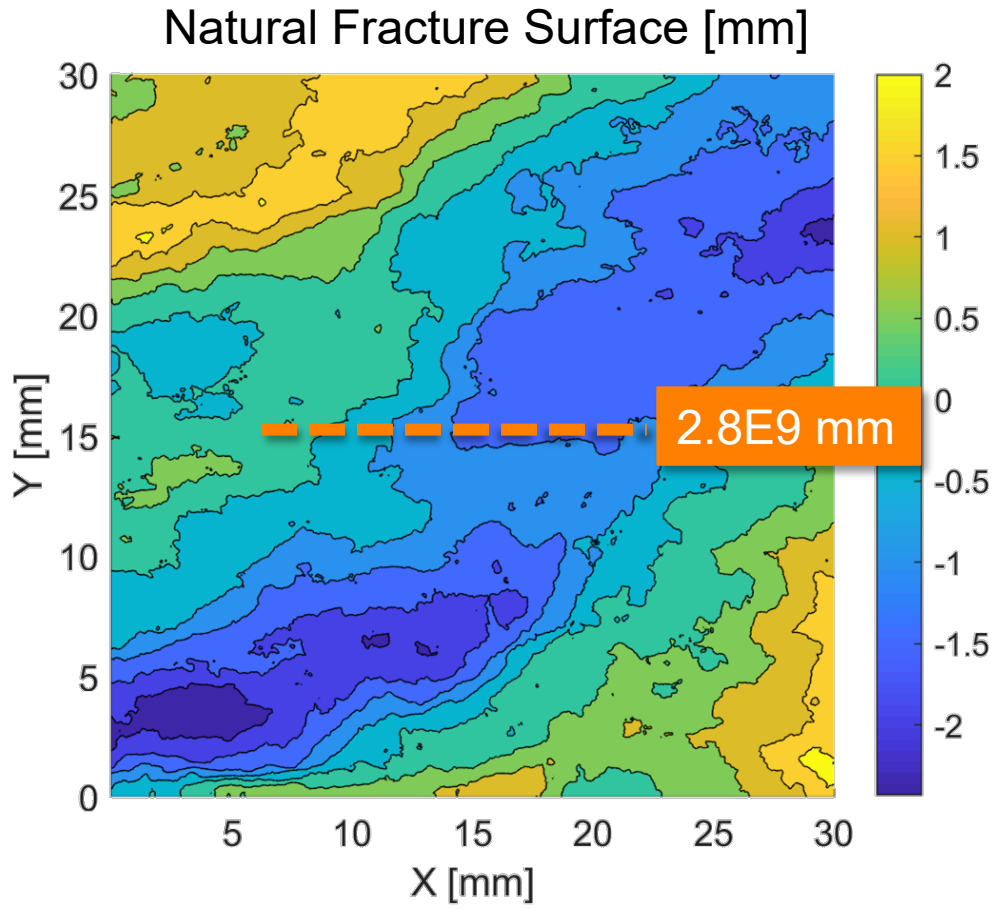

Figure. Natural fracture surface distribution with measured transect(s).

VI-D. Fracture Surface Characterization

- Variogram used to estimate correlation length of granite surface at variable orientations
- Unbounded exponential model used to fit data

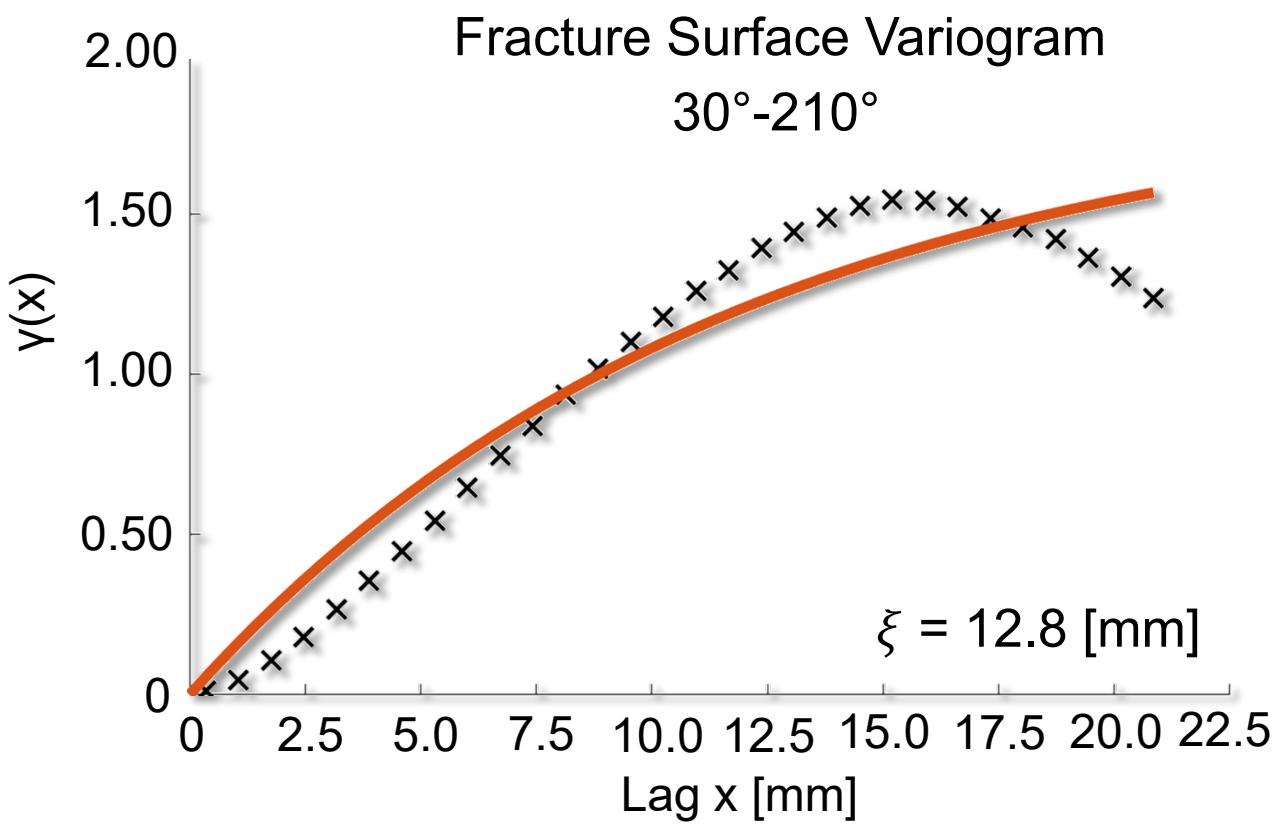

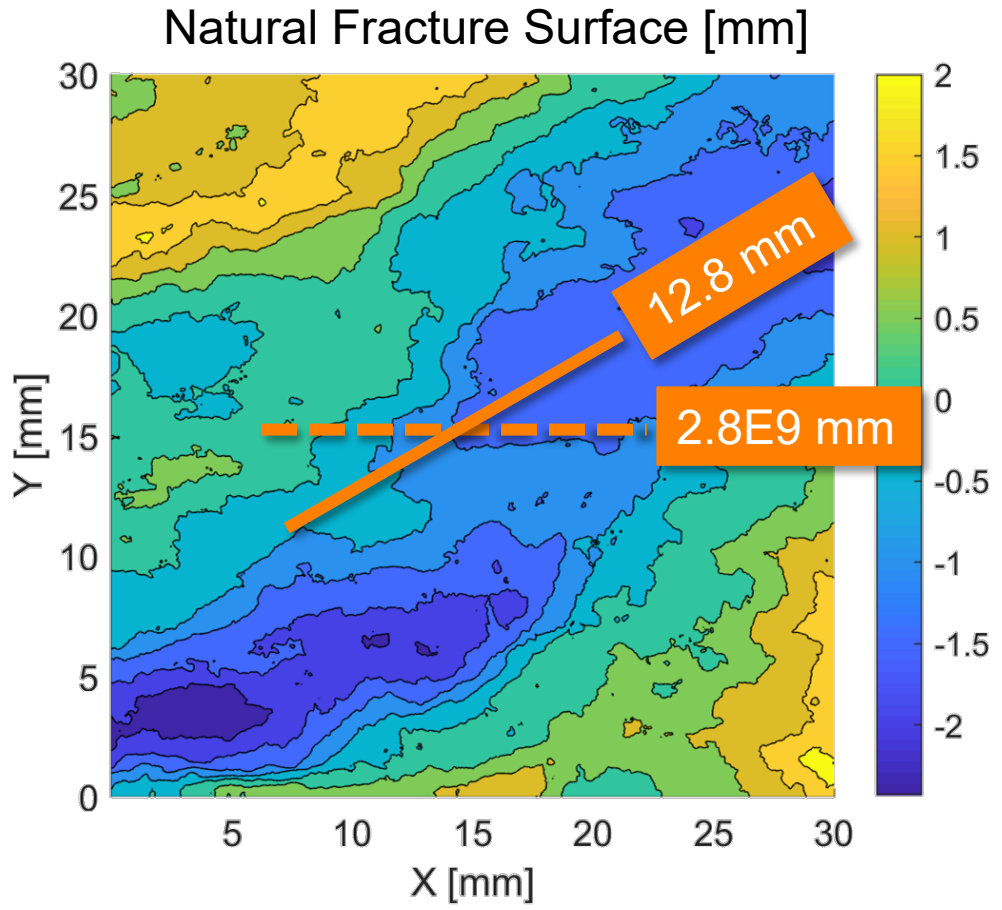

Figure. Natural fracture surface distribution with measured transect(s).

VI-D. Fracture Surface Characterization

- Variogram used to estimate correlation length of granite surface at variable orientations
- Unbounded exponential model used to fit data

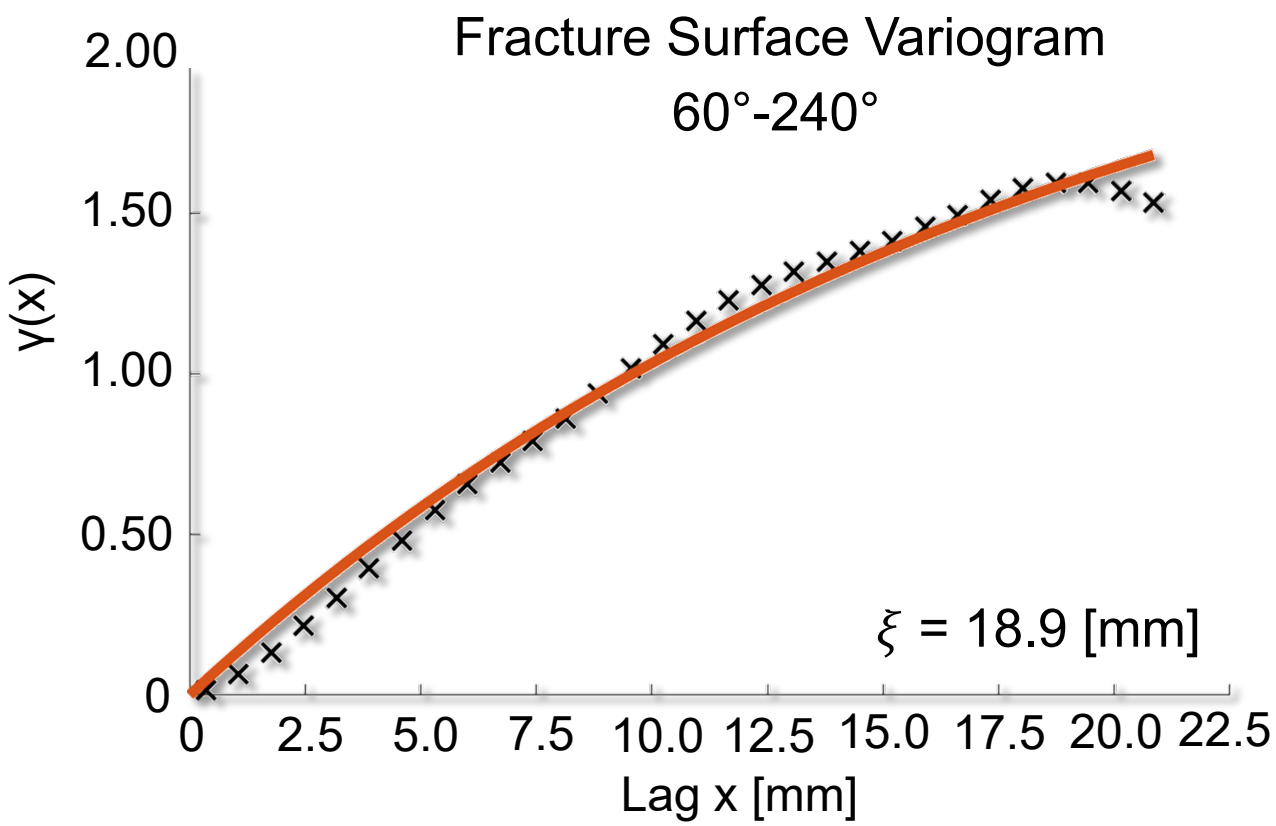

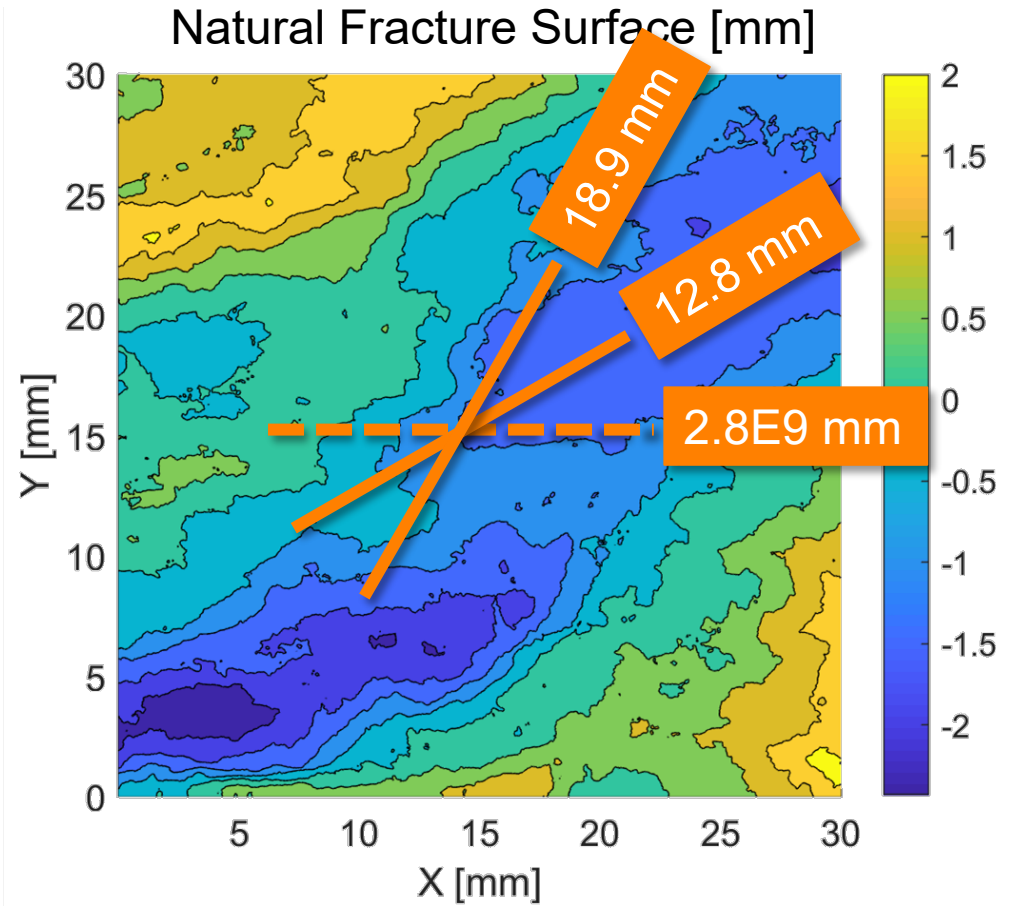

Figure. Natural fracture surface distribution with measured transect(s).

VI-D. Fracture Surface Characterization

- Variogram used to estimate correlation length of granite surface at variable orientations
- Unbounded exponential model used to fit data

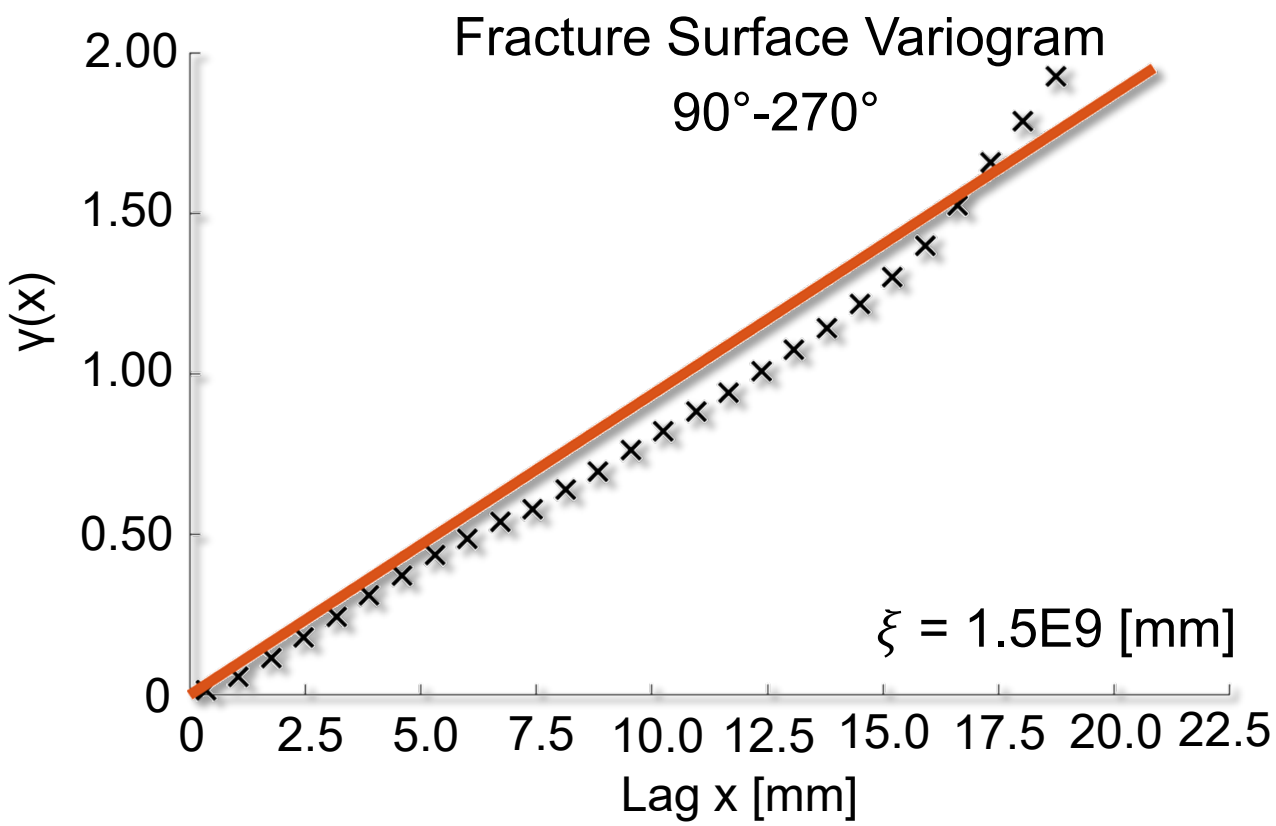

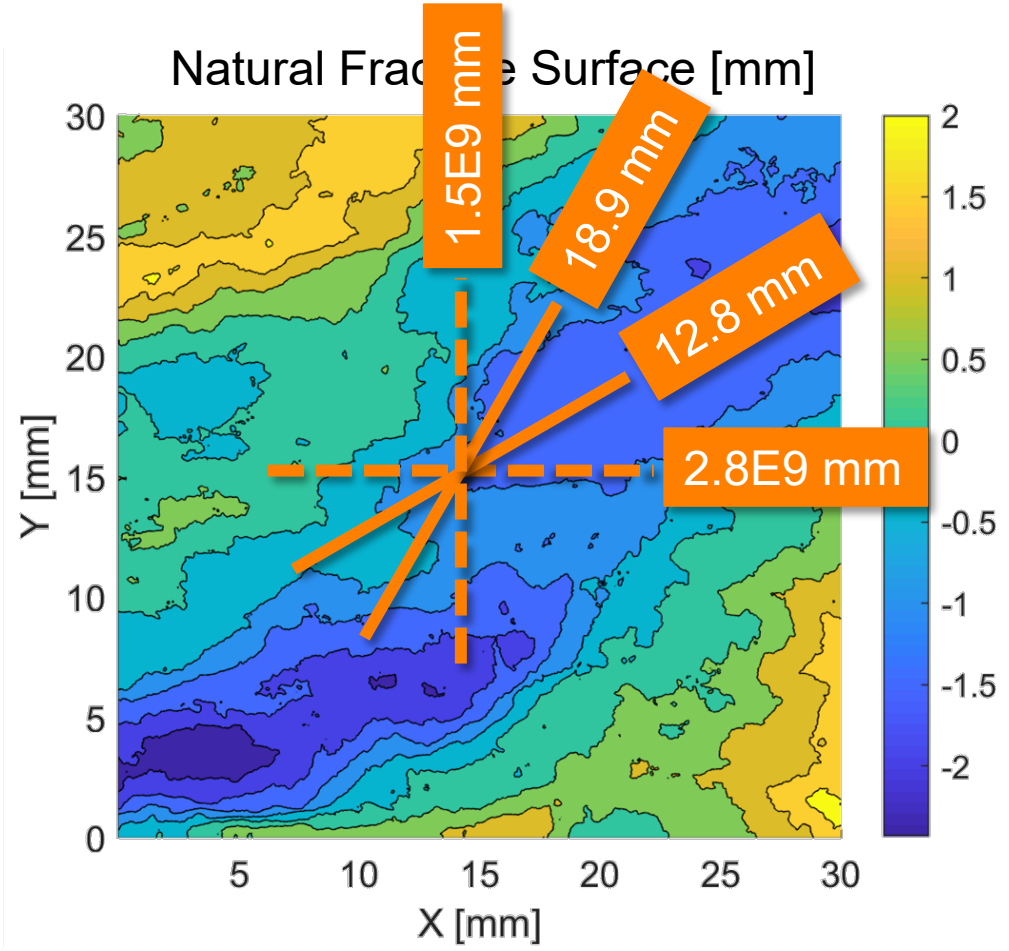

Figure. Natural fracture surface distribution with measured transect(s).

VI-D. Fracture Surface Characterization

- Variogram used to estimate correlation length of granite surface at variable orientations
- Unbounded exponential model used to fit data

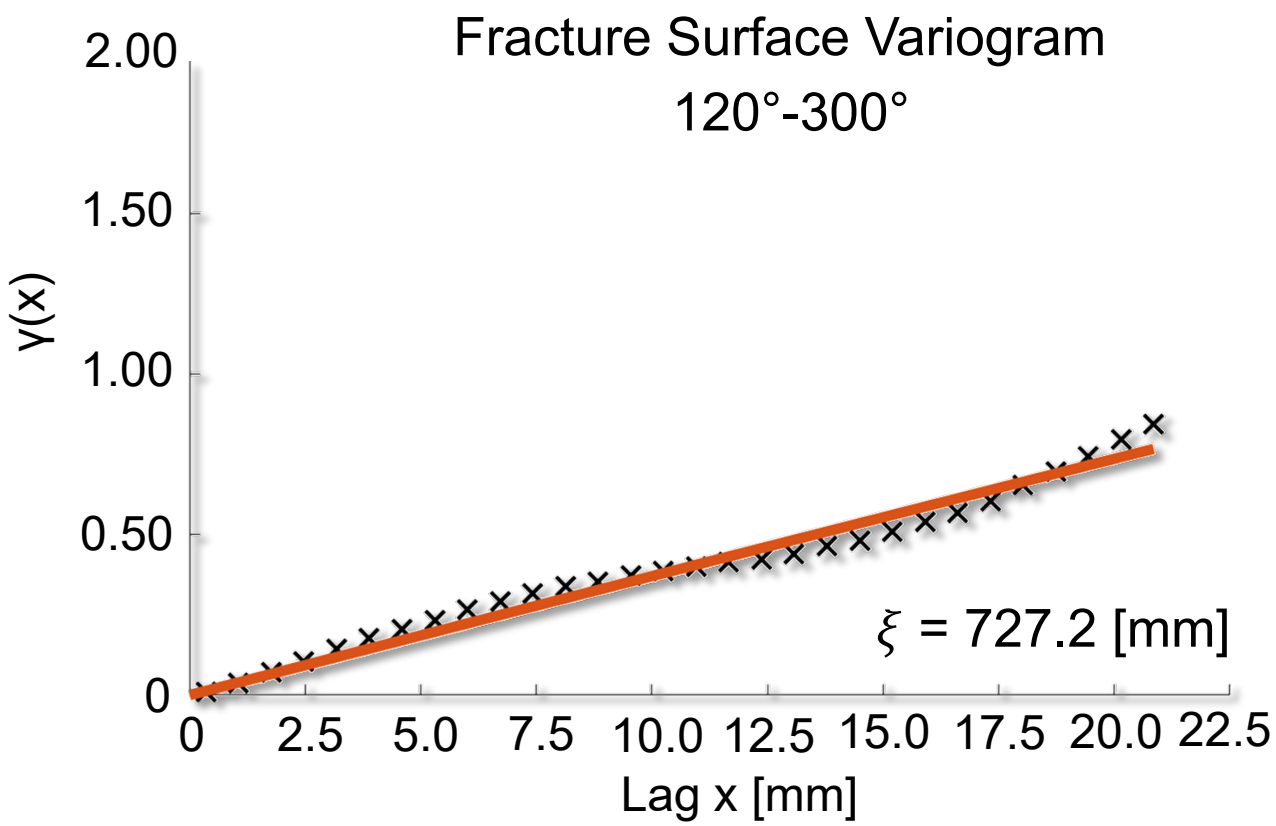

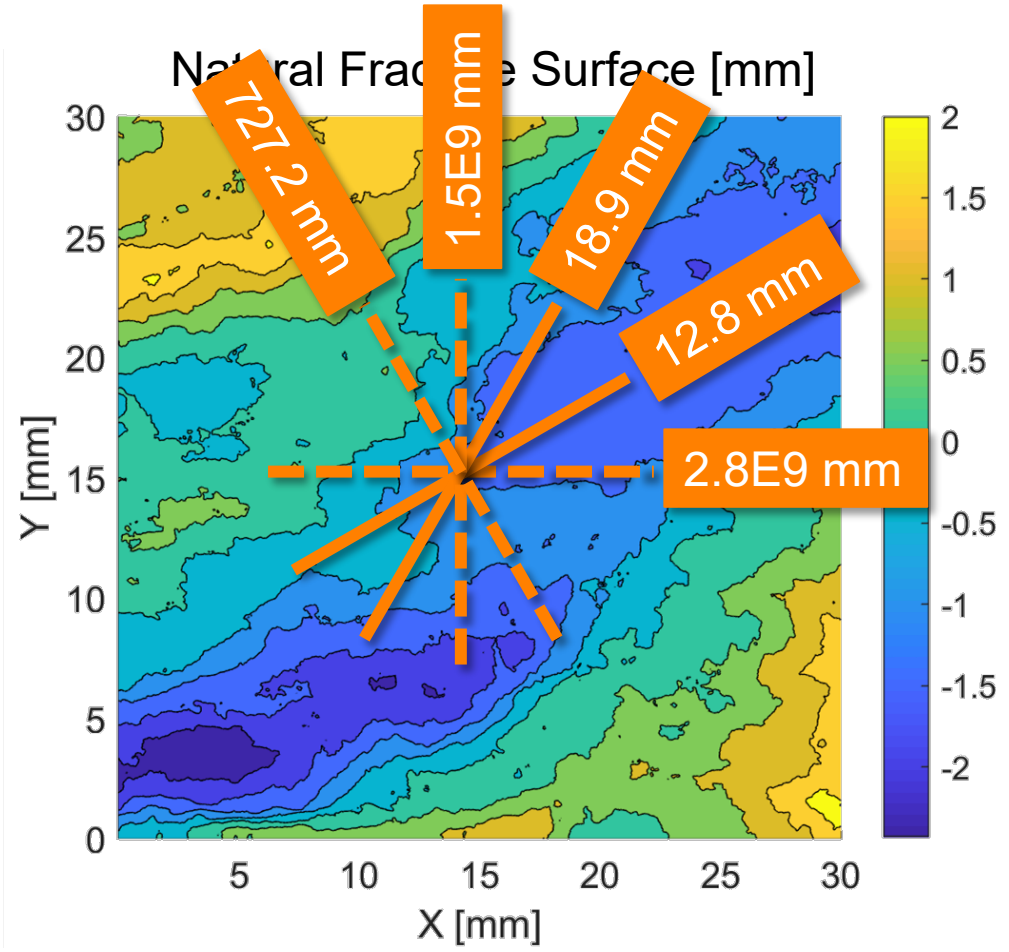

Figure. Natural fracture surface distribution with measured transect(s).

VI-D. Fracture Surface Characterization

- Variogram used to estimate correlation length of granite surface at variable orientations
- Unbounded exponential model used to fit data

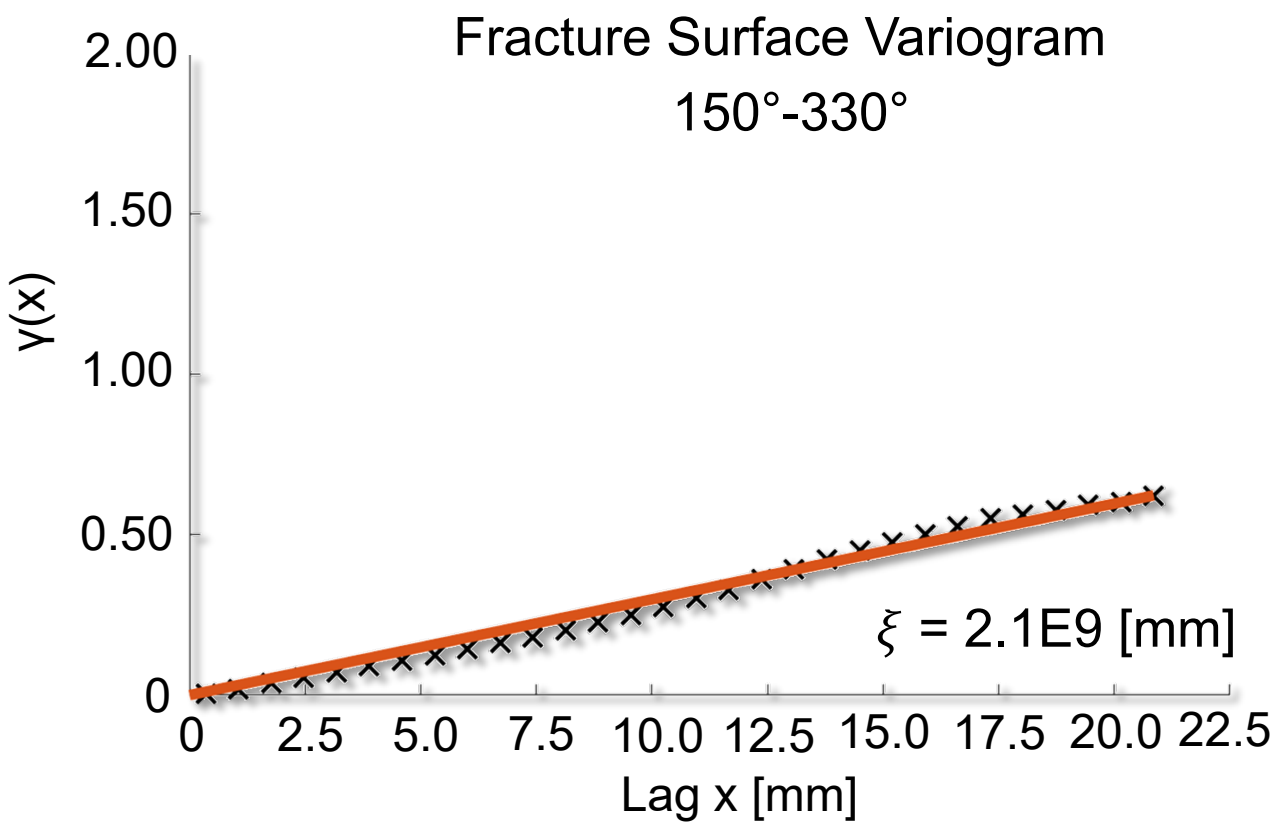

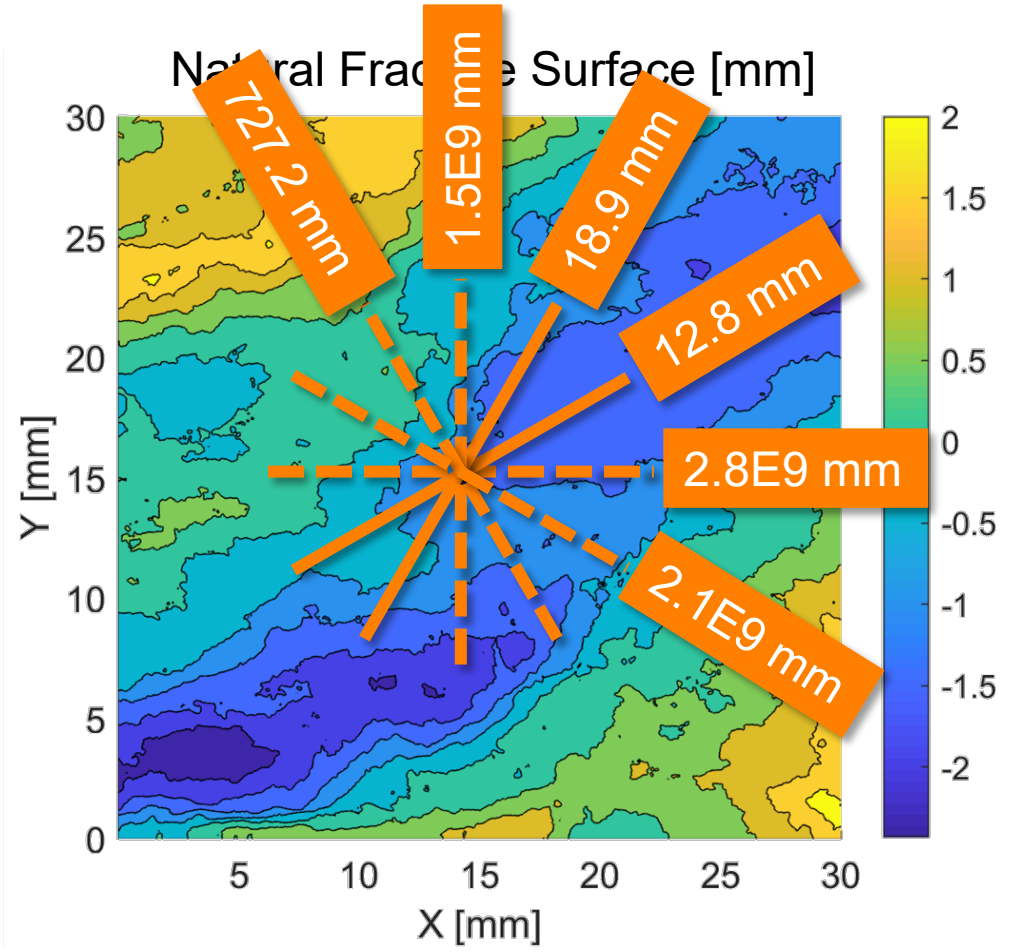

Figure. Natural fracture surface distribution with measured transect(s).

VI-E. Numerical Model Validation

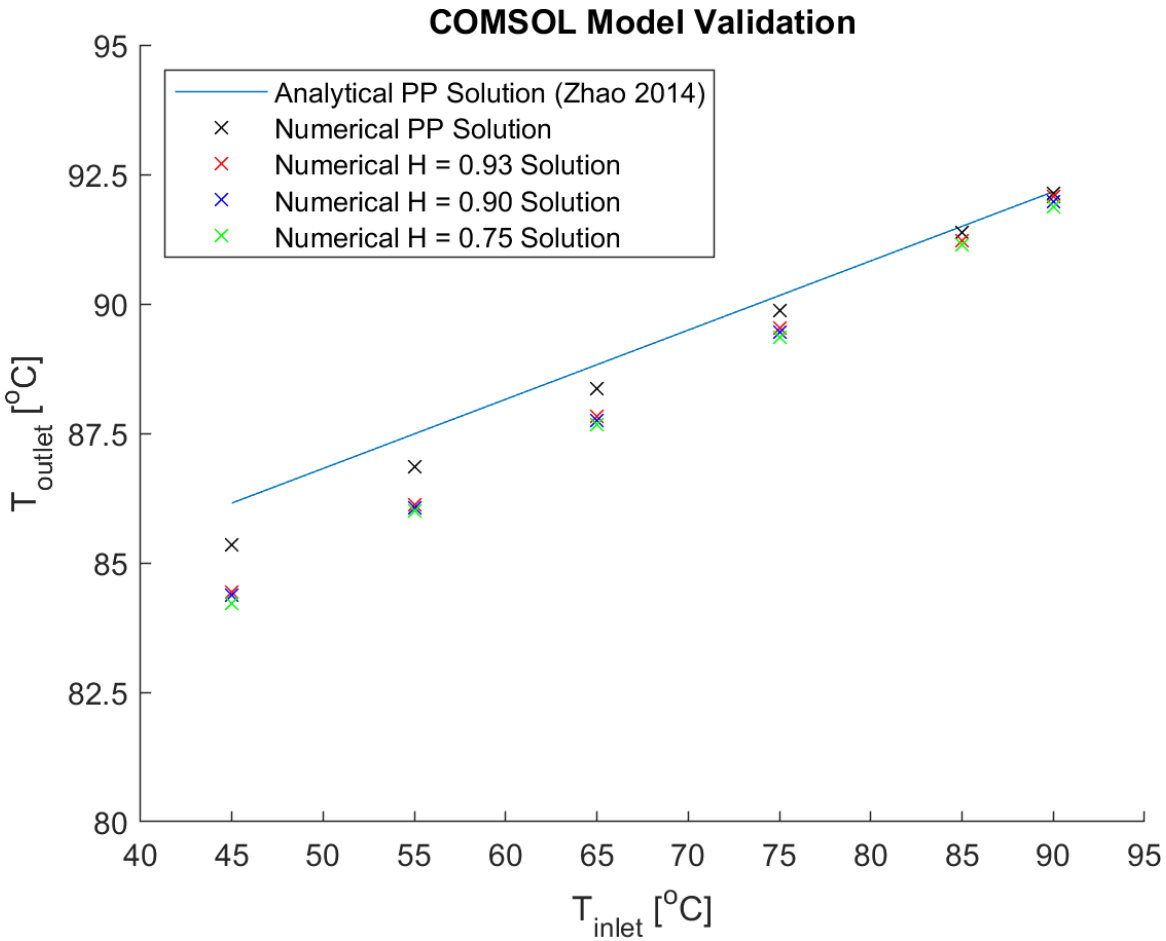

Figure. Comparison of numerical model outlet temperatures with the 1-dimensional analytical solution for flow between parallel plates. 'Numerical PP Solution' refers to the parallel plate FEM model built in COMSOL®. All models (H = 0.75_{HOM}, 0.90_{HOM}, 0.93_{HOM}) possess a homogeneous 0.5 mm mean aperture width, but surfaces of variable roughness.

Definitions

1. *Fracture* (n.): A discontinuity within an otherwise continuous formation, which may possess some magnitude of shear displacement.

2. *Aperture* (n.): The perpendicular width between two fracture faces.